

Gas Transport in Bentonite

M. V. Villar
V. Gutiérrez-Rodrigo
P. L. Martín
F. J. Romero
J. M. Barcala



Gas Transport in Bentonite

M. V. Villar

V. Gutiérrez-Rodrigo

P. L. Martín

F. J. Romero

J. M. Barcala

Toda correspondencia en relación con este trabajo debe dirigirse al Servicio de Información y Documentación, Centro de Investigaciones Energéticas, Medioambientales y Tecnológicas, Ciudad Universitaria, 28040-MADRID, ESPAÑA.

Las solicitudes de ejemplares deben dirigirse a este mismo Servicio.

Los descriptores se han seleccionado del Thesauro del DOE para describir las materias que contiene este informe con vistas a su recuperación. La catalogación se ha hecho utilizando el documento DOE/TIC-4602 (Rev. 1) Descriptive Cataloguing On-Line, y la clasificación de acuerdo con el documento DOE/TIC.4584-R7 Subject Categories and Scope publicados por el Office of Scientific and Technical Information del Departamento de Energía de los Estados Unidos.

Se autoriza la reproducción de los resúmenes analíticos que aparecen en esta publicación.

Catálogo general de publicaciones oficiales

<http://www.060.es>

Depósito Legal: M -26385-2011

ISSN: 1135 - 9420

NIPO: 721-13-057-7

Editorial CIEMAT

CLASIFICACIÓN DOE Y DESCRIPTORES

S58

BENTONITE; GASES; PERMEABILITY; POROSITY; SAMPLING; TESTING;
PRESSURE EFFECTS

Gas Transport in Bentonite

Villar, M.V.; Gutiérrez-Rodrigo, V.; Martín, P.L.; Romero, F.J.; Barcala, J.M.

63 pp. 81 figs. 14 refs 12 tables

Abstract:

The gas permeability of the Spanish FEBEX bentonite compacted at dry densities of between 1.4 and 1.8 g/cm³ with high water contents was measured for different confining, injection and backpressures. The results were compared with results obtained in previous investigations for lower degrees of saturation. It was checked that gas permeability was greatly affected by dry density, decreasing about three orders of magnitude when it increased from 1.5 to 1.8 g/cm³ for similar water content. The increase of water content caused also a decrease in gas permeability. It was found that both gas permeability and the relative gas permeability were mainly related to the accessible porosity. These relationships could be fitted to potential expressions with exponents between 3 and 4, as well as the relationship between intrinsic permeability and void ratio.

For gas pressures below 1.2 MPa no effect of the injection or confining pressures on the value of permeability was detected. For a given confining pressure the permeability value decreased as the effective pressure increased, especially if the increase in effective pressure was due to a decrease in gas backpressure. It was checked that the Klinkenberg effect was not significant for this material in the range of pressures applied in the tests.

The gas breakthrough pressure values in FEBEX saturated bentonite were determined for different dry densities. They increased clearly with dry density and were always higher than the swelling pressure of the bentonite. In high density samples gas flow tended to stop abruptly after breakthrough, whereas in lower density samples gas flow decreased gradually until a given pressure gradient was reached. The permeabilities computed after breakthrough (which usually did not stabilise) were inversely related to dry density. This would indicate that, even if the flow took place predominantly through preferential pathways that sometimes closed quickly after breakthrough and others remained open allowing decreasing gas flow, the swelling capacity of the bentonite matrix (lower as the density is lower) had also an effect on path formation and consequently on permeability. After resaturation of the bentonite the same breakthrough pressures and permeabilities were found, pointing to the perfect healing of these preferential pathways. A sealed interface along the bentonite did not seem to affect the breakthrough pressure or permeability values.

Transporte de Gas en Bentonita

Villar, M.V.; Gutiérrez-Rodrigo, V.; Martín, P.L.; Romero, F.J.; Barcala, J.M.

63 pp. 81 figs. 14 refs 12 tablas

Resumen:

Se ha medido la permeabilidad al gas de la bentonite FEBEX compactada con humedad elevada a densidades secas entre 1.4 y 1.8 g/cm³ para diferentes presiones de confinamiento, inyección y cola. Los resultados se han comparado con los de una investigación anterior realizada en muestras con grados de saturación más bajos. La permeabilidad depende en gran medida de la densidad, con la que disminuye, pero también de la humedad. Tanto la permeabilidad al gas como la permeabilidad intrínseca y la relativa se correlacionan fundamentalmente con la porosidad accesible mediante expresiones potenciales con exponentes entre 3 y 4.

Para presiones de gas inferiores a 1.2 MPa no se ha identificado influencia de la presión de inyección o la confinante en el valor de la permeabilidad. Se ha comprobado que el efecto Klinkenberg no es relevante para este material en el rango de presiones aplicadas. Se determinaron las presiones de paso (breakthrough) de muestras de bentonita saturada y compactada a diferentes densidades. Éstas aumentan claramente con la densidad seca y son mayores que la presión de hinchamiento correspondiente a esa densidad. En muestras de densidad alta el paso de gas tiende a parar abruptamente, mientras que en muestras de menor densidad una vez establecido el flujo disminuye lentamente hasta alcanzarse un determinado gradiente hidráulico. Las permeabilidades calculadas después del paso de gas considerando que el flujo fuera bifásico, están relacionadas inversamente con la densidad seca. Esto podría indicar que aunque el flujo se produzca predominantemente por caminos preferentes que unas veces se cierran rápidamente tras el paso de gas y otras permanecen abiertos permitiendo un flujo decreciente, la capacidad de hinchamiento de la matriz de bentonita también tiene influencia en la formación de trayectorias y consecuentemente en la permeabilidad. Tras resaturación de las muestras se han medido las mismas presiones de paso y permeabilidades, lo que indica que el sellado de estos hipotéticos caminos preferentes es efectivo. Incluso una junta entre bloques de bentonita queda sellada tras saturación de tal manera que no repercute en la presión necesaria para el paso de gas, que dependerá sólo de la densidad media del bloque.

CONTENTS

1	Introduction	1
2	Material	2
3	Methodology.....	3
3.1	Gas permeability.....	3
3.2	Breakthrough tests	7
3.3	Tests in interfaces.....	11
4	Results	13
4.1	Gas permeability.....	13
4.2	Breakthrough tests	17
4.3	Tests in interfaces.....	41
5	Discussion	50
5.1	Analysis of the Klinkenberg effect on gas permeability	50
5.2	Intrinsic and relative gas permeability	55
5.3	Breakthrough pressure	57
6	Conclusions	61
	Acknowledgements	62
	References.....	63

1 Introduction

The multiple barrier concept is the cornerstone of all proposed schemes for underground disposal of radioactive wastes. The concept invokes a series of barriers, both engineered and natural, between the waste and the surface. Achieving this concept is the primary objective of all disposal programmes, from site appraisal and characterisation to repository design and construction. However, the performance of the repository as a whole (waste, buffer, engineering disturbed zone, host rock), and in particular its gas transport properties, are still not completely understood. Gas will be generated within the repository by several mechanisms, such as the anaerobic corrosion of metals, the microbial degradation of organic wastes and the radiolysis of water, which generate hydrogen, oxygen, methane and carbon dioxide. The gas pressure could rise and build up if the generation rates are high and the transport within the repository is somehow hindered. This pressure may be sufficient to affect the repository structure and properties and may drive contaminated water into the geosphere if breakthrough occurs. Thus, the knowledge of the movement of gases through the repository structure is required to determine the magnitude of these effects and the need to accommodate them in the repository design and safety calculations. Issues still to be adequately examined that relate to understanding basic processes include: dilational versus visco-capillary flow mechanisms; long-term integrity of seals, in particular gas flow along contacts; role of the EDZ as a conduit for preferential flow; laboratory to field up-scaling.

Understanding gas generation and migration is thus vital in the quantitative assessment of repositories and is the focus of the research in the integrated, multi-disciplinary project FORGE. The FORGE project was a pan-European project with links to international radioactive waste management organisations, regulators and academia, specifically designed to tackle the key research issues associated with the generation and movement of repository gasses. FORGE intended to gather further experimental data to reduce uncertainty relating to the quantitative treatment of gas in performance assessment and this was addressed through a series of laboratory and field-scale experiments, including the development of new methods for up-scaling allowing the optimisation of concepts through detailed scenario analysis.

This report includes the work performed by CIEMAT in WP3.2 of the FORGE project “Gas permeability and breakthrough pressure as a function of dry density, water content and pressure in buffer materials” and WP3.3 “Gas transport through joints between buffer blocks and between host rock/buffer”. All the laboratory work included was performed at CIEMAT facilities and the results were presented at the following Conferences:

- Villar, M.V.; Martín, P.L.; Romero, F.J., Barcala, J.M. & Gutiérrez-Rodrigo, V. 2012. Gas transport through bentonite: influence of dry density, water content and boundary conditions. In: Skoczylas, F.; Davy, C.A.; Agostini, F. & Burlion, N. (eds.): *Propriétés de Transfert des Géomatériaux. Transfert 2012, Actes du Colloque*: 379-389.
- Gutiérrez-Rodrigo, V.; Villar, M.V.; Martín, P.L. & Romero, F.J. 2012. Determinación de las propiedades de transporte de gas en bentonita. *Macla* 16: 126-127.
- Villar, M.V.; Gutiérrez-Rodrigo, V.; Martín, P.L. & Romero, F.J. 2012. Gas transport through saturated bentonite and interfaces. ANDRA 5th International Meeting Clays in Natural and Engineered Barriers for Radioactive Waste Confinement. Abstracts, pp 704-705, GPTP/5. Montpellier, 22-25 October 2012.

Villar, M.V.; Gutiérrez-Rodrigo, V.; Martín, P.L.; Romero, F.J. & Barcala, J.M. 2013. Gas Permeability and Breakthrough Pressures of FEBEX Bentonite. FORGE Final Symposium. Luxembourg, 5-7 February 2013.

2 Material

The FEBEX bentonite was extracted from the Cortijo de Archidona deposit (Almería, Spain) and the processing at the factory consisted of disaggregation and gently grinding, drying at 60°C and sieving by 5 mm. The physico-chemical properties of the FEBEX bentonite, as well as its most relevant thermo-hydro-mechanical and geochemical characteristics obtained during the projects FEBEX I and II are summarised in the final reports of the project (ENRESA 2000, 2006).

The montmorillonite content of the FEBEX bentonite is above 90 wt.% (92±3 %). The smectitic phases are actually made up of a smectite-illite mixed layer, with 10-15 wt.% of illite layers. Besides, the bentonite contains variable quantities of quartz (2±1 wt.%), plagioclase (3±1 wt.%), K-felspar (traces), calcite (1±0.5 wt.%), and cristobalite-trydimite (2±1 wt.%).

The cation exchange capacity is 102±4 meq/100g, the main exchangeable cations being calcium (35±2 meq/100g), magnesium (31±3 meq/100g) and sodium (27±1 meq/100g). The predominant soluble ions are chloride, sulphate, bicarbonate and sodium.

The liquid limit of the bentonite is 102±4 %, the plastic limit 53±3 %, the density of the solid particles 2.70±0.04 g/cm³, and 67±3 % of particles are smaller than 2 µm. The hygroscopic water content in equilibrium with the laboratory atmosphere (relative humidity 50±10 %, temperature 21±3 °C, total suction about 100 MPa) is 13.7±1.3 %. The external specific surface area is 32±3 m²/g and the total specific surface area is 725 m²/g.

The saturated hydraulic conductivity to deionised water (k_w , m/s) of samples of untreated FEBEX bentonite compacted at different dry densities is exponentially related to dry density (ρ_d , g/cm³). A distinction may be made between two different empirical fittings depending on the density interval:

for dry densities of less than 1.47 g/cm³:

$$\log k_w = -6.00 \rho_d - 4.09 \quad [1]$$

for dry densities in excess of 1.47 g/cm³:

$$\log k_w = -2.96 \rho_d - 8.57 \quad [2]$$

The determinations were done at room temperature. The variation in the experimental values with respect to these fittings is smaller for low densities than it is for higher values, with an average –in absolute values– of 30 percent.

The swelling pressure (P_s , MPa) of FEBEX samples compacted with their hygroscopic water content and flooded with deionised water up to saturation at room temperature and constant volume conditions can be related to dry density (ρ_d , g/cm³) through the following equation:

$$\ln P_s = 6.77 \rho_d - 9.07 \quad [3]$$

In this case, the difference between experimental values and this fitting is, on average, 25 percent. This dispersion, which is wider for higher dry densities, is due both to the natural variability of bentonite and to the measurement method used, which does not allow high degrees of accuracy.

Some isothermal infiltration tests and heat flow tests at constant overall water content were performed during the FEBEX I project (ENRESA 2000, 2006) and they were backanalysed using CODEBRIGHT. The experimental data were fitted using a cubic law for the relative permeability and a value of 0.8 for the tortuosity factor.

3 Methodology

Different kinds of tests were performed: gas permeability tests, breakthrough tests and tests in interfaces. The buffer material used in all of them was the FEBEX bentonite compacted at different dry densities.

3.1 GAS PERMEABILITY

Gas permeability was measured in specimens of compacted FEBEX bentonite. Prior to compaction (several days earlier), the granulated bentonite was mixed with different quantities of deionised water, in order to obtain water contents of between 18 and 22%. Cylindrical samples of 3.8 cm diameter and 7.8 cm height were obtained by uniaxial compaction of the wet bentonite. Compaction pressures of between 30 and 152 MPa were applied to manufacture specimens of dry densities of between 1.4 and 1.8 g/cm³.

The cylindrical samples were placed in a triaxial cell confined between two porous stones and wrapped in two latex membranes, between which vacuum grease was applied in order to prevent the loss of gas. The cell walls were made of methacrylate and were capable of withstanding pressures up to 3 MPa (Figure 1). The cells had three inlets drilled in the base, one for the sample bottom drainage/backpressure, one for the sample top injection pressure, and another one for the confining pressure. In one of the tests (test FBX16), a stainless steel triaxial cell able to withstand pressures of up to 20 MPa was used (Figure 1, right).

The setup to perform gas permeability measurements was designed to work as a constant head permeameter under different gas pressures, allowing the change of the head pressure value, the control of the confining pressure and the measurement of the gas inflow and outflow (Figure 2). The cell was filled with water and pressurised with nitrogen, which was separated from the water in the cell through an elastic membrane contained in an OLAER's pressure accumulator capable of withstanding pressures of up to 33 MPa. The injection and downstream pressures could be independently varied and kept constant by HI-TEC gas forward pressure controllers during the period of time necessary to get steady flow. Associated to the pressure controllers, DRUCK pressure transmitters (PTX1400 series, 100 bar a, 0.15% typical accuracy, overpressure 2 x FS), were placed for redundancy at the inlet and outlet of the cell. Different range HITECH gas mass flowmeters measured the inward and outward flows (0.2-10, 2-100 and 20-1000 STP cm³/min). Gas mass flowmeters were used to prevent the potential impact of deviation from the ideal behaviour of gas on the measurement of the molecular flow rate and, hence, on the calculated permeability coefficients. Nitrogen gas was used as fluid. The technical details of the equipment were given in Villar *et al.* (2010).

The system applied the pressures to the sample and registered flow and pressures from the measurement devices. In and outflow gas rates, up and downstream pressure, temperatures and the confining pressure were monitored.



Figure 1: Bentonite sample inside a methacrylate triaxial cell (left) and high-pressure cell (right)

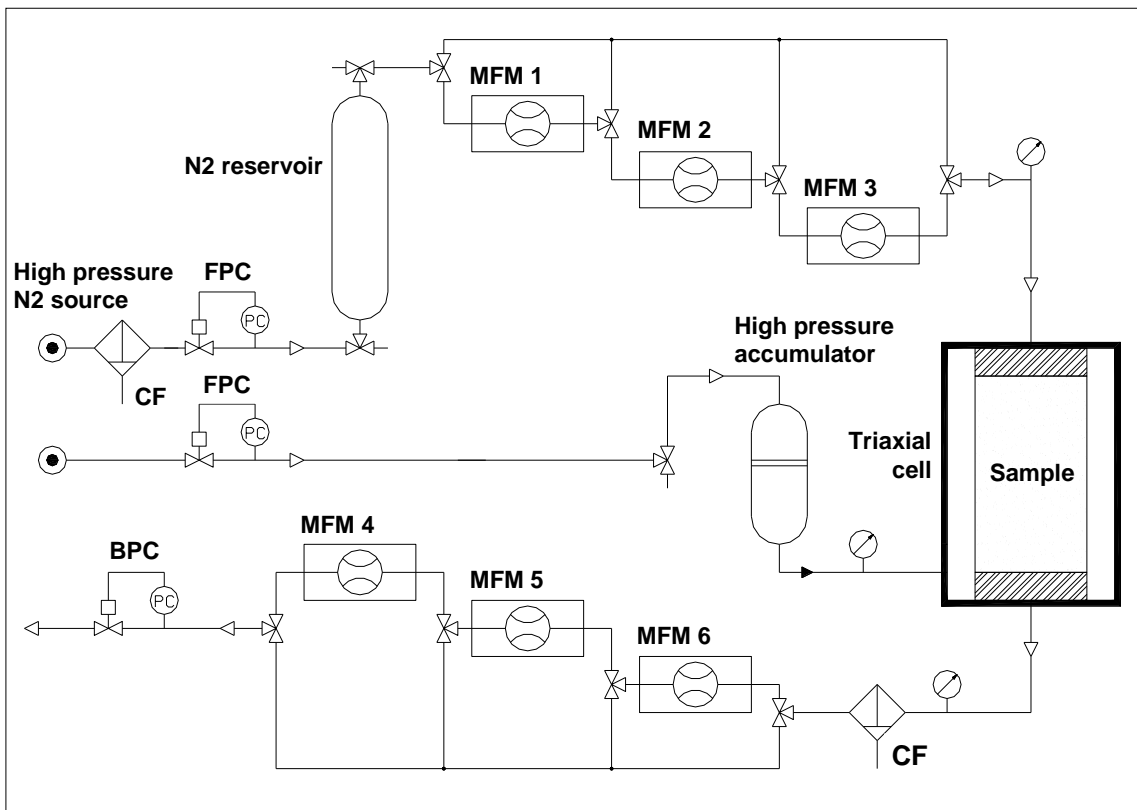


Figure 2: Schematic diagram of the setup for the gas permeability tests before modification (CF: coalescing filter; FPC: forward pressure controller; BPC: back pressure controller; MFM: mass flow meter (1000 mLn/min: 1&6; 100 mLn/min: 2&5; 10 mLn/min: 3&4); black arrow: water line for confining pressure)

After all the gas permeability measurements were performed, the setup was modified and divided into two separate measurement lines that were used for some breakthrough tests and tests in interfaces. In the new version of the setup, the backpressure was kept atmospheric and only the gas outflow was measured (by means of different range HITECH gas flowmeters).

It must be pointed out that no sample was completely dry (0% water content) during the determinations and therefore the intrinsic permeability could not be directly obtained from the measurements performed, since to determine the intrinsic permeability with air flow the sample must be completely dry. In order to obtain completely dry samples it would have been necessary to dry them in the oven at 110°C and this would have caused changes in the microstructure of the bentonite and consequently in its hydraulic properties. When there are two fluids present in the porous material (gas and water in this case), the permeabilities of each fluid depend upon the saturation of each fluid: these are called effective permeabilities. Hence the value obtained in the determinations (apart from the gas permeability, k_g) is the intrinsic permeability measured with gas flow, k_{ig} , multiplied by the relative permeability to gas, k_{rg} . The relative permeability to gas is the ratio of the effective permeability of gas at a particular saturation to the absolute permeability of gas at total gas saturation, i.e. in completely dry material, where the k_{rg} value would be 1.

To compute the permeability the inflow or outflow measurements can be used, applying the following equation for incompressible media with compressible pore fluids (Scheidegger 1974):

$$k_{ig} \cdot k_{rg} = \frac{Q_m \times \mu_g \times L \times 2P_m}{A \times (P_{up}^2 - P_{dw}^2)} \quad [4]$$

where Q_m is the measured flow (volume of fluid as a function of time), A is the sample surface area, μ_g is the fluid dynamic viscosity, L is the sample length and P_{up} and P_{dw} are the upstream and downstream pressures applied at the top (inlet) and the bottom (outlet), respectively, of the sample, and P_m is the pressure of the measured flow (in our case, due to the STP conditions of the gas mass flowmeters, the atmospheric pressure). In turn gas permeability, k_g , can be computed taking into account the gas density and viscosity change with upstream or downstream pressures (P):

$$k_g = \frac{\rho_g \times g \times P}{\mu_g} \times k_{ig} \times k_{rg} \quad [5]$$

It is considered that the viscosity of nitrogen did not change during the tests because they were isothermal, whereas density changed with pressure. The change in density was considered as that of an ideal gas, and thus computed as the product of the density of nitrogen at atmospheric pressure times the pressure, either the injection or the backpressure, depending on which flow was used for the computation. This solution assumed that steady state flow was established, what meant that the quantity of gas exiting the sample in the low pressure side was equal to that entering the sample in the high pressure side. This aspect was verified in the tests performed to measure the bentonite gas permeability. In any case, the underestimation of the calculated permeability coefficients should be less than 1.3%.

To analyse the effect of injection, back and confining pressures on permeability, the tests consisted of several steps, which followed the paths shown in Figure 3:

- Stage 1: under constant confining (0.6 MPa) and backpressure (atm), the injection pressure was increased in steps.
- Stage 2: under constant injection (0.4 MPa) and backpressure (atm), the confining pressure was increased from 0.6 to 1.0 MPa.

- Stage 3: under constant confining (1.0 MPa) and backpressure (atm), the injection pressure was increased in steps.
- Stage 4: under constant confining (1.0 MPa) and injection pressures (0.8 MPa), the backpressure was increased in steps.
- Stage 5: finally, the injection and backpressures decreased simultaneously under constant confining pressure (1.0 MPa).

In test FBX14, after these five stages, the confining pressure was increased to 1.2 MPa and the effect of changing both the injection and the backpressure under this confining pressure was checked. Test FBX16 was performed in a stainless steel cell (Figure 1, right) in order to be able to apply higher injection pressures, since the sample had a very high initial water degree of saturation. The backpressure was kept atmospheric all through the test, while the confining and injection pressures followed the path shown in Figure 4.

At the end of the tests, the bentonite specimens were measured and weighed and the water content at three different levels along the cylindrical specimens was determined by oven-drying at 110°C for 48 h.

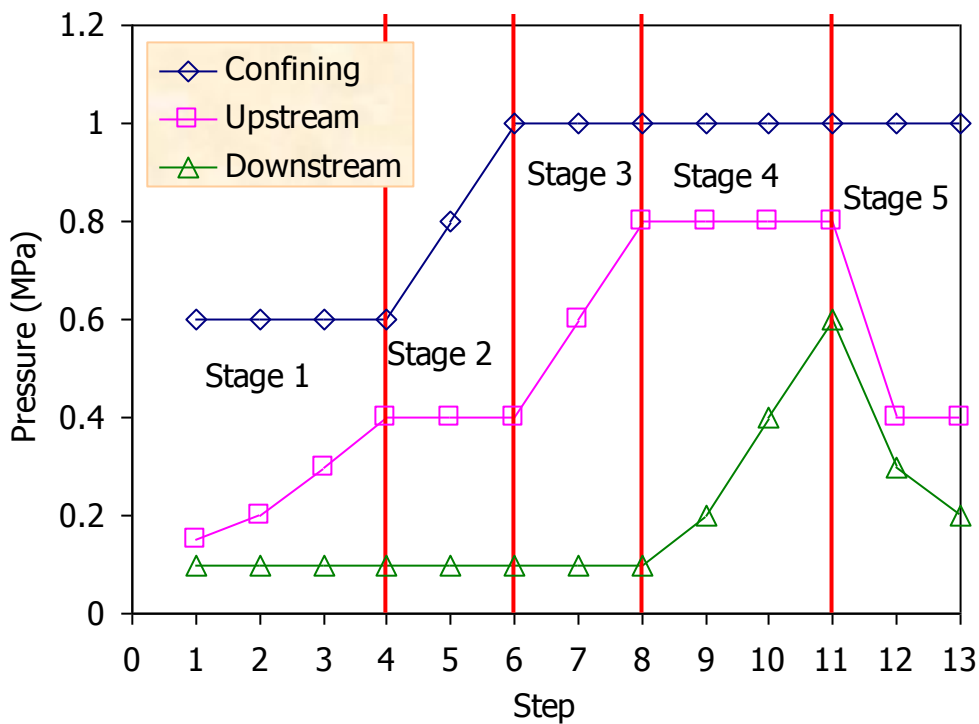


Figure 3: Pressure paths followed during the gas permeability tests PGFBX3 to PGFBX14

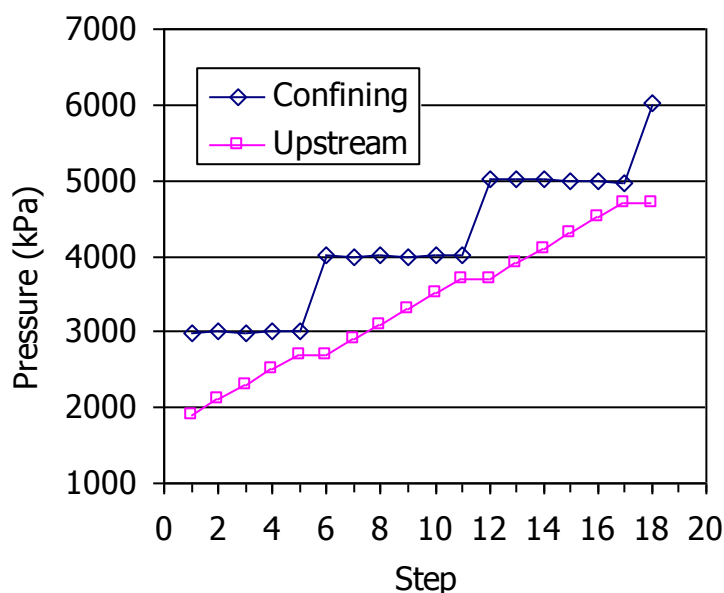


Figure 4: Pressure path followed during the gas permeability test FBX16. Backpressure was kept at atmospheric

3.2 BREAKTHROUGH TESTS

To perform these tests cylindrical bentonite samples were obtained by uniaxial compaction and saturated with deionised water. The cells and procedures were the same for all the tests except for test HP18_38:

- In test HP18_38 a sample of 7.8 cm in height and 3.8 cm in diameter was inserted in a stainless steel jacket with porous stones on top and bottom. The jacket was placed in a triaxial cell during saturation, so that to avoid vertical deformation. Saturation with deionised water was accomplished by applying injection pressures on top and bottom of 0.6 and 0.8 MPa. Saturation was followed online by measurement of water intake through a volume change apparatus. For the gas breakthrough test, the jacket on the base of the triaxial cell with the cell cap on top was placed in a frame to avoid vertical deformation of the bentonite (Figure 5). The test was performed in the modified setup described in section 3.1, in which the gas injection pressure on top was increased in 1.0-MPa steps while backpressure at the bottom was atmospheric and the outflow was measured by a series of three different range online flowmeters. No bentonite vertical or lateral deformation was allowed but the mechanical stresses during saturation and breakthrough were not measured.

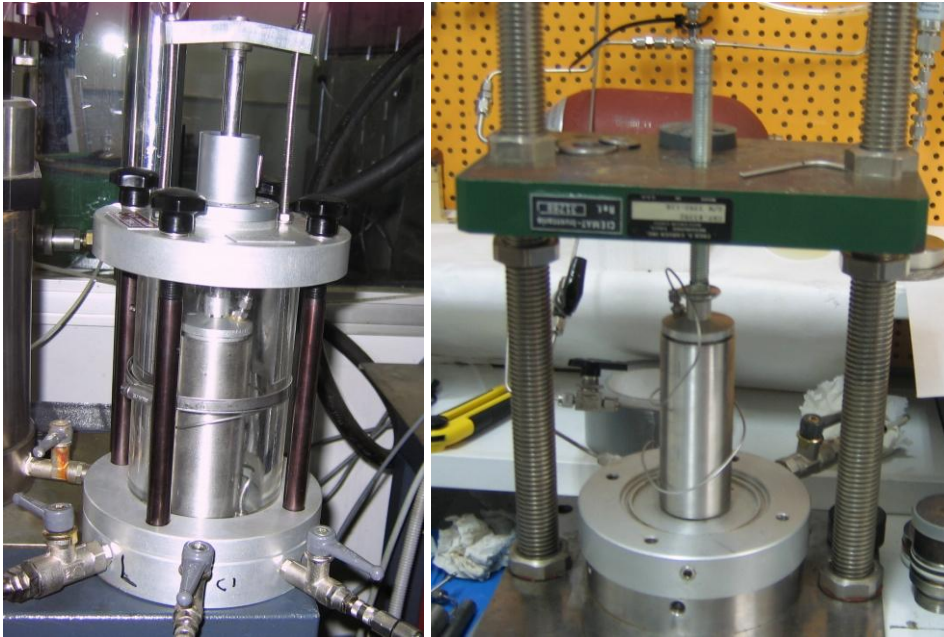


Figure 5: Cell with stainless steel jacket for breakthrough test HP18_38: during saturation (left) and breakthrough measurement (right)

- A series of stainless steel cells were designed and manufactured to perform gas breakthrough tests in saturated bentonite. The cells consisted of a body, in which the cylindrical sample was held, pistons with o-rings at both ends of the samples and threaded caps (Figure 6). The samples, of 3.8 and 5.0 cm in diameter and 2.0 or 5.0 in height, were obtained by uniaxial compaction of the bentonite with its hygroscopic water content directly inside the cell body. Saturation with deionised water was accomplished by applying injection pressures from 0.2 to 1.0 MPa (depending on the dry density) to one end to allow air escaping from the bentonite. Later, the pressure was applied on top and bottom. In the higher density samples saturation was followed online by measurement of water intake through volume change apparatuses, whereas for lower density samples saturation was checked by weighing. Once saturated the cells were weighed and the bentonite specimen indirectly measured, the filters on top and bottom of the samples were replaced by dry ones, the cells were again closed, and they were connected to a setup specially designed to measure breakthrough pressure (Figure 7). It consisted of two stainless steel deposits (SWAGELOK 304L-HDF4-75, SS Double-Ended DOT-Compliant Sample Cylinder, 75 cm³, 124 bar) connected to the ends of the cell and equipped with pressure transmitters DRUCK PMP 4070 (inlet pressure 135 bar a, outlet pressure 70 bar a, accuracy $\pm 0.04\%$ FS, over pressure 4 x FS). Vacuum was applied to the downstream deposit (the one at the bottom of the sample) and the other one was pressurised with nitrogen gas to 400 kPa. If no changes in pressure were recorded during 24 h, the injection pressure was increased by 200 kPa and kept constant for 24 h. The process was repeated until gas started to flow through the sample, causing a decrease of pressure in the upstream deposit and an increase in the downstream one. An HP 34970A data acquisition and switching mainframe, connected to a PC, recorded the data and monitored the tests in progress. The time required for the completion of a particular experiment was determined by the material and the conditions of the sample being studied.

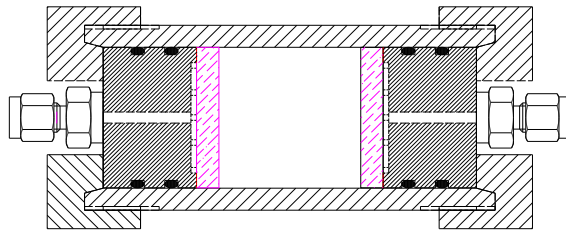


Figure 6: Schematic cross-section and appearance of the breakthrough cells

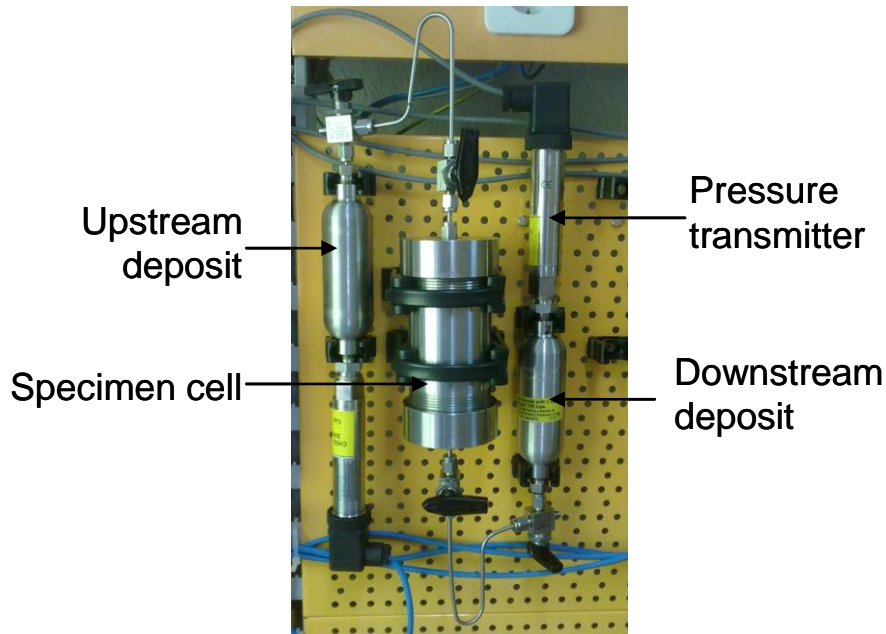


Figure 7: Setup for measurement of breakthrough pressure in bentonite

Although, these tests were not intended to measure permeability, after breakthrough in the setup just described, the flow of gas under the imposed pressure gradient could be estimated from the decay of the pressure difference across the sample with elapsed time, as in a variable head permeameter. An indirect method was used to determine the volume flow rate entering in or coming from the sample (Loosveldt et al. 2002). The mean volume flow rate Q_m was calculated as:

$$Q_m = V_v \times \left(\frac{\Delta\rho}{\rho} \right) \times \frac{1}{\Delta t} \quad [6]$$

where V_v is the volume of the deposit (inlet or outlet, about 50 or 75 cm³), $\Delta\rho/\rho$ is the relative change in gas density, and Δt is the time interval in which the change in gas density took place. To compute the change in gas density for almost steady-state conditions, it has to be taken into account that the (mass) flow rate (in standard conditions) is constant everywhere in the system at any pressure. From the equation of state for real gases:

$$\left(\frac{PV}{ZT}\right)_{\text{MEASURED}} = \left(\frac{PV}{ZT}\right)_{\text{STP}} \quad [7]$$

where P , T and V are the actual conditions of pressure, temperature and volume, respectively; and $Z(T, P)$ is the compressibility factor that expresses the deviation between compressibility (density) of the real gas and the ideal gas at identical conditions of temperature and pressure; the sub-indexes indicate the conditions of measurement or the standard conditions (STP: $T_0 = 273.15$ K and $P_0 = 101.325$ kPa).

The application of the real gas law immediately gives de value of ρ :

$$\rho = \rho_0 \frac{P}{P_0} \cdot \frac{T_0}{T} \cdot \frac{Z_0}{Z} = \frac{M}{V_0} \frac{P}{P_0} \cdot \frac{T_0}{T} \cdot \frac{Z_0}{Z} \quad [8]$$

where ρ_0 is the density and V_0 is the molar volume (0.0224143 m³/mol) of the supposedly ideal gas at reference conditions (STP); M is the molecular weight of the gas, T and P are the actual conditions.

Fluid physics equations and experimental observations have led to the determination of values of Z , which are listed in numerical tables (L'Air Liquide 1976). They show that the Z value for nitrogen in the range of pressure and temperature of our tests corresponding to the maximal difference with respect to the ideal gas is 0.99364 (N₂ at 20°C and 48 bar-a). This Z value indicates an underestimation of 0.64% in the actual density value when the gas is considered ideal and pressures are used to obtain the flow rate.

Note that when the actual densities deduced from Equation 6 are introduced in Equation 4, the compressibility factor Z is eliminated from the equation. If the test is considered isothermal, then:

$$Q_m = V_v \times \left(\frac{\Delta P}{P_{av}}\right) \times \frac{1}{\Delta t} \quad [9]$$

where ΔP is the pressure change and P_{av} is the average pressure (upstream or downstream) in the deposit (inlet or outlet) during the time interval considered. The computation of permeability from the pressure decrease was performed then applying Equation 4, which became:

$$k_{ig} \cdot k_{rg} = V_{v, \text{up,dw}} \times \left(\frac{\Delta P}{P_{av}}\right)_{\text{up,dw}} \times \frac{1}{\Delta t} \times \frac{\mu_g \times L \times 2 P_m}{A \times (P_{up}^2 - P_{dw}^2)} \quad [10]$$

In this kind of tests the pressure of the measurement P_m and the average pressure of the interval P_{av} are the same.

The accuracy of this analysis depends on the assumption that the gas behaved as an ideal gas and that a pseudo-steady state flow was established, *i.e.* that the quantity of gas exiting the high pressure vessel was approximately equal to that entering the low pressure vessel. The permeability coefficient thus measured represents the sum of the permeability coefficient of the material and any additional contribution (cracks or incomplete sealing between sample and body cell). So the measured value could be higher than the permeability coefficient of the

material and, therefore, the best value of the permeability coefficient of the material would be the lowest value obtained in a series of tests.

At the end of the tests, the bentonite specimens were measured and weighed and the water content and dry density at three different levels along the cylindrical specimens was determined. To determine the dry mass the samples were oven-dried at 110°C for 48 h, and to compute the dry density, the volume of the same specimens was determined by immersing them in mercury prior to drying.

3.3 TESTS IN INTERFACES

These tests were carried out to check the gas transport performance of the interfaces between bentonite blocks and between bentonite and granite once the materials were saturated. Consequently, the first step was the preparation of the interfaces and their saturation.

3.3.1 Bentonite/bentonite interfaces

The samples for tests on bentonite interfaces were prepared by uniaxially compacting cylindrical specimens that were later longitudinally cut with a saw (Figure 8). The clay was compacted with its hygroscopic water content to dry densities between 1.6 and 1.8 g/cm³. After cutting the cylinders, the halves were put together inside stainless steel cells of 3.8 cm internal diameter and 5 cm height (Figure 6) with geotextile on top and bottom. The cutting process implied mass loss, and consequently a reduction in overall dry density (Figure 9). Saturation took place with deionised water through both ends under an injection pressure of 0.2 MPa during several days and then under an injection pressure of 0.6 MPa.

After saturation, the procedure followed for the gas breakthrough tests was the same described in section 3.2, and the experimental setup was that shown in Figure 7.



Figure 8: Appearance of sample BTJ17_38 prepared for bentonite interfaces testing



Figure 9: Appearance of sample BTJ16_38 prior to saturation inside the cell

3.3.2 Granite/bentonite interfaces

For the granite/bentonite interface two preliminary tests were performed in methacrylate cells (tests GB1 and GB2). A granite core of 5.2 cm in diameter and 6.6 cm in height was longitudinally cut in two halves, what resulted in rough granite surfaces. One of the halves was glued to a methacrylate cell with an epoxy adhesive (Figure 10, left). Additionally, three bentonite samples of 5.0 cm diameter and 2.2 cm height were obtained by uniaxial compaction of the clay. They were longitudinally cut in two halves using a Brazilian test apparatus. Those halves of the most appropriate size and consistency were stacked inside the methacrylate cell (Figure 10, right). Porous stones were placed on top and bottom and the cell was closed with stainless steel covers. Saturation proceeded from the bottom with deionised water, initially under a low pressure. Once saturated the cell GB1 was opened and weighed, to check the final bentonite water content, the porous filters were replaced by dry ones, and the cell was closed again. The sample was tested for gas breakthrough in the modified version of the setup described in section 3.1 (Figure 11).



Figure 10: Preparation of the preliminary test for granite/bentonite interface GB2



Figure 11: Methacrylate cell during the granite/bentonite interface gas breakthrough test GB1

4 Results

4.1 GAS PERMEABILITY

Gas permeability was measured in samples compacted at dry densities of between 1.4 and 1.8 g/cm³ with water contents between 18 and 22%, corresponding to initial degrees of saturation between 62 and 97%. The gas pressures applied during the tests were those shown in Figure 3, with a maximum injection pressure of 0.8 MPa and a maximum confining pressure of 1.0 MPa, which was well below the expected swelling pressure. It was checked that for a given sample and test step the gas outflow was equal to the gas inflow, and thus the gas permeability calculated as $k_{ig} \cdot k_{rg}$ was the same despite the flow (in or out) used to compute it. However, when gas permeability was calculated taking into account the fluid properties (*i.e.* the permeability in m/s), the gas permeability upstream was usually slightly higher than downstream, up to a maximum of one order of magnitude when the upstream and downstream pressures were very different. This was due to the variation of the fluid properties with pressure and gives an idea of the possible range of variation of gas permeability inside the sample due to the gas pressure gradient.

A summary of the characteristics of the tests performed is given in Table I, where the initial and final dry density (ρ_d), water content (w), degree of saturation (S_r) and accessible void ratio ($e(1-S_r)$) are shown, along with the average permeability value obtained with the gas outflow for all the steps in which backpressure was atmospheric. The differences between the initial and final conditions were due to progressive decompression of the samples (since they were compacted applying very high pressures). Final checking of water content at different levels showed that the differences in water content along the samples were smaller than 0.4%, with a trend to find lower water contents towards the end of the sample where gas injection was applied (on top).

Table I: Summary of the gas permeability tests performed

Reference	Initial ρ_d (g/cm ³)	Initial w (%)	Initial S_r (%)	Final ρ_d (g/cm ³)	Final w (%)	Final S_r (%)	$e(1-S_r)$	k_g (m/s)	$k_{ig} \cdot k_{rg}$ (m ²)
PGFBX1	1.51	13.1	45		14.1	48	0.43	$7.3 \cdot 10^{-9}$	$1.1 \cdot 10^{-13}$
PGFBX2	1.40	21.3	62		21.4	62	0.36	$8.8 \cdot 10^{-8}$	$8.6 \cdot 10^{-14}$
PGFBX3	1.68	18.2	81	1.68	16.7	74	0.11	$1.4 \cdot 10^{-9}$	$2.0 \cdot 10^{-15}$
PGFBX4	1.76	18.4	93	1.73	17.7	89	0.04	$1.2 \cdot 10^{-10}$	$1.7 \cdot 10^{-16}$
PGFBX5	1.80	17.7	96	1.73	19.4	93	0.02	$2.3 \cdot 10^{-12}$	$3.4 \cdot 10^{-18}$
PGFBX6	1.78	18.6	97	1.74	18.9	93	0.01	$4.7 \cdot 10^{-12}$	$7.0 \cdot 10^{-18}$
PGFBX7	1.76	17.8	90	1.72	18.1	86	0.05	$4.2 \cdot 10^{-11}$	$6.2 \cdot 10^{-17}$
PGFBX8	1.78	18.1	94	1.72	19.3	91	0.03	$2.2 \cdot 10^{-12}$	$3.4 \cdot 10^{-18}$
PGFBX9	1.76	19.0	96	1.71	19.9	92	0.02	$5.5 \cdot 10^{-12}$	$8.3 \cdot 10^{-18}$
PGFBX10	1.62	22.7	92	1.55	22.1	80	0.06	$3.4 \cdot 10^{-9}$	$4.7 \cdot 10^{-15}$
PGFBX11	1.65	18.4	78	1.62	17.9	73	0.14	$1.5 \cdot 10^{-9}$	$2.3 \cdot 10^{-15}$
PGFBX12	1.70	18.3	85	1.68	18.4	81	0.09	$1.9 \cdot 10^{-10}$	$2.8 \cdot 10^{-16}$
PGFBX13	1.76	17.6	89	1.73	17.7	85	0.06	$2.3 \cdot 10^{-11}$	$3.6 \cdot 10^{-17}$
PGFBX14	1.78	18.5	97	1.72	19.7	93	0.02	$8.4 \cdot 10^{-12}$	$1.3 \cdot 10^{-17}$
PGFBX16	1.78	18.7	97	1.61	21.4	85	0.01	$1.1 \cdot 10^{-13}$	$1.9 \cdot 10^{-19}$

These values are plotted in Figure 12 grouped by the initial water content. The decrease of gas permeability with dry density was substantial, several orders of magnitude for an increase of dry density from 1.5 to 1.8 g/cm³. The effect of water content was not very noticeable due to the fact that the range tested was not broad, however, higher water content samples tended to have lower permeabilities. In fact, the samples could be separated in two widespan groups: those with water contents around 18% and those with water contents around 20%, which is the separation considered in the rest of the report.

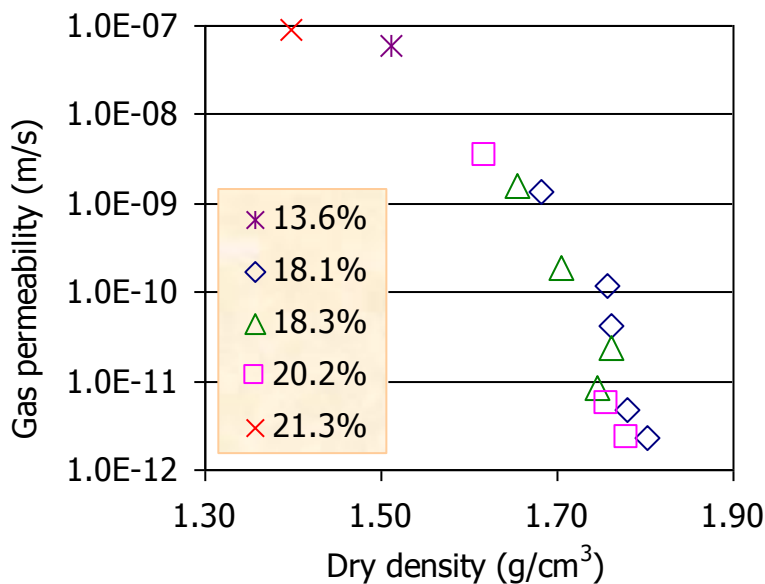


Figure 12: Average gas permeability (shown in Table I) for different water contents as a function of bentonite dry density

The permeability values obtained during Stage 1 (Figure 3) are plotted in Figure 13. The effect of dry density, and particularly degree of saturation, on gas permeability was very clear, both for the samples with water content 18% and 20%. The same comment could be made for the values obtained during Stage 3 (Figure 14), in which the confining pressure was 1.0 MPa instead of 0.6 MPa. For the samples with water content 20%, the increase in the degree of saturation from 80 to 90% gave place to a decrease in permeability of three orders of magnitude. In the range of pressures tested, no clear effect of the injection pressure on the permeability value obtained was observed.

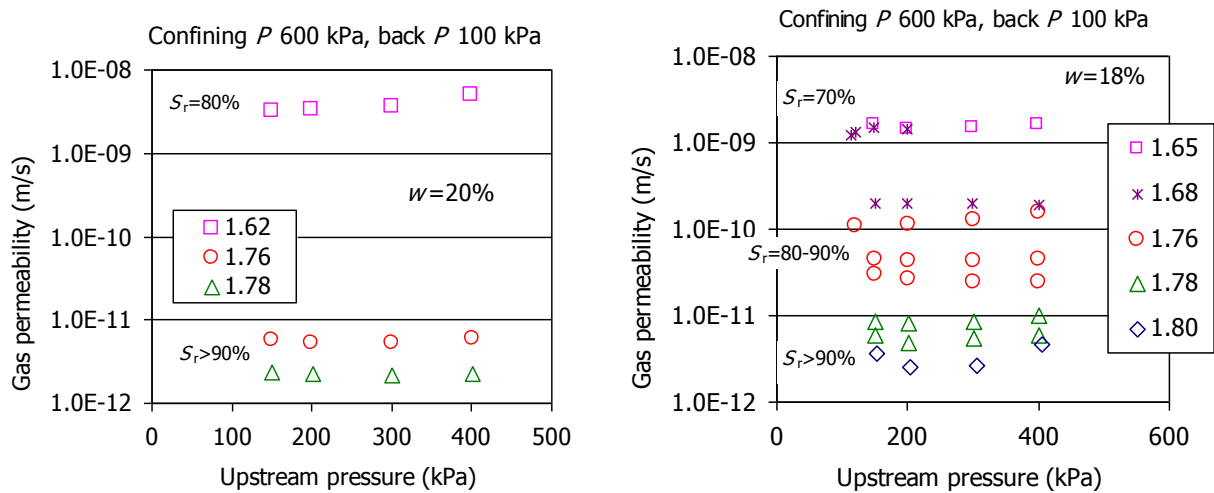


Figure 13: Gas permeability measured during Stage 1 for samples of average water content 20% (left) and 18% (right). The dry density of the samples is indicated in the legends in g/cm³

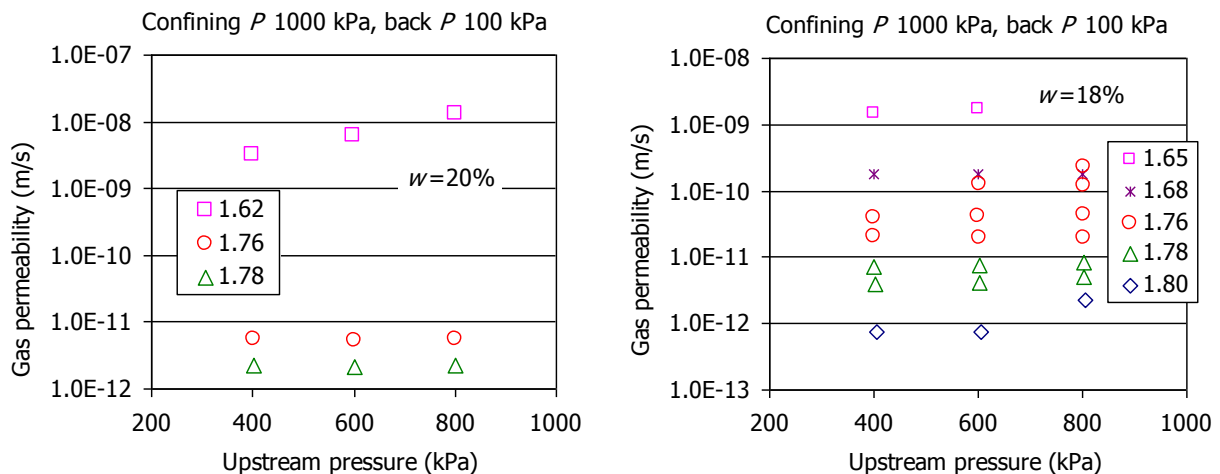


Figure 14: Gas permeability measured during Stage 3 for samples of average water content 20% (left) and 18% (right). The dry density of the samples is indicated in the legends in g/cm³

The effect of the confining pressure on permeability was checked during Stage 2, in which the confining pressure was increased from 600 to 1000 kPa, while the injection and backpressure were constant (Figure 15). In test FBX14 the confining pressure was increased up to 1200 kPa. For the range of pressures tested in this series of tests, the confining pressure did not affect the permeability value. Test FBX16 was performed in a cell that allowed the application of higher confining and injection pressures, since the degree of saturation was very high (97%) and the permeability expected very low. The pressure path followed in this test was shown in Figure 4. It was observed that each time the confining pressure was increased, the permeability value

decreased slightly (Figure 16). This decrease could be attributed to the increase in effective pressure resulting from the confining pressure increase while injection pressure was unchanged. In fact, for each confining pressure, as the injection pressure was increased, the permeability value increased also, due to the decrease in effective pressure. In any case, the changes observed are small.

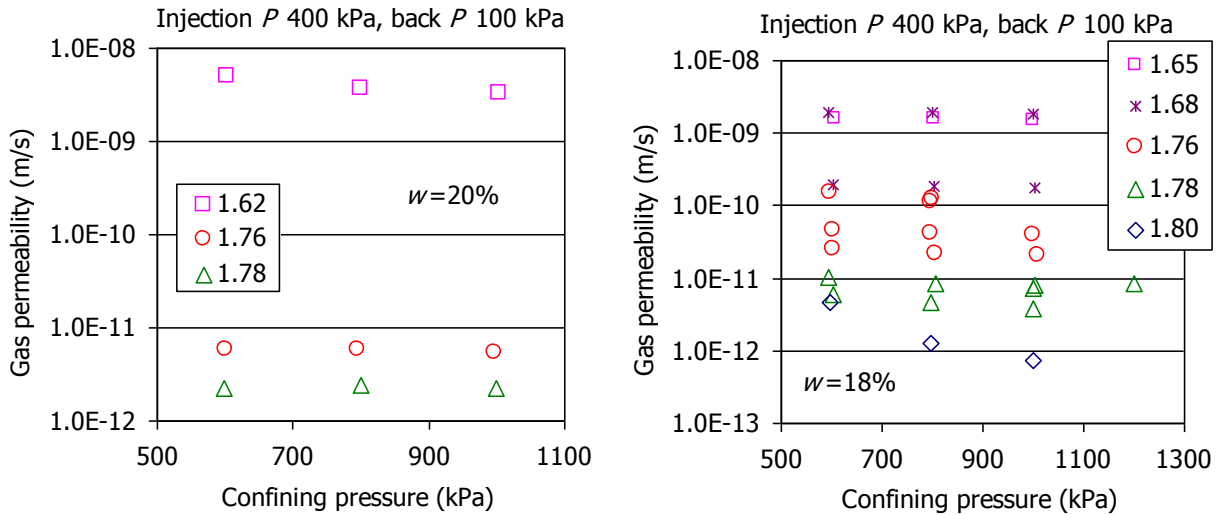


Figure 15: Effect of confining pressure on gas permeability measured during Stage 2 for samples of average water content 20% (left) and 18% (right). The dry density of the samples is indicated in the legends in g/cm^3

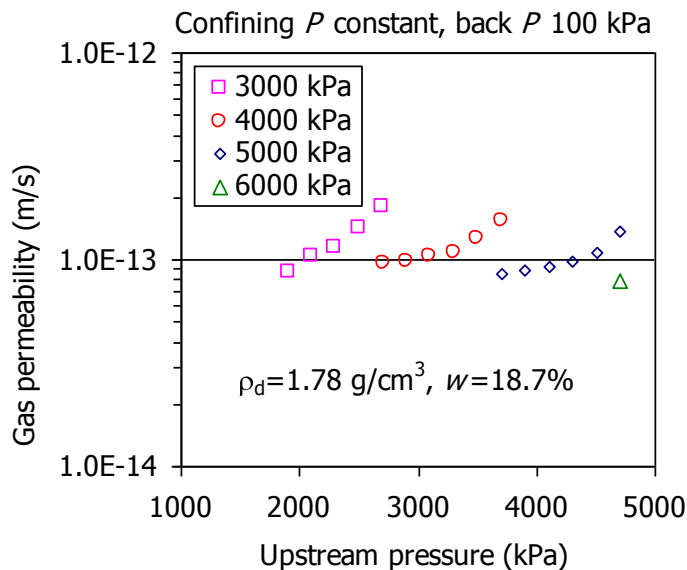


Figure 16: Gas permeability measured in test FBX16 (initial $S_r = 97%$) for different confining pressures (indicated in the legend)

Since the degree of saturation of tests FBX14 and FBX16 were the same, the permeability values, which were obtained under very different pressure conditions (lower for test FBX14 than for test FBX16), can be compared (Figure 17). Gas permeability tended to decrease with the increase in effective pressure, without major changes as confining pressure was varied.

However, the change from the low to the high range of confining (and consequently effective) pressure, did imply an almost 2-order of magnitude decrease in gas permeability.

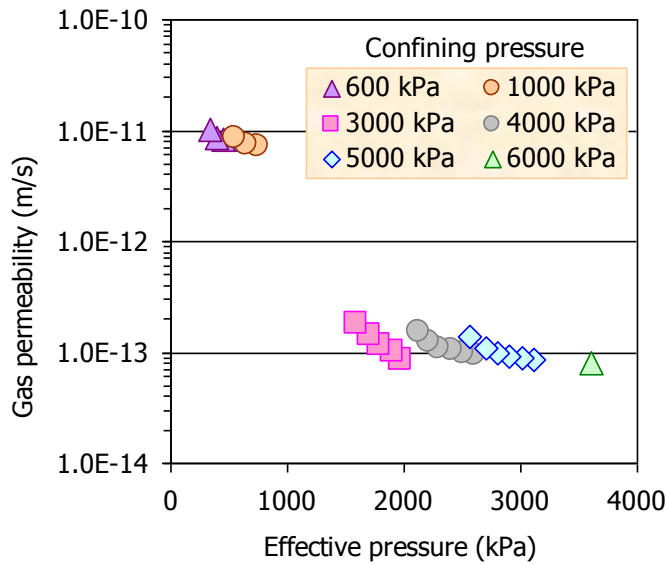


Figure 17: Comparison of gas permeability obtained in tests FBX14 and FBX16 (initial $S_r=97\%$) for different effective pressures. Backpressure was atmospheric

The effect of backpressure on permeability was tested during Stage 4 and 5 of the tests (Figure 3). The gas permeability values obtained during these stages are shown in Figure 18. The increase in backpressure implied a decrease in effective pressure and consequently an increase in gas permeability. As explained above, this effect is not observed when the gas permeability is expressed as $k_{ig} \cdot k_{rg}$, *i.e.* without taking into account the fluid properties.

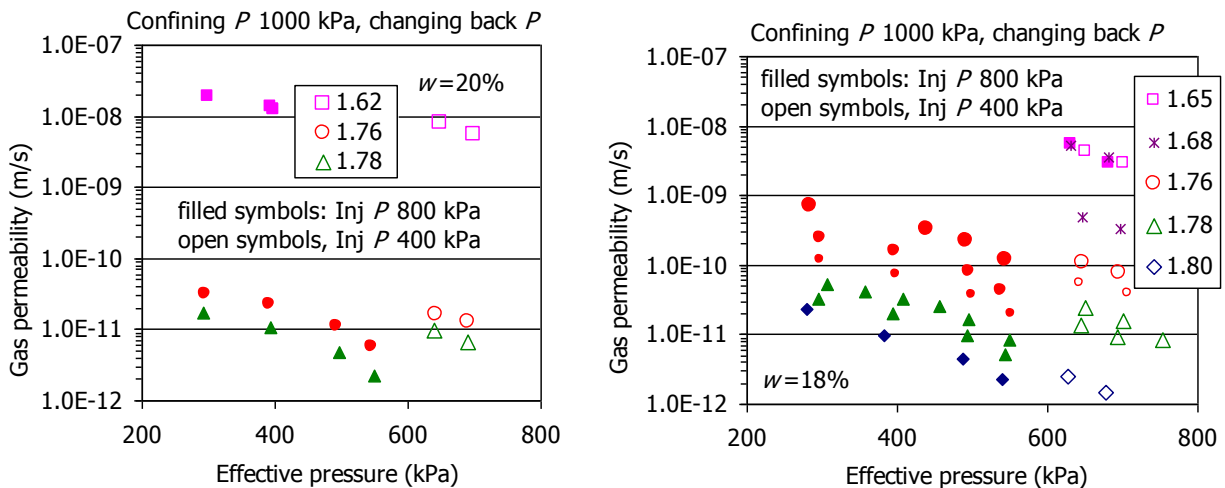


Figure 18: Effect of effective pressure on gas permeability measured during Stages 4 and 5 for samples of average water content 20% (left) and 18% (right). The dry density of the samples is indicated in the legend in g/cm^3

4.2 BREAKTHROUGH TESTS

The breakthrough tests were performed in samples previously saturated in stainless steel cells to which progressive higher gas pressures were applied at one end while the other end was under vacuum (except for test HP18_38). Once the breakthrough was achieved, gas flow

through the sample was allowed until no pressure change was recorded in the deposits. The pressure change over time was used to compute the gas permeability, as explained in section 3.2. There was no further water supply once the gas pressures started to be applied.

The characteristics of the samples prepared for the breakthrough tests are shown in Table II and the results of each finished test are detailed below. In most cases a dry density decrease was observed after saturation, due to the slight expansion allowed by the cell and the geotextile used as saturation interface. Hence, the breakthrough pressures and permeabilities reported below correspond to the dry densities after saturation.

Table II: Characteristics of the samples saturated for the breakthrough pressure tests

Reference	Initial ρ_d (g/cm ³)	Initial w (%)	Diameter (cm)	Initial height (cm)	Saturation time (days)	Saturation P (kPa)	w after saturation (%)	ρ_d after saturation (g/cm ³)
HP18_38	1.72	20	3.8	7.8	225	600	28.2	
BT13_50 (2)	1.34	12.8	5.0	5.0	163	200-600	37.5	1.28
BT14_38	1.42	14.6	3.8	5.0	82	600	31.0	
BT14_50	1.49	14.7	5.0	5.0	79	600	35.2	1.36
BT15_38	1.51	13.6	3.8	5.0	174	600-1000	27.9	
BT15_50	1.51	13.7	5.0	5.0	154	600-1000	30.5	1.39
BT16_38	1.60	13.7	3.8	2.0	180	200-600	35.6	1.42
BT17_38	1.69	14.3	3.8	2.0	222	1000	31.6	1.54

4.2.1 Test HP1.8_38

A sample of 7.8 cm in height and 3.8 cm in diameter was saturated with deionised water inside a stainless steel jacket by applying injection pressures on top and bottom of 600 kPa for 225 days. The initial dry density and water content of the sample were 20% and 1.72 g/cm³, respectively. The water content at the end of the saturation phase was 28.2%, and the density probably decreased, due to the vertical deformation allowed which was not measured.

For the gas breakthrough test the jacket with the sample inside was placed in a frame to avoid vertical deformation of the bentonite (Figure 5). The gas injection pressure on top was increased from 2.2 to 10 MPa in 0.2-MPa steps while backpressure at the bottom was atmospheric. Each step was held for between 24 and 72 h. No outflow was recorded in any of the steps. An injection pressure of 10 MPa was kept for 40 days without any outflow being recorded. The sample was then inverted, so that to apply the gas pressure through the opposite end. Again a gas pressure of 10 MPa was applied and kept for 98 days without no measurable flow on the opposite end. The injection pressure was then increased from 10.0 to 15.5 MPa in 0.5-MPa steps applied every 24 h. At this pressure value breakthrough was achieved and the outflow suddenly increased as the injection pressure decreased. The whole pressure and flow evolution during the test is shown in Figure 19, and the detail of the breakthrough episode in Figure 20.

After breakthrough permeability could be computed either from the outflow, using Equation 4, or from the pressure decrease in the upstream vessel (volume 300 cm³), using Equation 10, and

both calculations coincided quite well. The values obtained are plotted in Figure 21. The increase of permeability over time can be attributed to the progressive drying of the sample due to the gas flow. In fact, the final water content of the bentonite was 22.6% and the dry density 1.67 g/cm^3 .

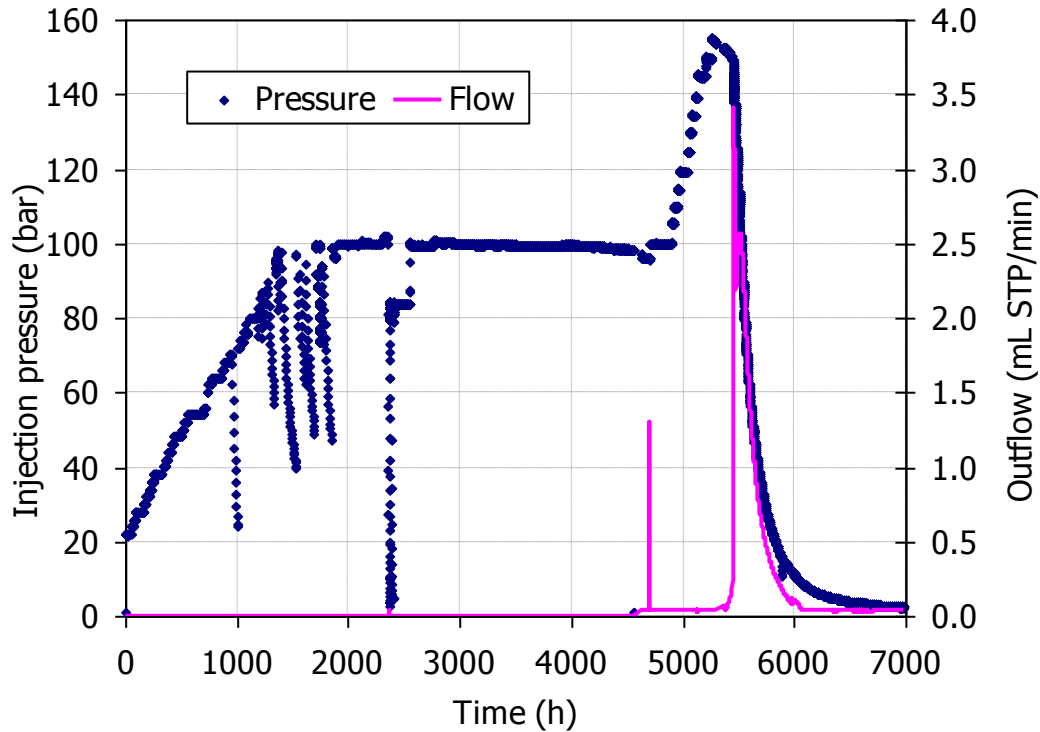


Figure 19: Injection pressure and outflow during test HP18_38

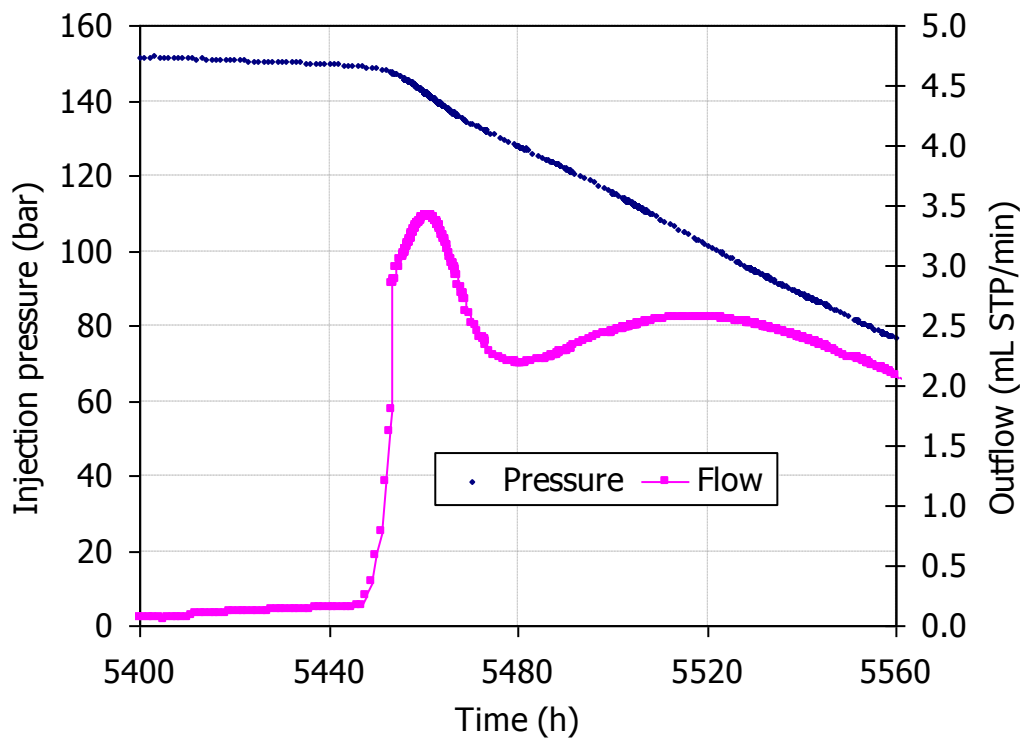


Figure 20: Injection pressure and outflow during the breakthrough episode in test HP18_38

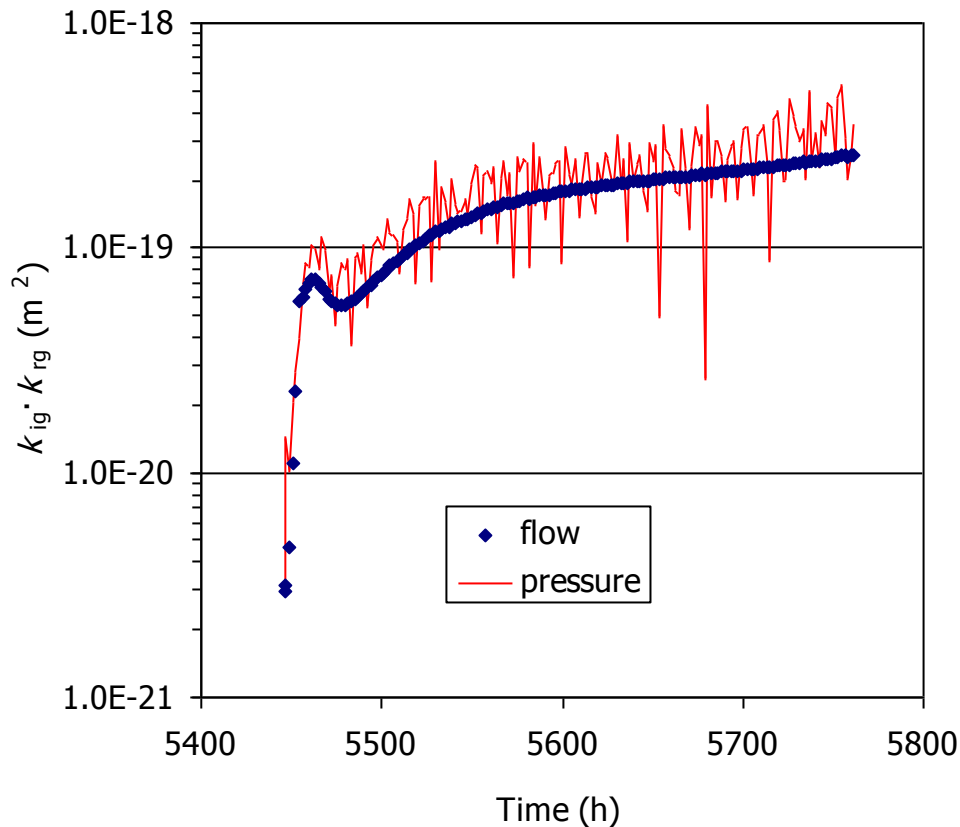


Figure 21: Evolution of gas permeability after breakthrough as computed from the gas outflow (Equation 4) and from the pressure decrease in the upstream deposit (Equation 10)

4.2.2 Tests in small samples

In addition to the test just presented, a series of stainless steel cells were used to perform gas breakthrough tests in 5- and 2-cm high specimens of saturated bentonite (Figure 6). The bentonite was compacted inside the cell with its hygroscopic water content to different nominal dry densities. The tests followed these phases:

1. Saturation of the bentonite with deionised water by applying injection pressures of 0.2-0.6-0.8 MPa initially on one side and then on both. This pressure was sometimes increased to values of up to 1.0 MPa. The water intake during the saturation phase was some times measured online and finally checked by weight difference. Once saturated the filters through which saturation occurred were removed and replaced by dry filters before moving the cells to the setup shown in Figure 7.
2. An initial pressure of 400 kPa was fixed in the upstream deposits, while a vacuum of 260 mbar-a was applied to the downstream deposits. The pressure in the upstream deposit was increased every 24 h by 200 kPa until breakthrough occurred. Then flow through the sample was allowed until the pressures in both deposits stopped changing. Gas permeability could be computed from these pressure changes using Equation 10. Once flow stopped, the pressure in the downstream deposit was decreased first every 24 h by 200 kPa, in order to increase the hydraulic head, and if flow was not achieved before the downstream deposit pressure came to 0, the pressure in the upstream deposit was increased following the previous procedure. Once a new breakthrough occurred, the pressures in the two deposits

were let stabilise again. In some cases this procedure was repeated a third time in order to obtain a new breakthrough.

3. After flow stopped, the tubes were checked in search of water and the cells were removed from the setup, weighed and measured and set for resaturation. After this phase the samples were weighed and measured and the filters replaced by dry ones.
4. The cells were moved to the gas breakthrough setup and the procedure described in bullet 2 repeated.

Finally the cells were dismantled, the samples extracted, weighed, measured, and the dry density and water content were determined in three or two levels along them (depending on their height).

Equation 10 was used for the computation of permeability over short periods of time (10 min) corresponding to successive pressure changes (ΔP). Due to the changes of temperature in the laboratory and to the uncertainties inherent to the sensors and data acquisition system, oscillations in pressure were recorded (even if there was a constant increase or decrease trend) and this gave place to a quite large dispersion in the permeability values computed, especially as the change of pressure in the deposits became smaller. To avoid this artefact it was considered advisable to fit the pressure values to an equation and compute permeability from the values resulting from the fitted equations. An approximating function is also the finest form of data smoothing in the time domain. It can also be differentiated or integrated, both numerically and analytically, resulting in far more accurate aspects of data analysis. Since a parametric model is also a continuous function, smooth data can be reconstructed at exactly the x values and density desired (SYSTAT 2002).

The equations used to fit the pressure evolution were a First and Second Order Independent Decay, Intercept Form, for the decrease of pressure (Equation 11) and a First and Second Order Independent Formation, Intercept Form, for the increase of pressure (Equation 12):

$$y = a + b \exp -cx + \frac{d}{1+dex} \quad [11]$$

$$y = a + b \left(1 - \exp -cx \right) + d \left(1 - \frac{1}{1+dex} \right) \quad [12]$$

where x is time in h and y is pressure in bar.

An example of the improvement achieved with this procedure is shown in Figure 22. The permeability values computed from the pressure values measured show a large dispersion, whereas those computed from the pressure values fitted with Equation 11 show a steady, clear trend. The goodness of the pressure fitting is also highlighted.

The details of the tests finished so far are given below. The breakthrough pressure values correspond to the difference in pressure between the upstream and downstream deposits at the moment of breakthrough, i.e. the hydraulic head. In the Tables, the gas permeability values given correspond to the average of the values computed from the pressure increase and decrease once they were stable, which usually coincided, although in most cases a range of permeability is given, since it did not stabilised. The changes in water content and dry density caused by the different phases of the tests (saturation, gas testing, resaturation, gas testing) are also reflected in the Tables.

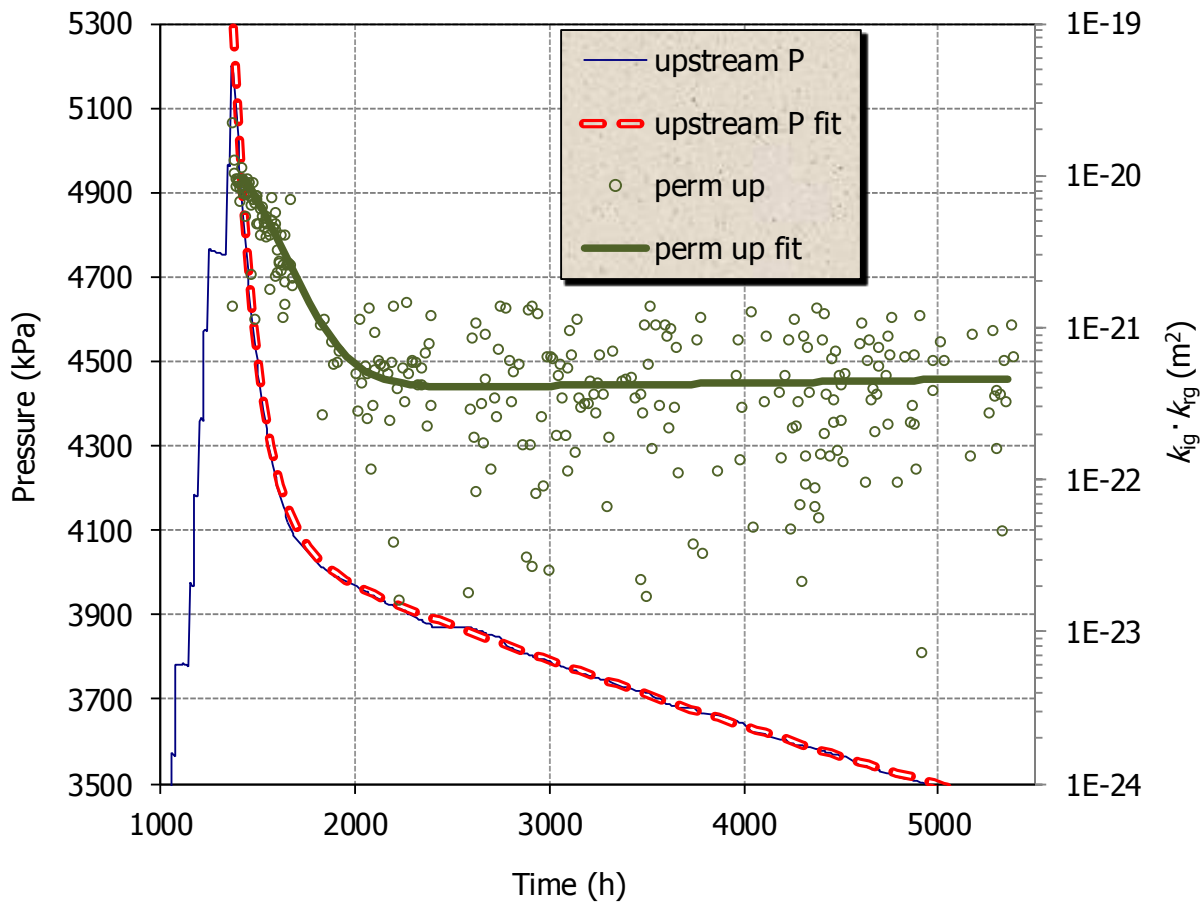


Figure 22: Pressure decrease in upstream deposit measured and fitted during Phase 2 of test BT1.4_38 and permeability values computed with Equation 10 from the pressure values measured and from those fitted

Test BT1.3_50(2)

The characteristics and results of test BT1.3_50(2) are shown in Table III, and the evolution of pressures in the upstream and downstream deposits during the first breakthrough test in Figure 23. The breakthrough was reached at a very low pressure, 1.4 MPa. Gas flow continued after breakthrough, with permeability decreasing. The second breakthrough took place at an even lower pressure, flow decreasing slowly afterwards. Figure 24 shows the two breakthrough episodes in detail.

Table III: Results of test BT1.3_50(2)

Phase	Duration (days)	w (%)	ρ_d (g/cm ³)	S_r (%)	Saturation/BT P (MPa)	$k_{ig} \cdot k_{rg}$ (m ²)
1. Saturation	172	37.4	1.28	91	0.2-0.4-0.6	
2. Gas breakthrough	62	36.7	1.36	100	1.4	$3.3 \cdot 10^{-18}$ - $4.2 \cdot 10^{-20}$
		37.3		101	1.0	$9.3 \cdot 10^{-19}$ - $3.4 \cdot 10^{-19}$
3. Resaturation	154	37.3	1.35	102	0.2	
4. 2 nd gas breakthrough	72	37.4	1.36	91	1.6	$1.8 \cdot 10^{-19}$ - $1.6 \cdot 10^{-21}$
					0.8	$2.1 \cdot 10^{-21}$ - $1.5 \cdot 10^{-21}$

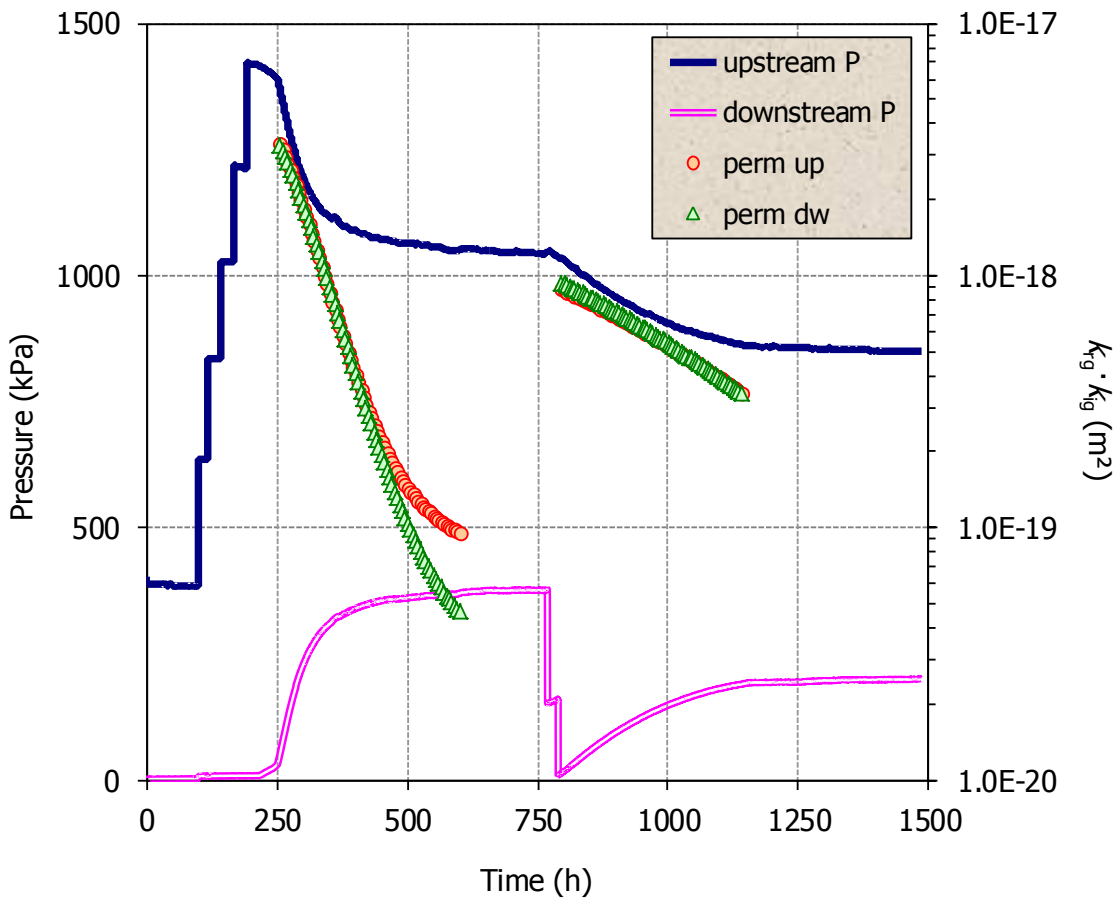


Figure 23: Evolution of pressure in the upstream and downstream deposits during Phase 2 of test BT1.3_50(2) and permeabilities computed from it

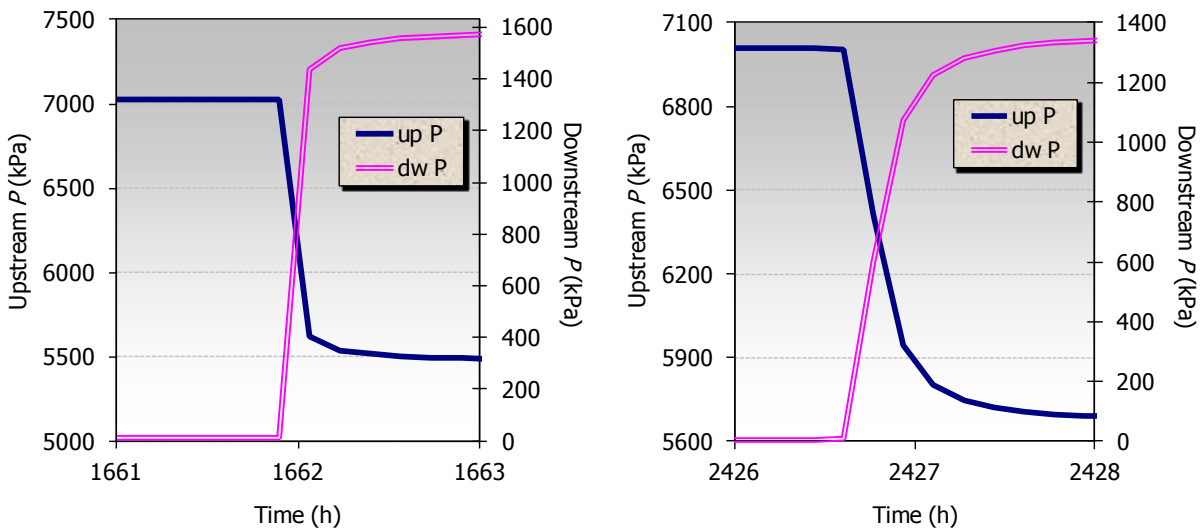


Figure 24: Evolution of pressure in the upstream and downstream deposits during the two breakthrough episodes in Phase 2 of test BT1.3_50(2)

After resaturation another BT test was performed. The results obtained are shown in Figure 25, which provides another example of two consecutive breakthrough episodes being the first pressure higher than the second one. The first took place at 1.6 MPa and the pressure in the deposits changed quickly, giving place to a sharp decrease of the permeability computed from this assumed flow. Figure 26 shows an enlargement of the two breakthrough episodes.

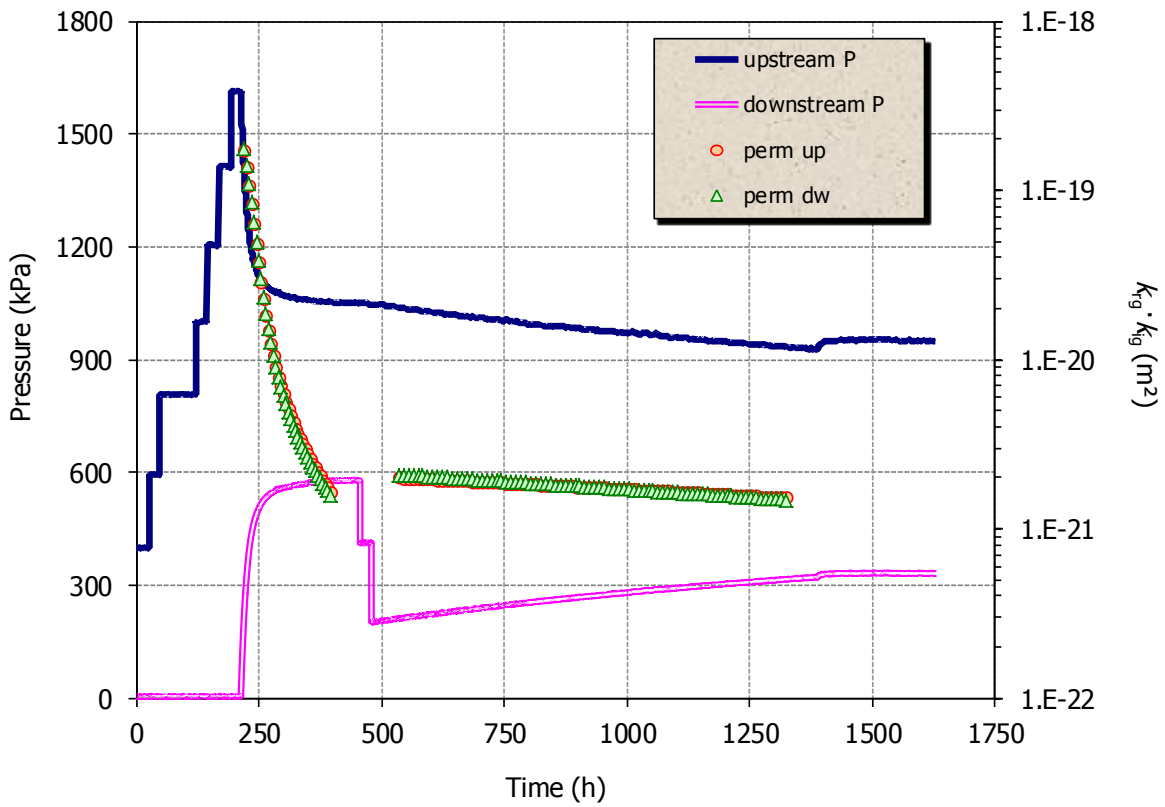


Figure 25: Evolution of pressure in the upstream and downstream deposits during Phase 4 of test BT1.3_50(2) and permeabilities computed from it

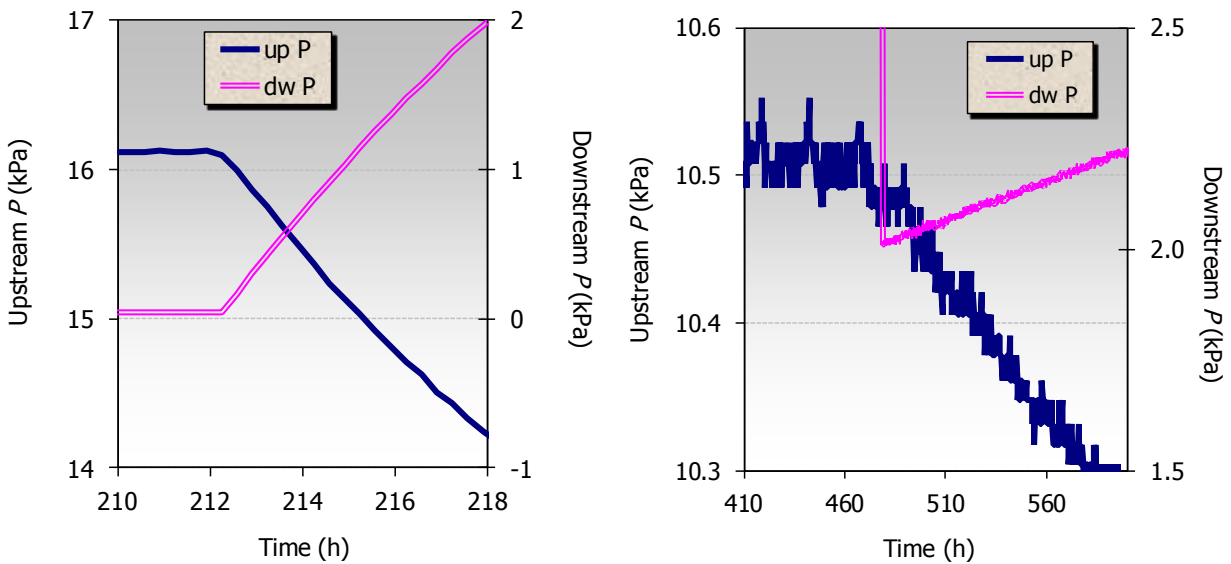


Figure 26: Evolution of pressure in the upstream and downstream deposits during the two breakthrough episodes in Phase 4 of test BT1.3_50(2). Note the detail of the upstream pressure scale in the right figure

Test BT1.4_38

The characteristics of test BT1.4_38 are shown in Table IV and the evolution of pressure in the upstream and downstream deposits during the first breakthrough is shown in Figure 27. When

the injection pressure was increased to 5.2 MPa, the pressure in the upstream deposit started to decrease while that in the downstream deposit remained constant for about an hour more and then increased, which could be the interval between the air entry and the breakthrough (Figure 28). The evolution of gas permeability after breakthrough as computed with Equation 10 from the fitting to the upstream and downstream pressure changes is also shown in Figure 27. At first, the permeability dropped by more than one order of magnitude and then kept constant. After resaturation the gas test was performed again and the results obtained are shown in Figure 29. The first breakthrough was very sudden, the permeability decreased almost instantly one order of magnitude and no stable permeability value could be computed from it. The second one was reached at a lower hydraulic head by decreasing the pressure in the downstream deposit, and flow was established for long time after it, although the permeability value did not stabilise. The two breakthrough episodes are shown in detail in Figure 30.

Table IV: Results of test BT1.4_38

Phase	Duration (days)	w (%)	ρ_d (g/cm ³)	S_r (%)	Saturation/BT P (MPa)	$k_{ig} \cdot k_{rg}$ (m ²)
1. Saturation	82	31.0	1.42	93	0.6	
2. Gas breakthrough	251	30.9	1.42	93	5.2	$4.3 \cdot 10^{-22}$
3. Resaturation	113	32.2	1.47	103	0.6	
4. 2 nd gas breakthrough	107	31.4	1.46	100	6.6	$1.1 \cdot 10^{-18} - 1.2 \cdot 10^{-19}$
					4.2	$3.1 \cdot 10^{-21} - 3.5 \cdot 10^{-22}$

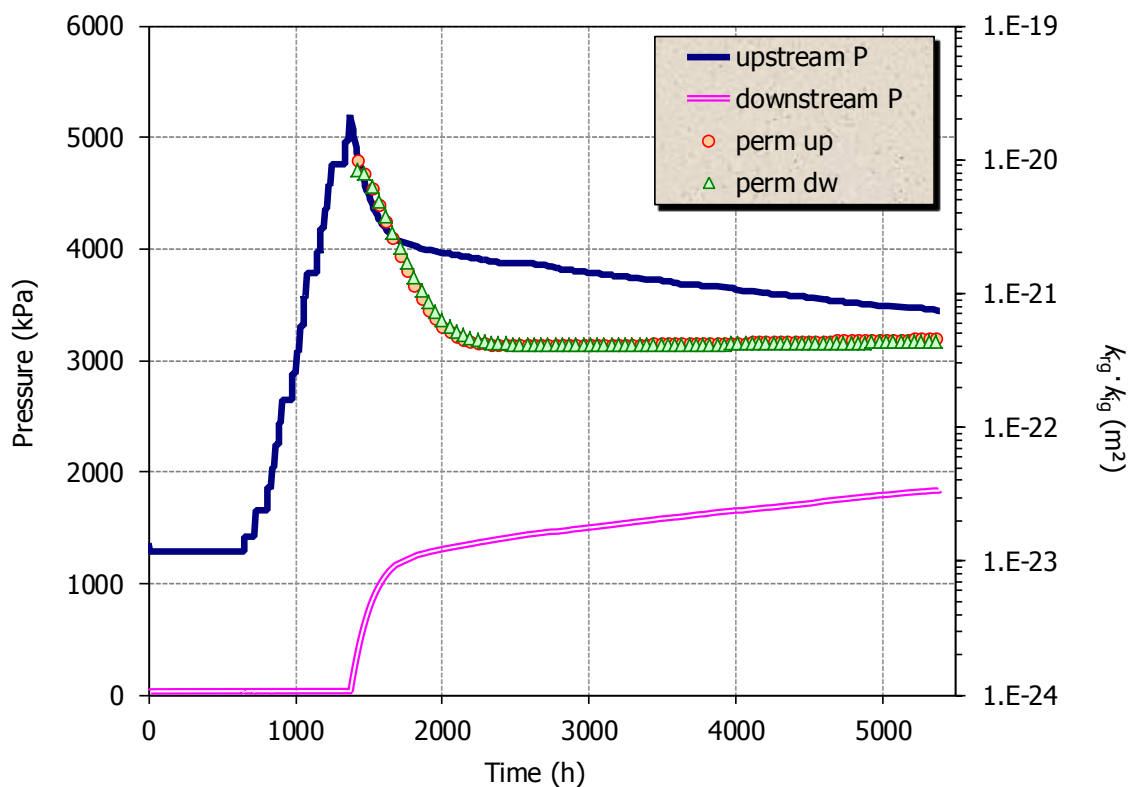


Figure 27: Evolution of pressure in the upstream and downstream deposits during Phase 2 of test BT1.4_38 and permeabilities computed from it

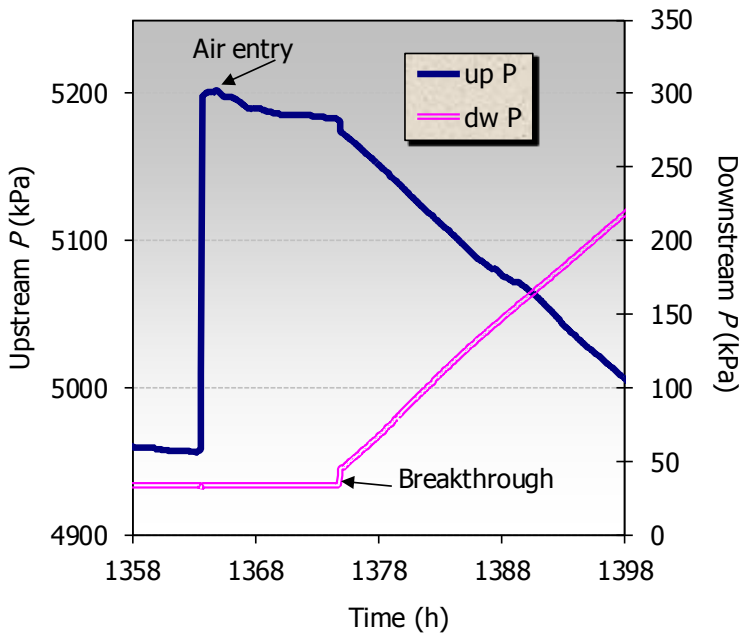


Figure 28: Evolution of pressure in the upstream and downstream deposits during the breakthrough episode in Phase 2 of test BT1.4_38

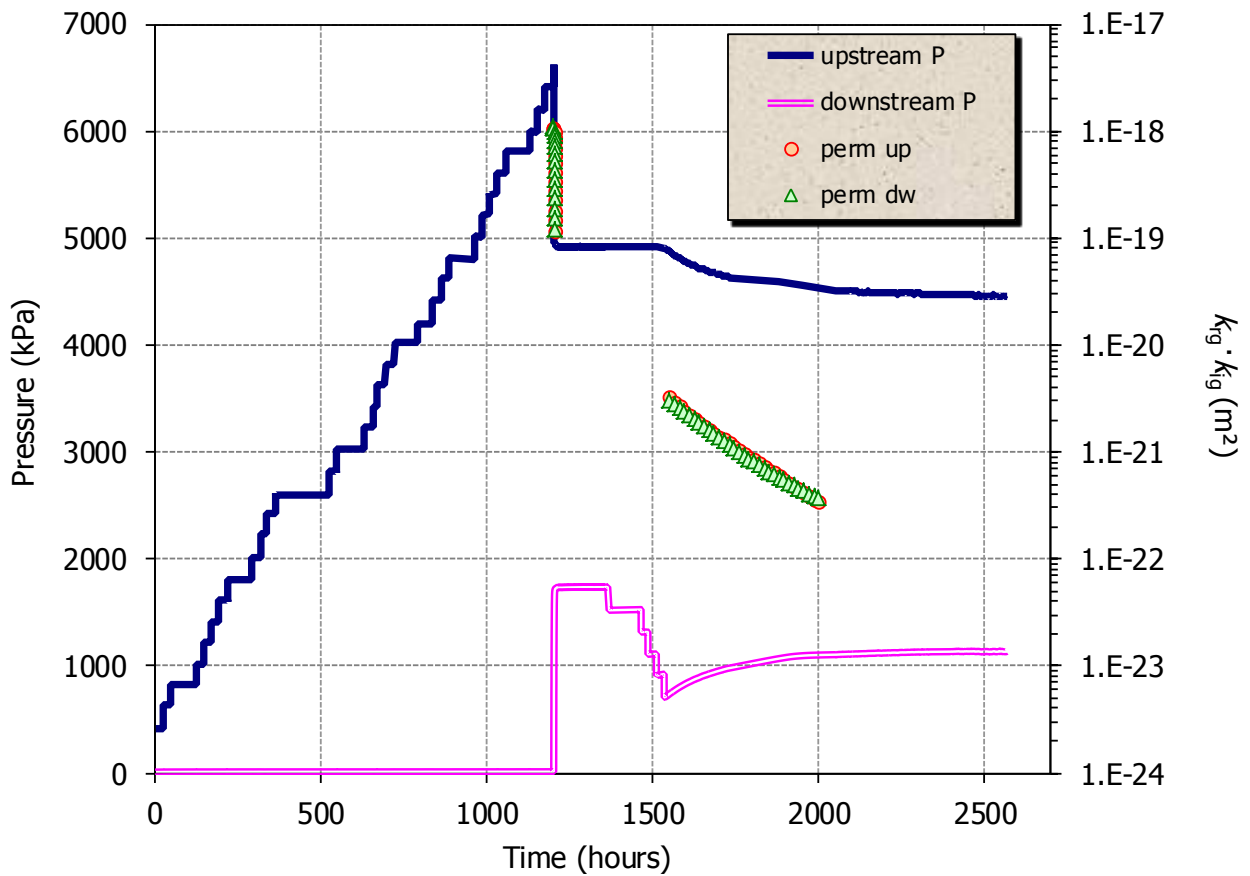


Figure 29: Evolution of pressure in the upstream and downstream deposits during Phase 4 of test BT1.4_38 and permeabilities computed from it

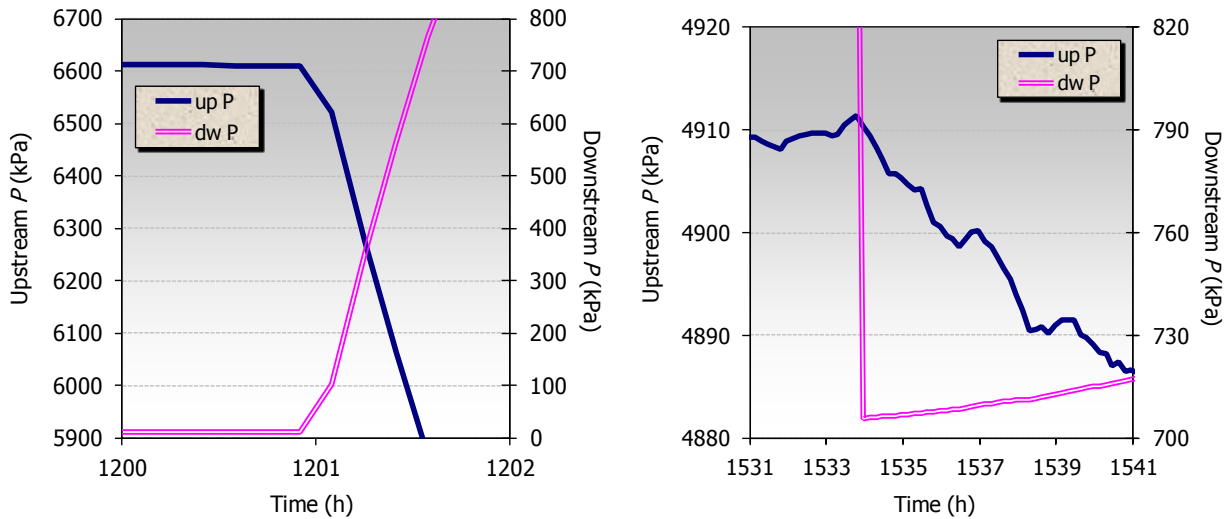


Figure 30: Evolution of pressure in the upstream and downstream deposits during the two breakthrough episodes in Phase 4 of test BT1.4_38

Test BT1.4_50

The characteristics and results of test BT1.4_50 are shown in Table V, and the evolution of pressures in the upstream and downstream deposits during the first breakthrough test in Figure 31. This sample recorded an inlet pressure decrease from the beginning of the test, *i.e.* for an injection pressure of 100 kPa. After 60 min (flight time) a linear downstream increase was recorded (Figure 32), what clearly indicated gas flow through the bentonite. If the pressures were plotted taking this moment as time 0, the pressure change in both deposits would be perfectly symmetrical.

Table V: Results of test BT1.4_50

Phase	Duration (days)	w (%)	ρ_d (g/cm ³)	S_r (%)	Saturation/BT P (MPa)	$k_{ig} \cdot k_{rg}$ (m ²)
1. Saturation	79	35.2	1.36	97	0.6	
2. Gas breakthrough	64	35.0	1.36	97	1	$2.0 \cdot 10^{-20}$
3. Resaturation	54	37.1	1.36	102	0.8-1.0	
4. 2 nd gas breakthrough	132	35.9	1.36	99	2.9	$6.7 \cdot 10^{-20} - 7.6 \cdot 10^{-22}$
					1.5	$1.9 \cdot 10^{-21} - 5.0 \cdot 10^{-22}$
					1.6	$3.6 \cdot 10^{-21} - 1.4 \cdot 10^{-21}$

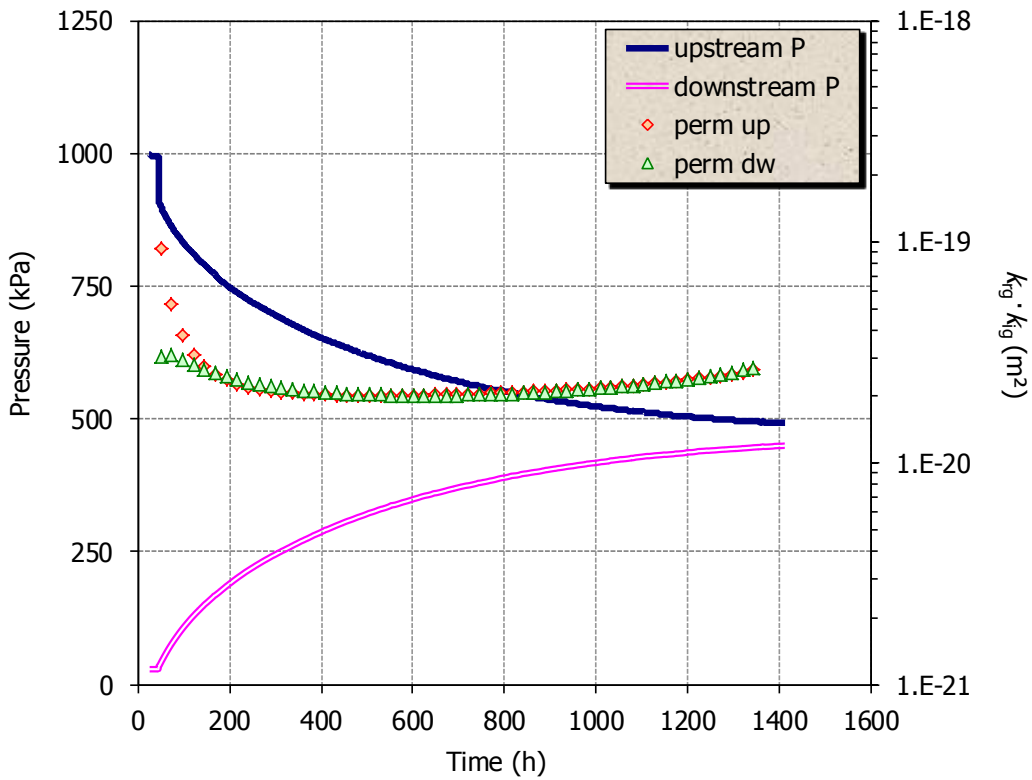


Figure 31: Evolution of pressure in the upstream and downstream deposits during Phase 2 of test BT1.4_50 and permeabilities computed from it

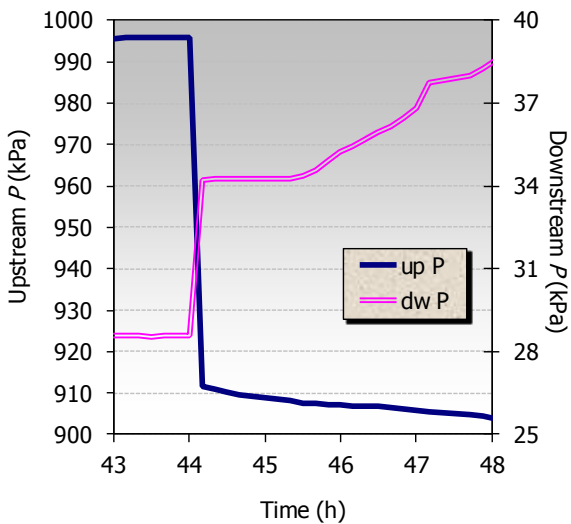


Figure 32: Evolution of pressure in the upstream and downstream deposits during the breakthrough episode in Phase 2 of test BT1.4_50

Figure 33 shows the evolution of pressures in the deposits during Phase 4 of the test, *i.e.* after resaturation, and the evolution of gas permeability as computed with Equation 11 from the fitted pressure changes in the deposits after breakthrough. The first breakthrough took place at a pressure higher than in Phase 2, and the permeability after it decreased two orders of magnitude in a few days. To reach new breakthroughs the hydraulic head was increased twice by decreasing the pressure in the downstream deposit. The enlargements of the three breakthrough episodes of Phase 4 of the test are shown in Figure 34.

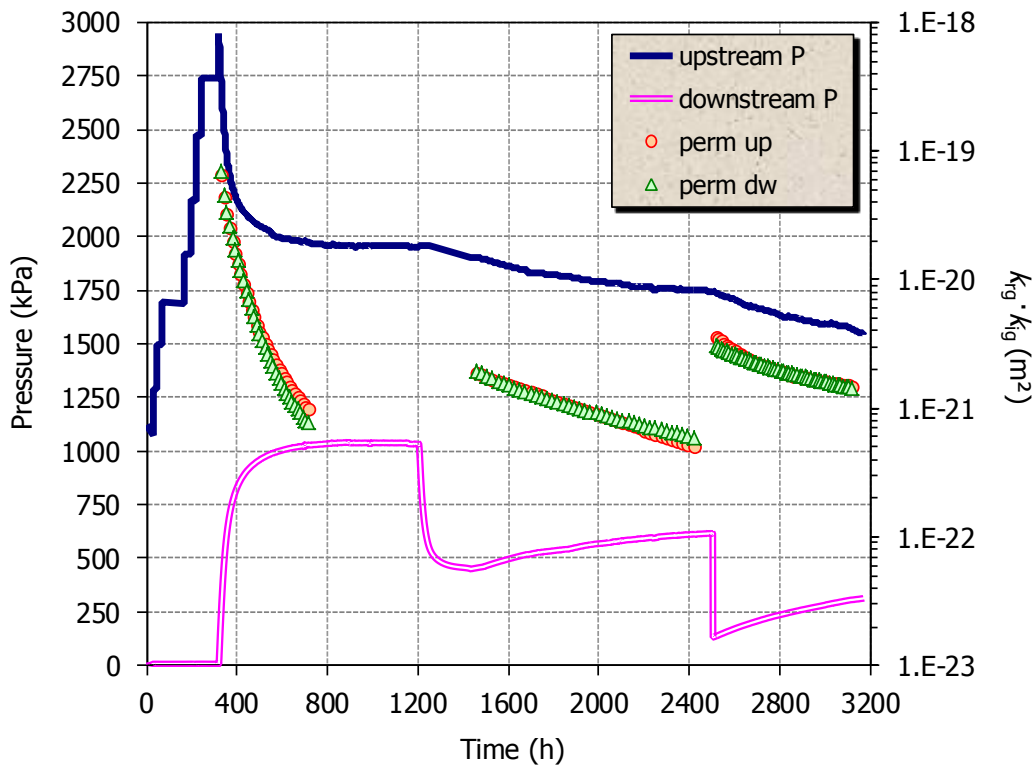


Figure 33: Evolution of pressure in the upstream and downstream deposits during Phase 4 of test BT1.4_50 and permeabilities computed from it

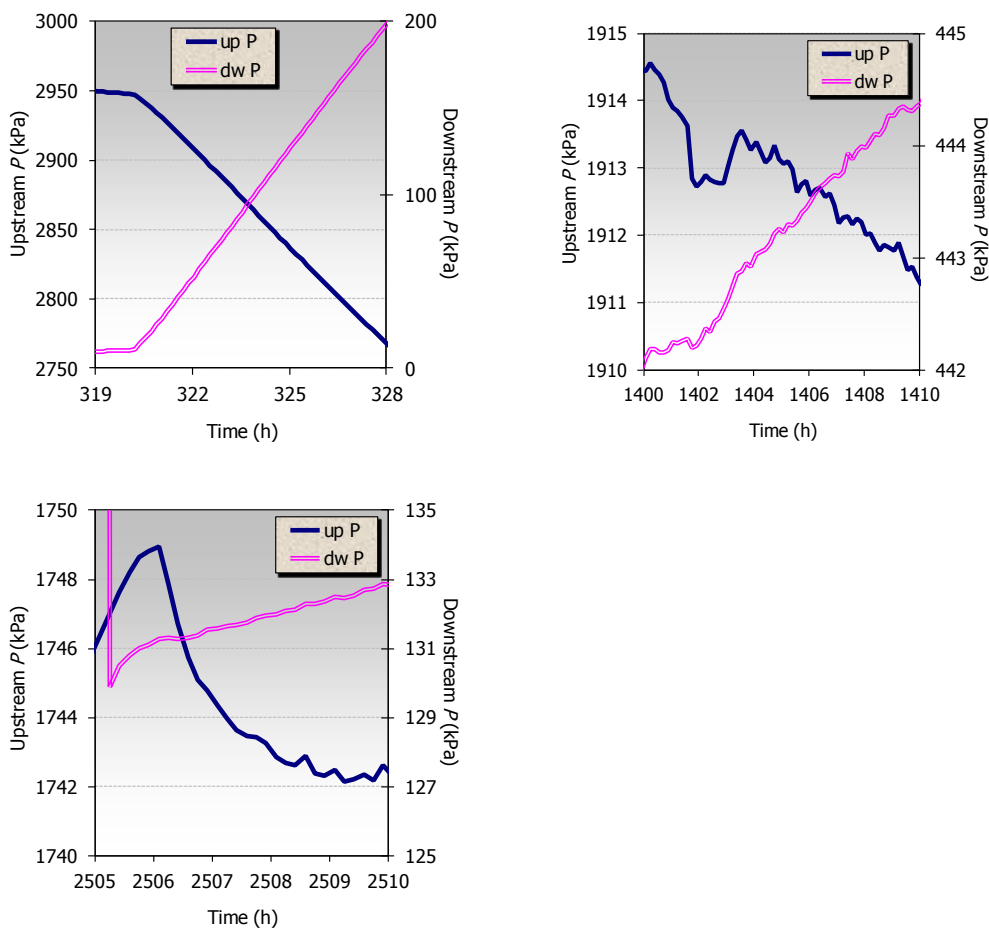


Figure 34: Evolution of pressure in the upstream and downstream deposits during the three breakthrough episodes in Phase 4 of test BT1.4_50

Test BT1.5_38

The characteristics and results of test BT1.5_38 are shown in Table VI. Figure 35 shows the evolution of pressures in both deposits during Phase 2 of the test and the evolution of gas permeability as computed with Equation 10 from the fitted pressure changes in the deposits after breakthrough. After the first breakthrough the pressures in both deposits stabilised in less than two hours and the permeability decreased sharply. Afterwards the pressure in the downstream deposit was stepwise reduced down to 140 kPa. Since no flow was detected, the pressure in the upstream deposit was progressively increased until flow was established again, what happened for the same hydraulic head as before. The flow gradually decreased and remained very low for a long time, indicating that the gas pathways remained partly open, although the permeability decreased continuously. In order to increase the hydraulic head and foster flow, the pressure in the downstream deposit was reduced until flow occurred again. Figure 36 shows an enlargement of the changes in pressure in both deposits during the three breakthrough episodes. The water content had only slightly decreased at the end of the test, probably because flow only occurred for very short periods of time.

Table VI: Results of test BT1.5_38

Phase	Duration (days)	w (%)	ρ_d (g/cm ³)	S_r (%)	Saturation/BT P (MPa)	$k_{ig} \cdot k_{rg}$ (m ²)
1. Saturation	174	27.9	1.51	95	0.6-1.0	
2. Gas breakthrough	200	27.5	1.51	94	9.1	$1.7 \cdot 10^{-18}$ - $3.8 \cdot 10^{-21}$
					9.3	$3.0 \cdot 10^{-20}$ - $2.6 \cdot 10^{-23}$
					8.2	$2.9 \cdot 10^{-21}$ - $1.3 \cdot 10^{-22}$
3. Resaturation	100	29.2	1.53	103	1.0	
4. 2 nd gas breakthrough	172	28.8	1.51	99	7.0	$4.6 \cdot 10^{-16}$ - $4.8 \cdot 10^{-19}$
					7.0	$1.7 \cdot 10^{-16}$ - $9.8 \cdot 10^{-20}$
					6.7	$3.0 \cdot 10^{-18}$ - $3.1 \cdot 10^{-21}$

Figure 37 shows the evolution of pressures in the deposits during Phase 4 of the test, *i.e.* after resaturation, and the evolution of gas permeability as computed with Equation 11 from the fitted pressure changes in the deposits after breakthrough. The first breakthrough took place at a pressure lower than in Phase 2, and the pressure in both deposits stabilised in one hour. After breakthrough the permeability decreased sharply. To reach a new breakthrough the hydraulic head was increased by decreasing the pressure in the downstream deposit and then by increasing it in the upstream deposit until flow occurred again. As in the previous case, this stopped very quickly (less than 2 h). The process was repeated and after the third breakthrough the stabilisation of pressure in both deposits was more gradual. The enlargement of the three breakthroughs episodes of Phase 4 of the test are shown in Figure 38. After the 3rd breakthrough the flow decreased slowly. Overall the breakthrough pressures were lower after resaturation and the permeability higher.

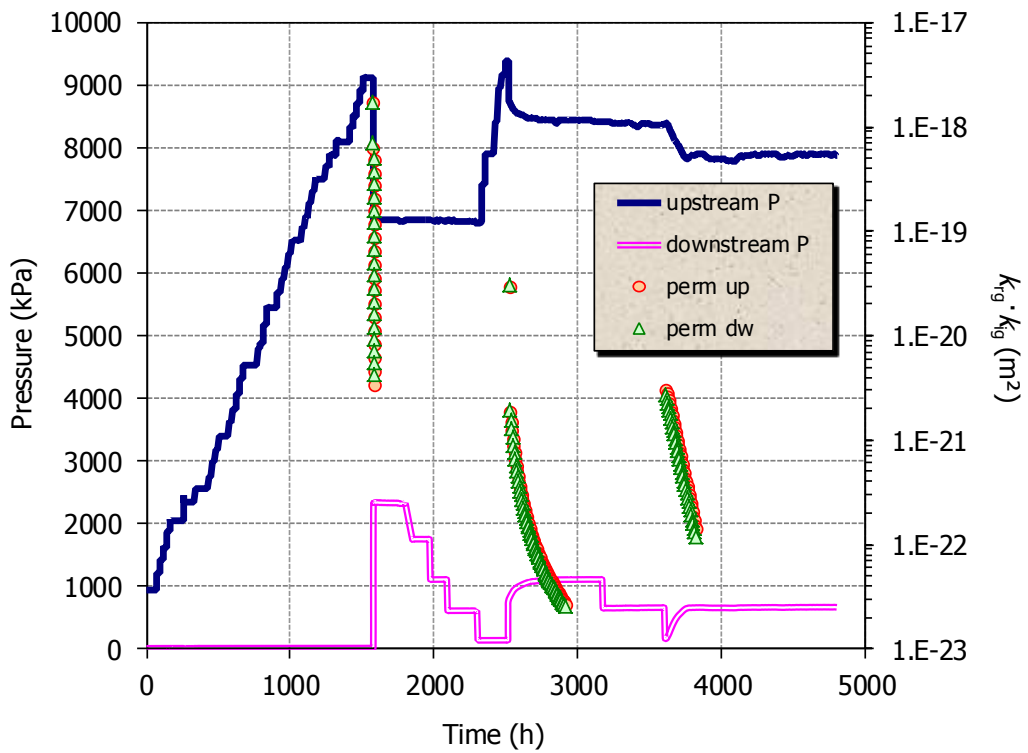


Figure 35: Evolution of pressure in the upstream and downstream deposits during Phase 2 of test BT1.5_38 and permeabilities computed from it

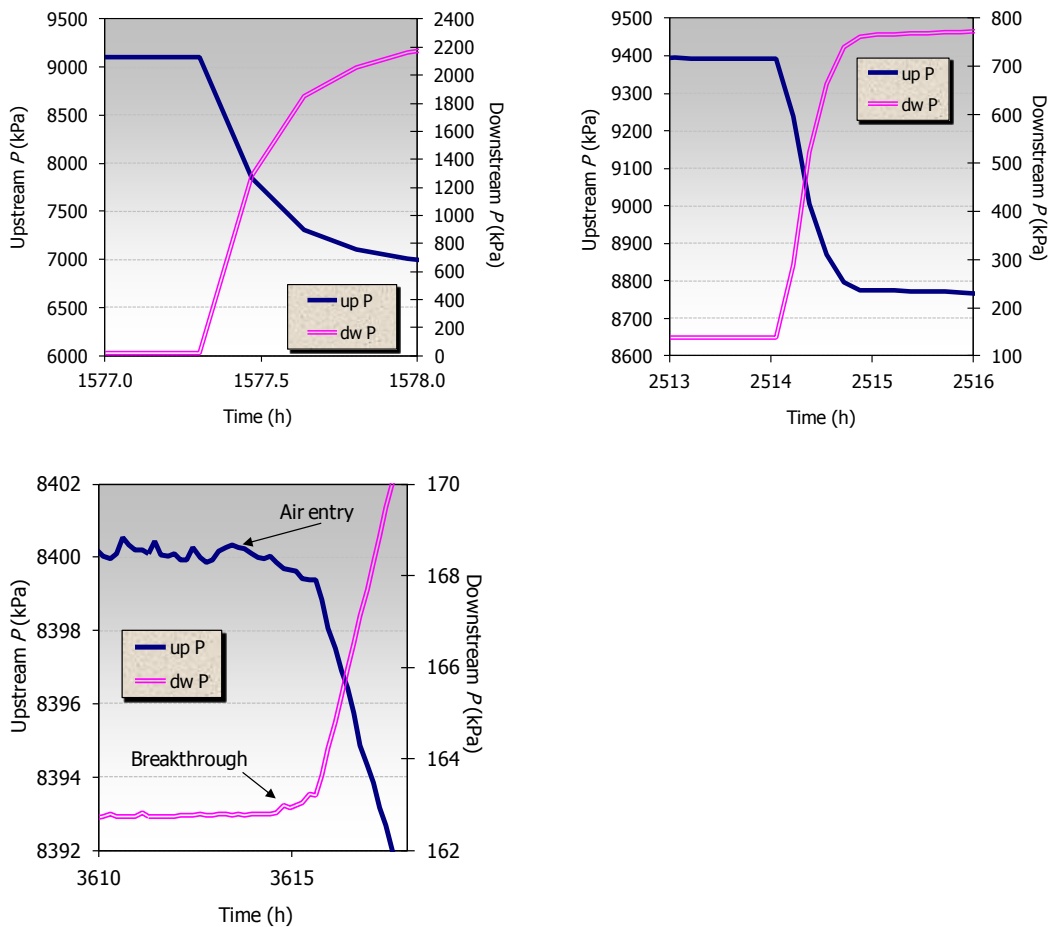


Figure 36: Evolution of pressure in the upstream and downstream deposits during the three breakthrough episodes in Phase 2 of test BT1.5_38

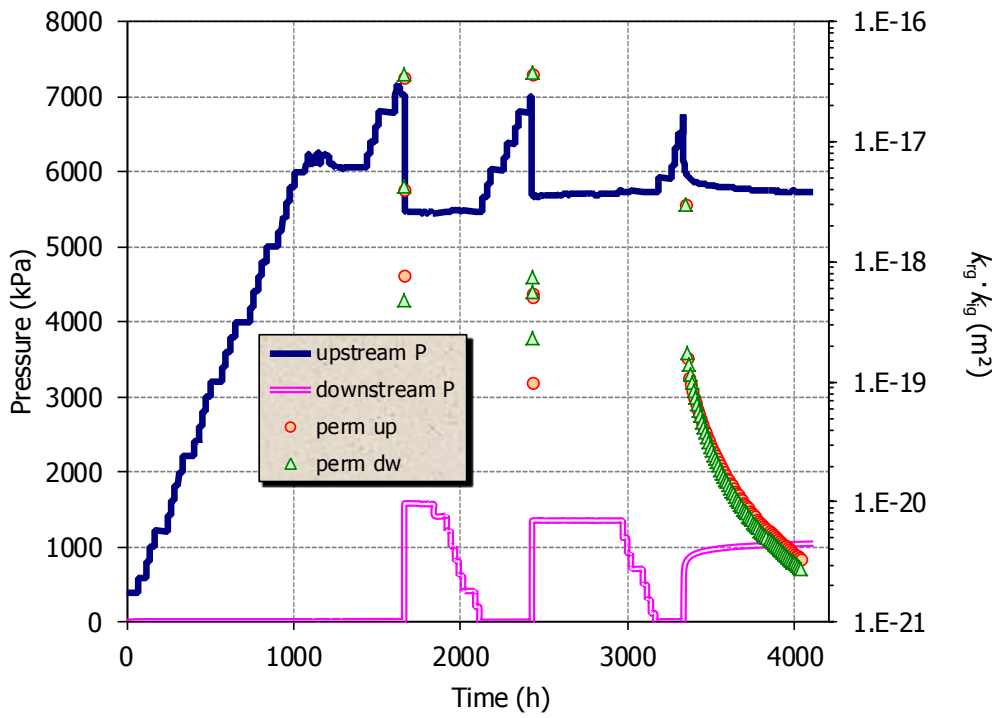


Figure 37: Evolution of pressure in the upstream and downstream deposits during Phase 4 of test BT1.5_38 and permeabilities computed from it

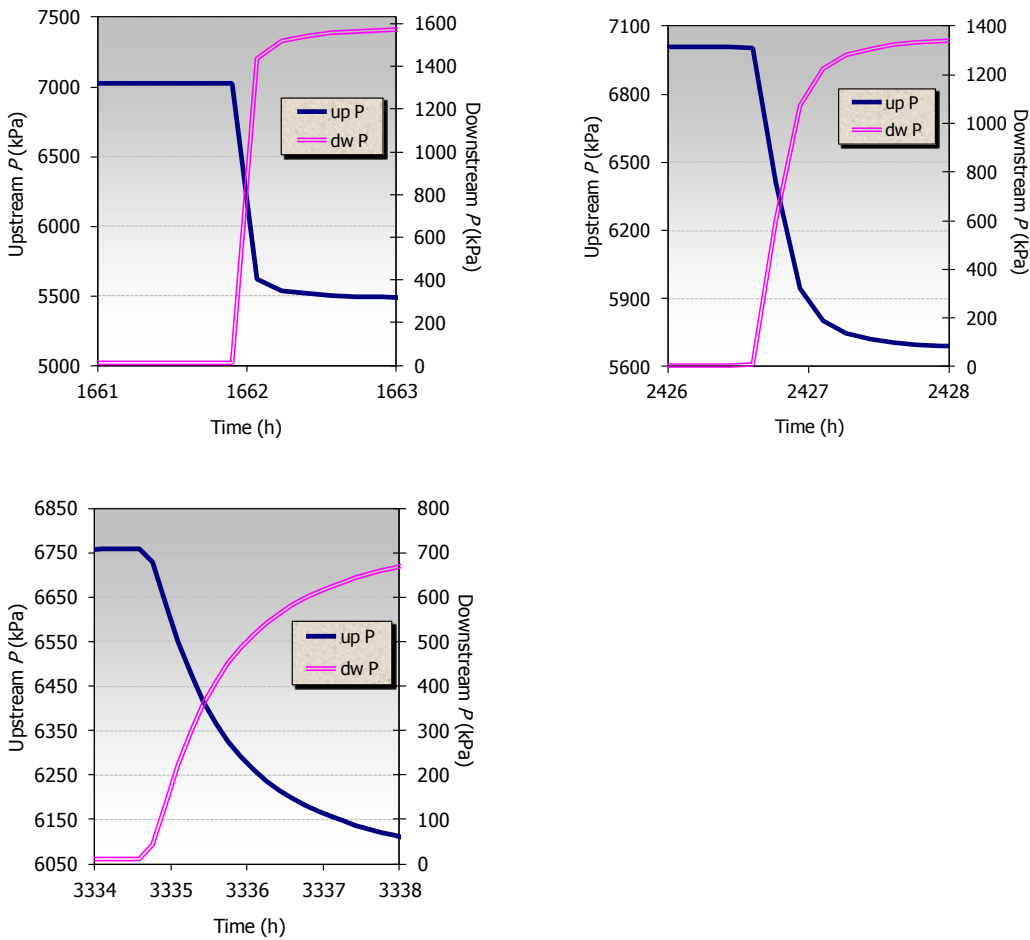


Figure 38: Evolution of pressure in the upstream and downstream deposits during the three breakthrough episodes in Phase 4 of test BT1.5_38

Test BT1.5_50

The characteristics and results of test BT1.5_50 are shown in Table VII. Figure 39 shows the evolution of pressures in both deposits during Phase 2 of the test and Figure 40 shows an enlargement of the changes in pressure in both deposits during breakthrough, which was quite sudden. The evolution of gas permeability as computed with Equation 10 from the fitted pressure changes in the deposits after breakthrough is shown in Figure 41. At the beginning of breakthrough the permeability decreased quickly and stabilised, eventually increasing slightly, which could be due to the drying of the sample caused by the gas flow.

Table VII: Results of test BT1.5_50

Phase	Duration (days)	w (%)	ρ_d (g/cm ³)	S_r (%)	Saturation/BT P (MPa)	$k_{ig} \cdot k_{rg}$ (m ²)
1. Saturation	154	30.5	1.39	88	0.6-0.8-1.0	
2. Gas breakthrough	64	29.3	1.39	84	7.1	$7.6 \cdot 10^{-20}$
3. Resaturation	153	31.3	1.39	90	1.0	
4. 2 nd gas breakthrough	68	29.4	1.40	86	7.5	$6.1 \cdot 10^{-19} - 1.9 \cdot 10^{-21}$
					0.3	$7.2 \cdot 10^{-20} - 4.3 \cdot 10^{-20}$

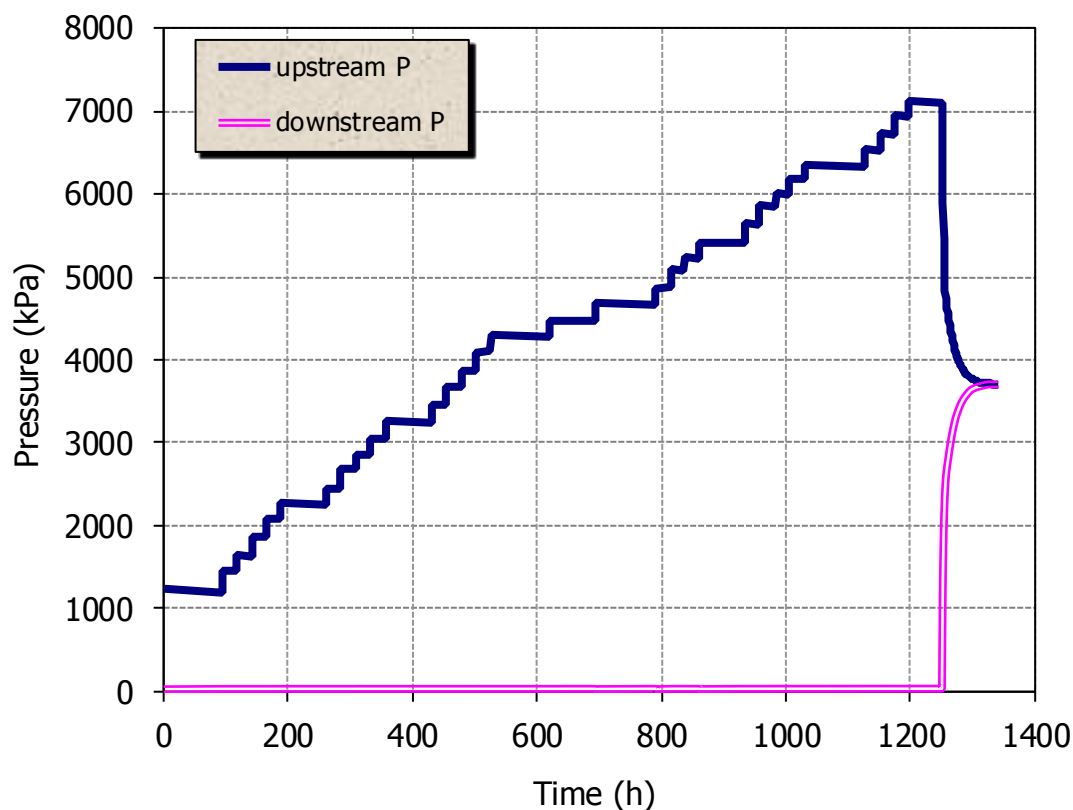


Figure 39: Evolution of pressure in the upstream and downstream deposits during Phase 2 of test BT1.5_50

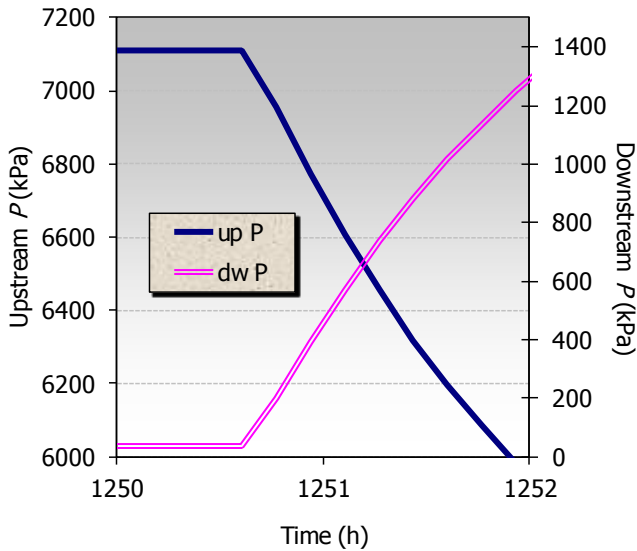


Figure 40: Evolution of pressure in the upstream and downstream deposits during the breakthrough episode of Phase 2 in test BT1.5_50

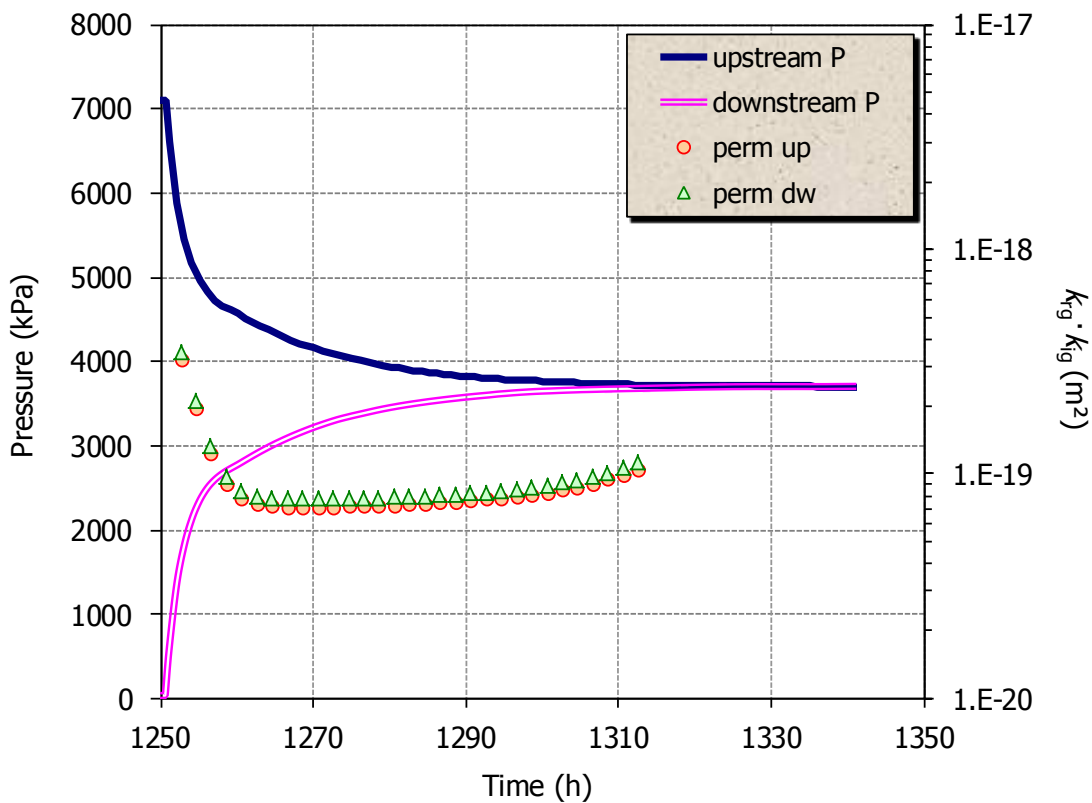


Figure 41: Evolution of pressure in the upstream and downstream deposits after breakthrough in Phase 2 of test BT1.5_50 and permeabilities computed from it

Figure 42 shows the evolution of pressures in the deposits during Phase 4 of the test, *i.e.* after resaturation. After the first breakthrough –which took place at a hydraulic head slightly higher than before– and once the pressures in both deposits had stabilised, the pressure in the downstream deposit was reduced in order to increase the hydraulic head. This resulted in sudden flow through the sample and change in the downstream and upstream pressures. The enlargements of the two breakthroughs episodes of Phase 4 of the test are shown in Figure 43.

The evolution of gas permeability as computed with Equation 10 from the pressure changes in the deposits after breakthrough is shown in Figure 44. Permeability decreased sharply just after breakthrough and then continuously increased, without reaching a stable value. This would indicate that the gas pathways remained open for a long time and easily opened again when the hydraulic head was slightly increased (second breakthrough). The permeability trends in this latter breakthrough episode as computed from the pressure changes in the upstream deposit or in the downstream deposit do not coincide initially, but tended eventually to the same value.

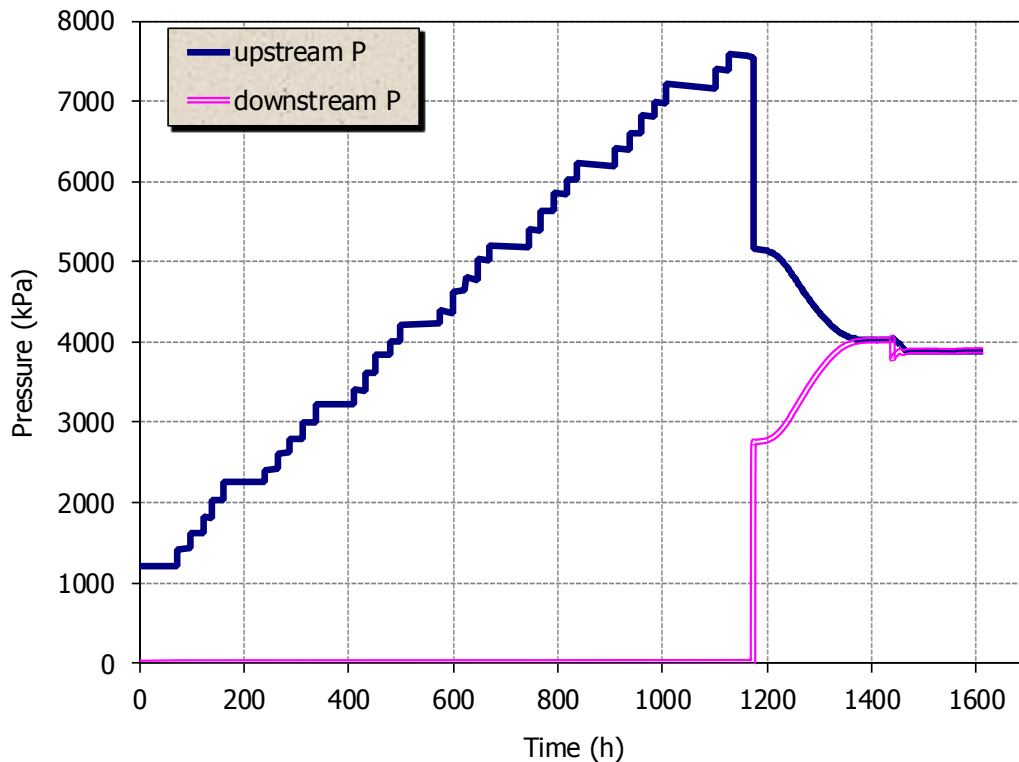


Figure 42: Evolution of pressure in the upstream and downstream deposits during Phase 4 of test BT1.5_50

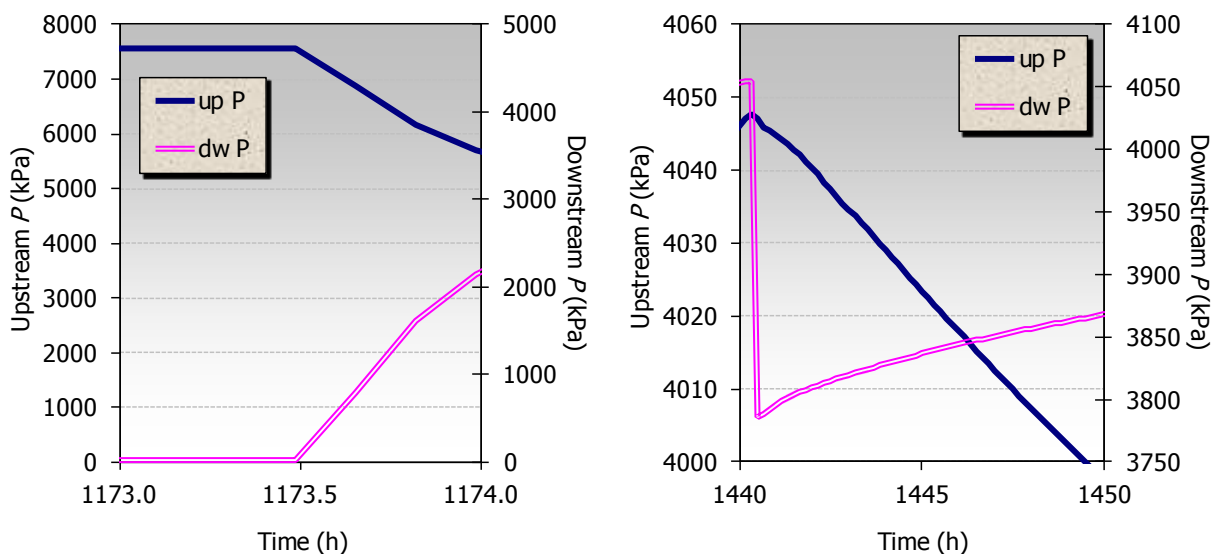


Figure 43: Evolution of pressure in the upstream and downstream deposits during the two breakthrough episodes in Phase 4 of test BT1.5_50

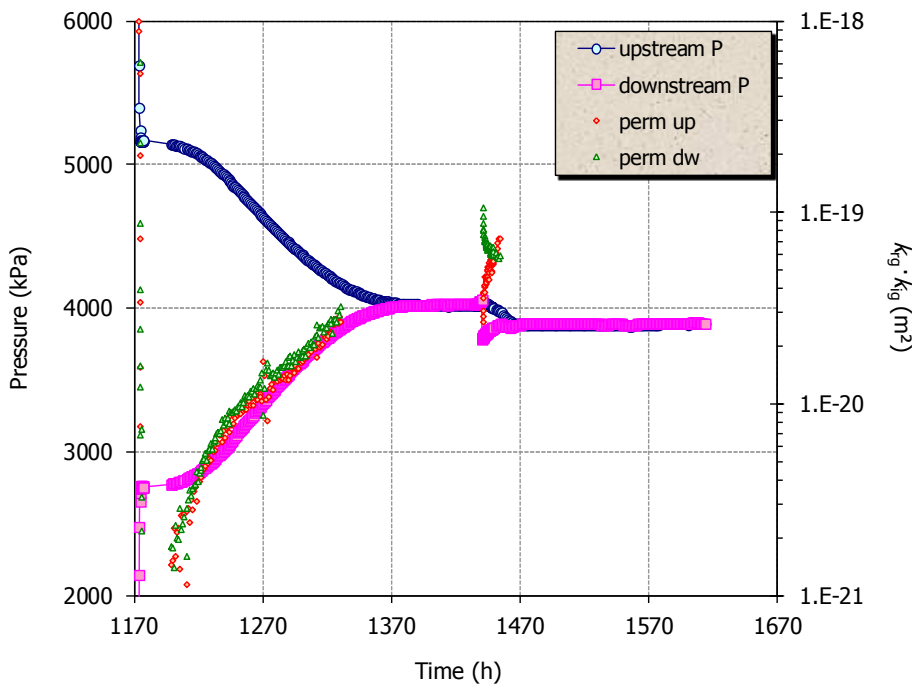


Figure 44: Evolution of pressure in the upstream and downstream deposits after breakthrough in Phase 4 of test BT1.5_50 and permeabilities computed from it

Test BT1.6_38

The characteristics and results of test BT1.6_38 are shown in Table VIII, and the evolution of pressures in the upstream and downstream deposits during the first breakthrough test in Figure 45. After the first breakthrough was achieved, flow in the downstream deposit decreased due to a leak in it. After solving the experimental problem, the initial conditions were restored and Phase 2 of the test continued. The pressure gradients required to produce the passage of gas through the sample became lower as the test progressed and after breakthrough the permeability values decreased continuously. Figure 46 shows an enlargement of the changes in pressure in both deposits during the three breakthrough episodes. It can be observed that in the first breakthrough, the pressure in the upstream deposit started to decrease while that in the downstream deposit remained constant for two hours more and then increased, which could be the interval between the air entry inside de sample and the breakthrough. In the third breakthrough, the upstream pressure fluctuated due to technical problems.

Table VIII: Results of test BT1.6_38

Phase	Duration (days)	w (%)	ρ_d (g/cm ³)	S_r (%)	Saturation/BT P (MPa)	$k_{ig} \cdot k_{rg}$ (m ²)
1. Saturation	180	35.6	1.42	106	0.2-0.6	
2. Gas breakthrough	203	34.5	1.41	103	3.4	$1.3 \cdot 10^{-21} - 9.1 \cdot 10^{-22}$
					2.3	$4.1 \cdot 10^{-21} - 7.4 \cdot 10^{-22}$
					1.8	$1.5 \cdot 10^{-21} - 8.6 \cdot 10^{-22}$
3. Resaturation	164	35.3	1.46	112	0.6-1.0	
4. 2 nd gas breakthrough	51	33.8	1.45	106	3.8	$1.6 \cdot 10^{-17} - 8.1 \cdot 10^{-19}$
					2.9	$2.7 \cdot 10^{-17} - 3.7 \cdot 10^{-19}$

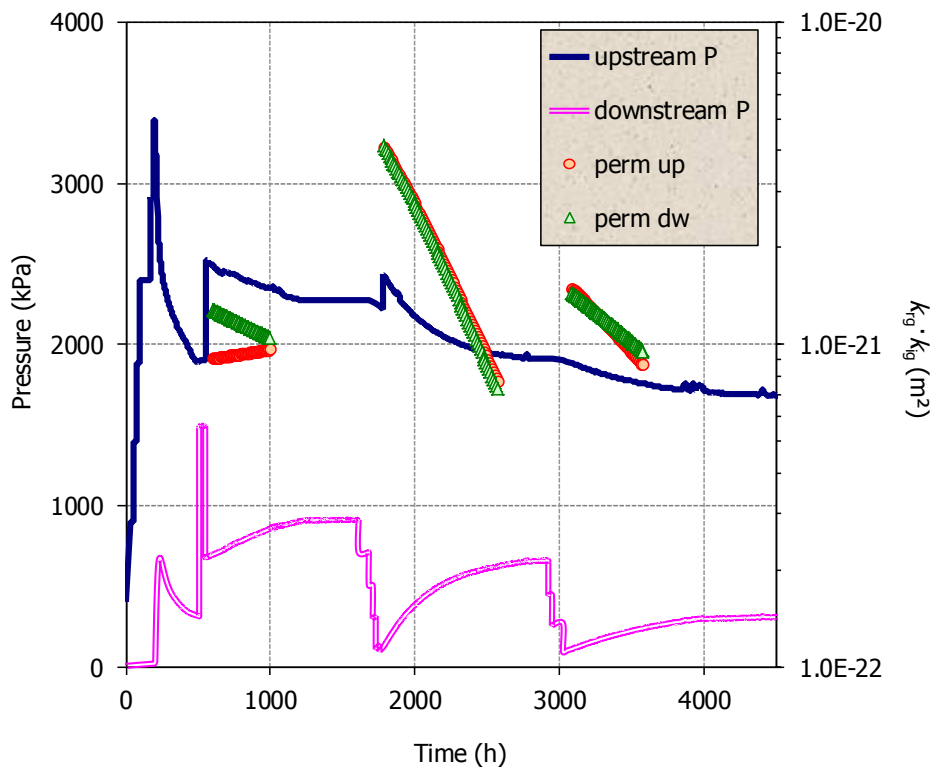


Figure 45: Evolution of pressure in the upstream and downstream deposits during Phase 2 of test BT1.6_38 and permeabilities computed from it (technical problem after the first BT)

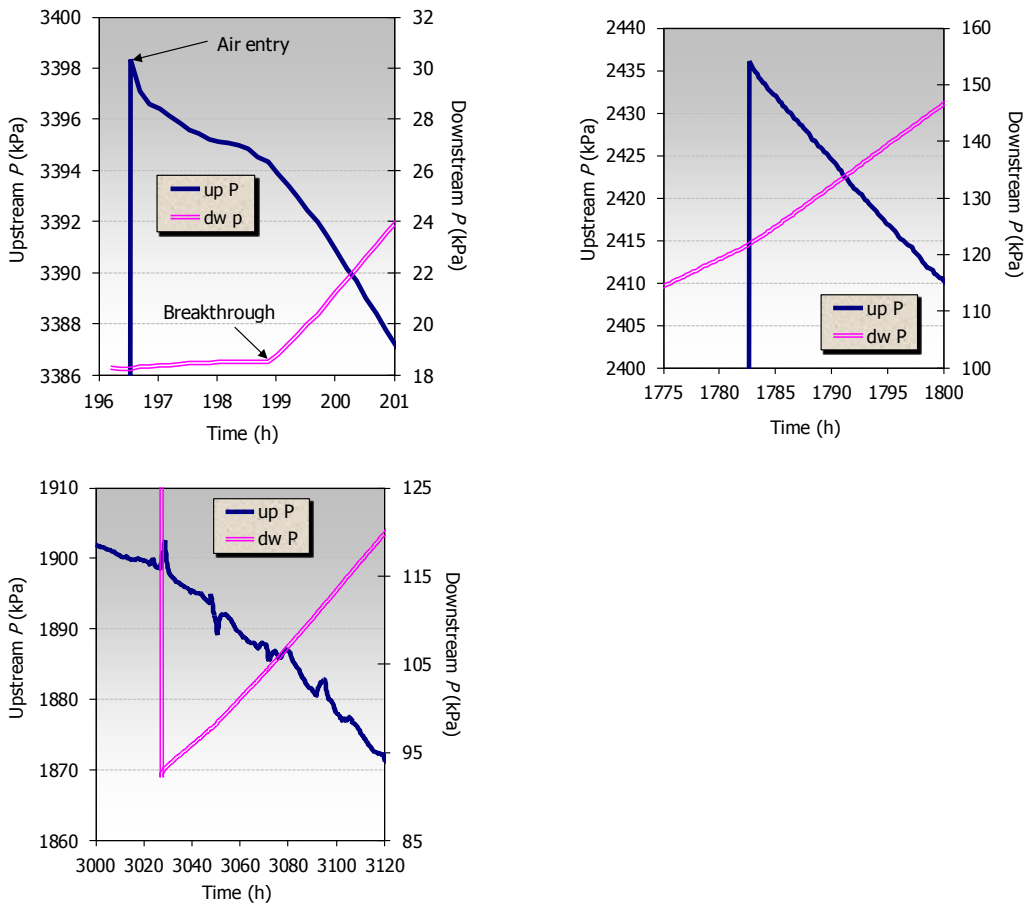


Figure 46: Evolution of pressure in the upstream and downstream deposits during the three breakthrough episodes in Phase 2 of test BT1.6_38

Figure 47 shows the evolution of pressures in the deposits during Phase 4 of the test, after sample resaturation. The first breakthrough took place at a pressure similar to that in Phase 2, and the pressure in both deposits stabilised in less than one hour. After this first breakthrough the permeability decreased quickly two orders of magnitude. The second breakthrough occurred at a lower pressure, but following the same pattern. The enlargements of the two breakthrough episodes of Phase 4 of the test are shown in Figure 48. In both cases flow ceased abruptly afterwards.

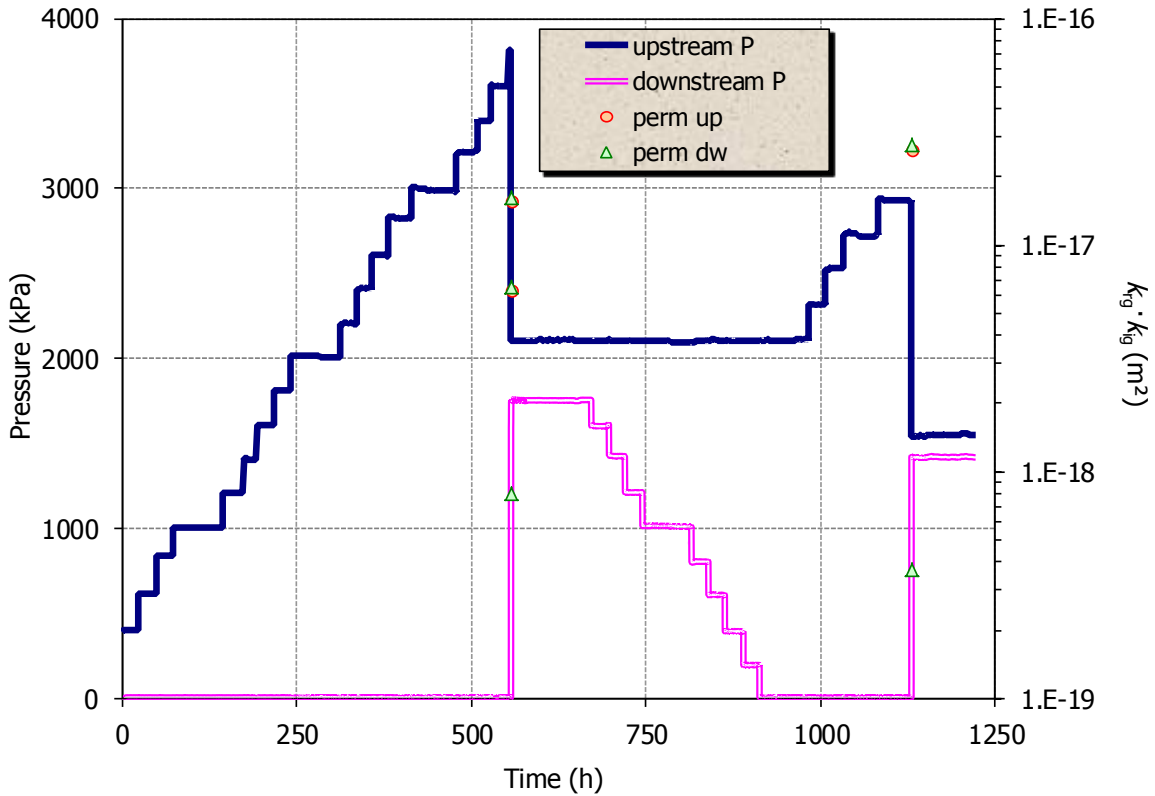


Figure 47: Evolution of pressure in the upstream and downstream deposits during Phase 4 of test BT1.6_38 and permeabilities computed from it

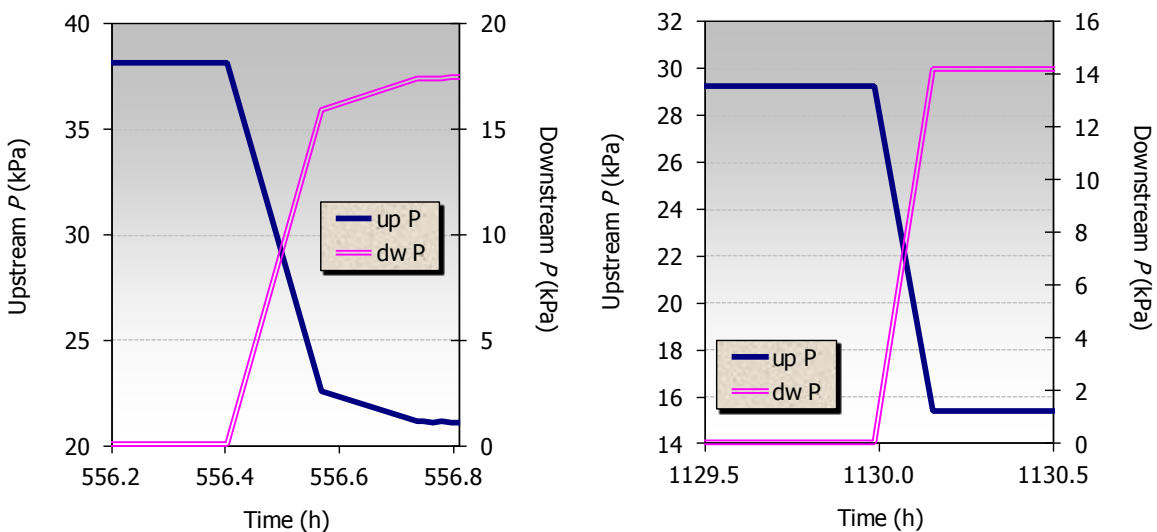


Figure 48: Evolution of pressure in the upstream and downstream deposits during the two breakthrough episodes in Phase 4 of test BT1.6_38

Test BT1.7_38

The characteristics and results of test BT1.7_38 are shown in Table IX, and the evolution of pressures in the upstream and downstream deposits during the first breakthrough test in Figure 49. After the first breakthrough the pressures in both deposits stabilised in less than one hour. The second breakthrough took place at a smaller pressure and the pressure in both deposits changed continuously for a long period of time, which indicates that flow occurred. The permeabilities computed during this phase decreased continuously until flow stopped. Figure 50 shows the details of the two breakthrough episodes. In the second breakthrough there was a delay between the moment when the pressure in the upstream deposit started to decrease and the moment when the pressure in the downstream deposit started to increase.

Table IX: Results of test BT1.7_38

Phase	Duration (days)	w (%)	ρ_d (g/cm ³)	S_r (%)	Saturation/BT P (MPa)	$k_{ig} \cdot k_{rg}$ (m ²)
1. Saturation	222	31.6	1.54	112	1.0	
2. Gas breakthrough	156	30.6	1.48	101	6.0	$9.5 \cdot 10^{-21} - 2.6 \cdot 10^{-21}$
					5.5	$2.5 \cdot 10^{-21} - 2.1 \cdot 10^{-22}$
3. Resaturation	164	31.7	1.51	109	0.6-1.0	
4. 2 nd gas breakthrough	141	30.7	1.50	103	6.8	$1.1 \cdot 10^{-17} - 4.1 \cdot 10^{-21}$
					6.2	$1.8 \cdot 10^{-21} - 3.9 \cdot 10^{-22}$

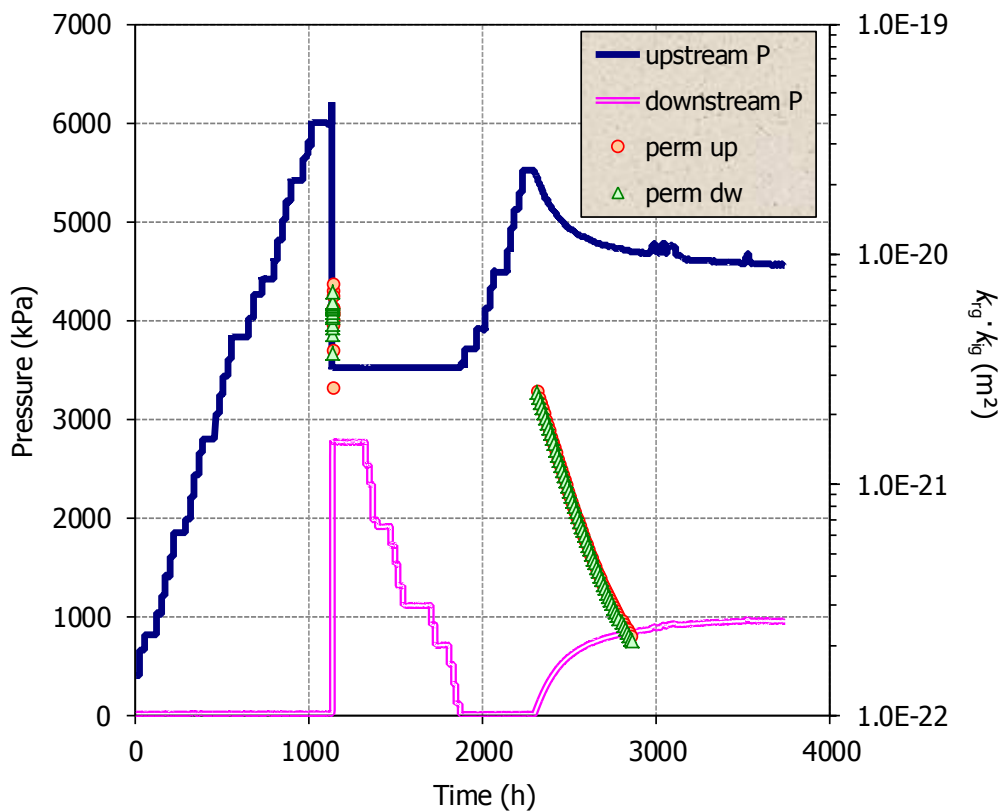


Figure 49: Evolution of pressure in the upstream and downstream deposits during Phase 2 of test BT1.7_38 and permeabilities computed from it

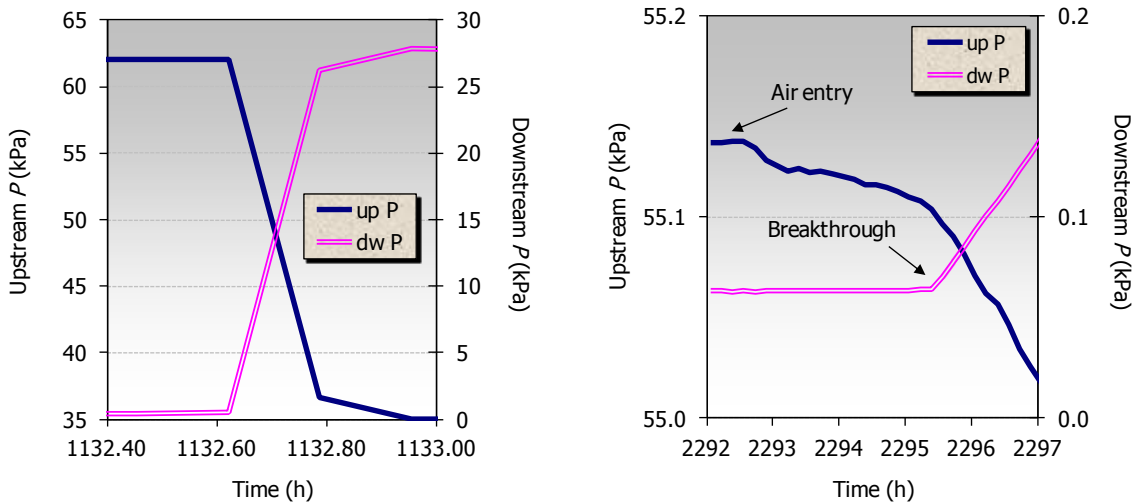


Figure 50: Evolution of pressure in the upstream and downstream deposits during the two breakthrough episodes in Phase 2 of test BT1.7_38

In Phase 4, after resaturation the first breakthrough took place at 6.8 MPa, a higher value than that obtained in Phase 2 (Figure 51). The gas flow ceased in less than one hour (Figure 52, left), with the permeability decreasing sharply. It has to be taken into account that these values were calculated assuming two-phase flow, thus they must be taken as approximate. The second breakthrough took place at a lower pressure and flow continued afterwards, ceasing slowly, which brought forward a decrease of the computed permeability.

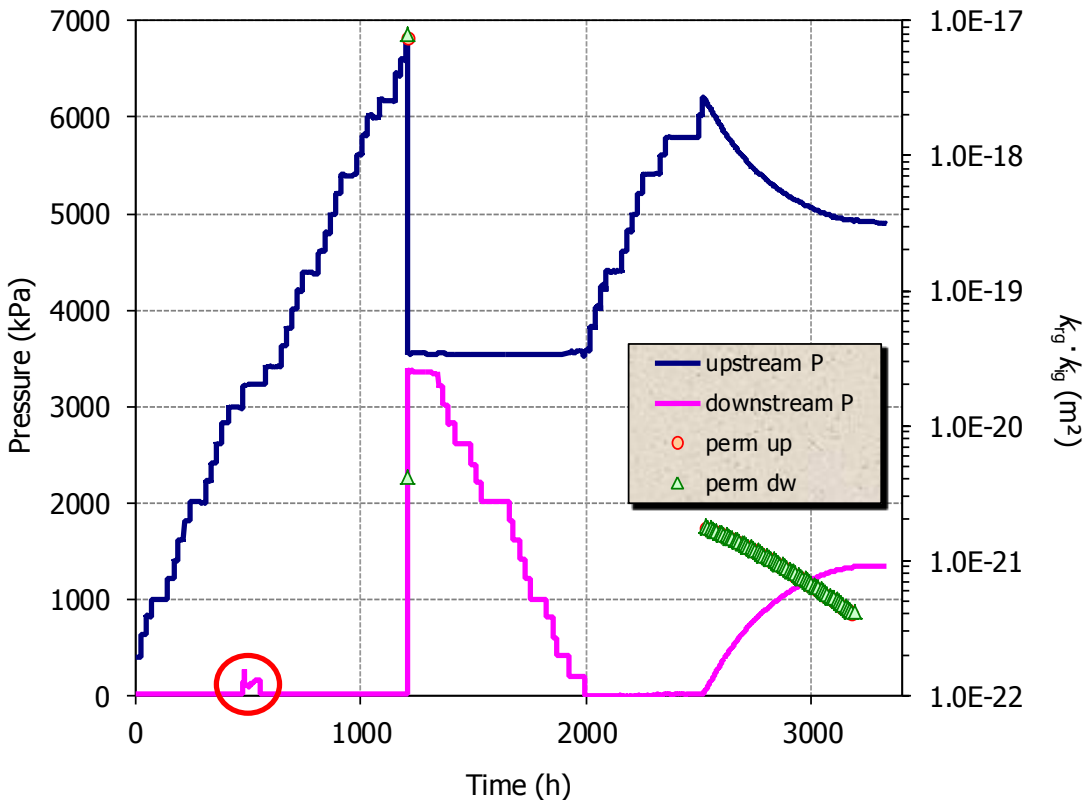


Figure 51: Evolution of pressure in the upstream and downstream deposits during Phase 4 of test BT1.7_38 and permeabilities computed from it (in a red circle, a problem with data acquisition equipment)

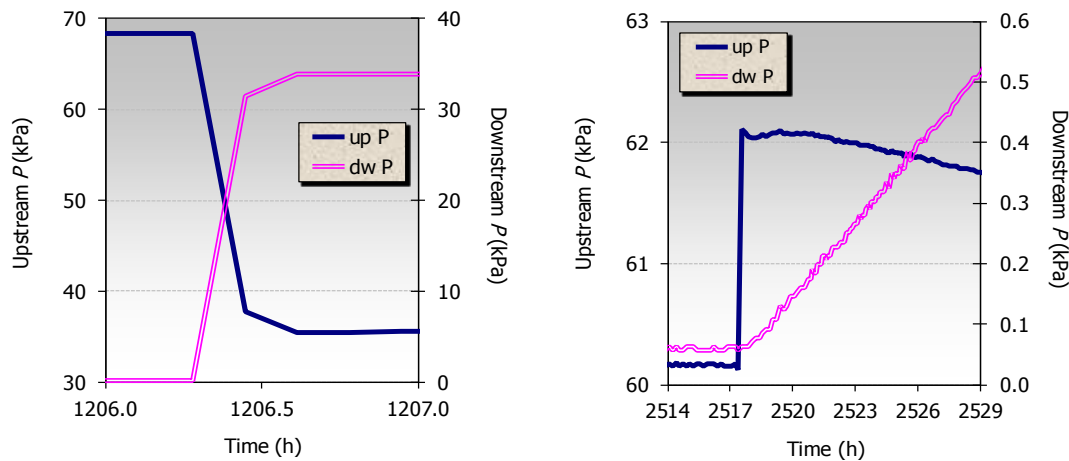


Figure 52: Evolution of pressure in the upstream and downstream deposits during the two breakthrough episodes in Phase 4 of test BT1.7_38

4.3 TESTS IN INTERFACES

4.3.1 Bentonite/bentonite interfaces

The samples for these tests were prepared according to the procedure described in section 3.3.1 and followed the same phases described in section 4.2.2.

The characteristics of the samples with interfaces prepared for the breakthrough tests are shown in Table X and the results of each test are detailed below.

Table X: Characteristics of the samples saturated for the breakthrough pressure tests

Reference	Compaction ρ_d (g/cm ³)	ρ_d after joint (g/cm ³)	Initial w (%)	Diameter (cm)	Initial height (cm)	Saturation time (days)	Saturation P (kPa)	w after saturation (%)
JB17_38	1.69	1.48	13.7	3.8	5.0	167	200-800	35.8
JB18_38	1.77	1.67	14.7	3.8	5.0	228	600-800	29.4

Test JB1.7_38

A bentonite sample was compacted at a nominal dry density of 1.7 g/cm³ (actual ρ_d 1.69 g/cm³) and cut longitudinally to create an interface. Upon cutting and placing in the stainless steel cell due to mass loss the dry density of the bentonite decreased considerably, to a value of 1.48 g/cm³. Saturation brought a new density reduction, due to the swelling of the bentonite and the slight deformation allowed by the cell. The characteristics and results of the different phases of the test are shown in Table XI. Figure 53 shows the evolution of pressure in the deposits during the tests and the permeabilities computed from it. The first breakthrough was very abrupt, whereas the second one, which occurred at a lower pressure, only implied a very small, continuous flow (Figure 54). This could indicate that the interface remained a weakness zone even after gas flow almost stopped after the first breakthrough. It must be taken into account that the BT tests were performed without water supply, for which reason the interface could not completely seal after the first breakthrough.

Table XI: Results of test JB1.7_38

Phase	Duration (days)	w (%)	ρ_d (g/cm ³)	S_r (%)	Saturation/BT P (MPa)	$k_{ig} \cdot k_{rg}$ (m ²)
1. Saturation	167	35.8	1.38	101	0.2-0.6-0.8	
2. Gas breakthrough	124	34.9	1.38	99	2.7	$7.8 \cdot 10^{-20}$ - $2.6 \cdot 10^{-21}$
					1.4	$4.9 \cdot 10^{-21}$ - $4.7 \cdot 10^{-22}$
3. Resaturation	168	36.6	1.40	106	0.4-0.6	
4. 2 nd gas breakthrough	131	34.7	1.40	100	2.8	$7.1 \cdot 10^{-20}$ - $8.3 \cdot 10^{-22}$
					2	$4.7 \cdot 10^{-20}$ - $1.1 \cdot 10^{-21}$

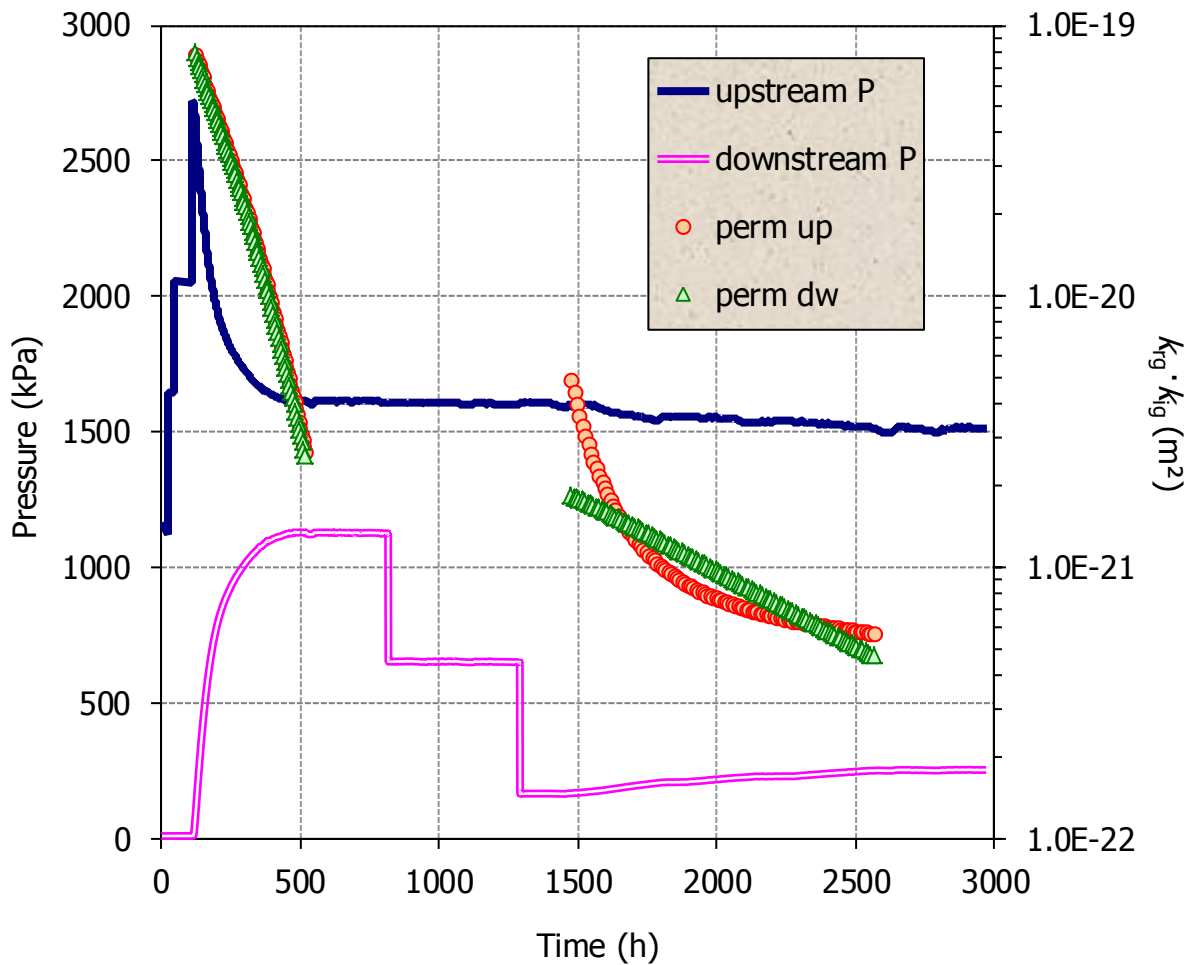


Figure 53: Evolution of pressure in the upstream and downstream deposits during Phase 2 of test JB1.7_38 and permeabilities computed from it

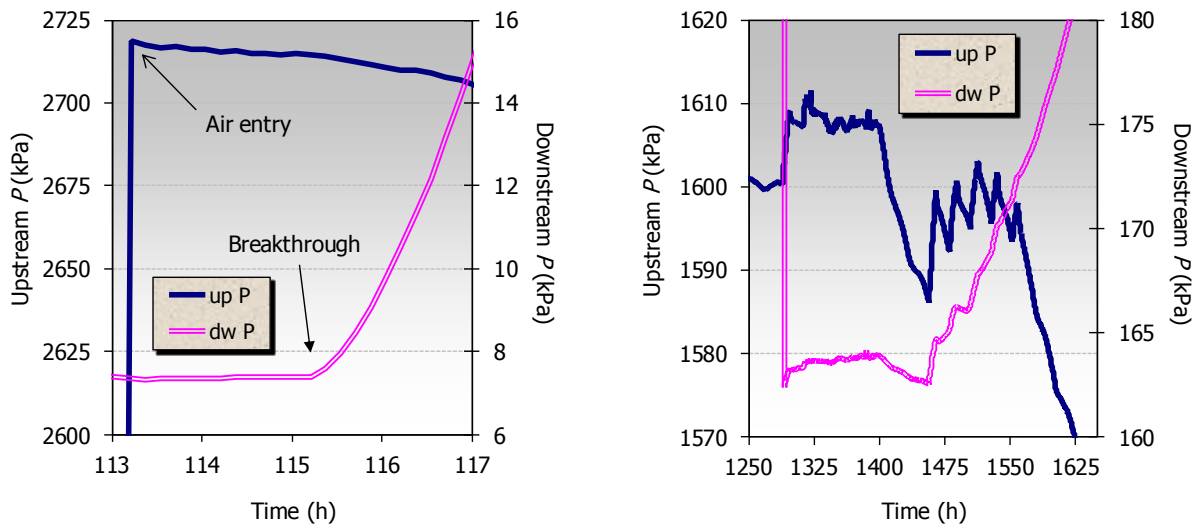


Figure 54: Evolution of pressure in the upstream and downstream deposits during the two breakthrough episodes of test JB1.7_38 during Phase 2

The behaviour during Phase 4 was similar to the previous stage. Figure 55 presents the evolution of pressures with two breakthrough episodes. The first one took place at a pressure similar to that in Phase 2, and the second one at a lower pressure. To reach the second breakthrough it was necessary to first decrease the pressure in the downstream deposit until 0 and then increase that in the upward deposit. The detail of the two BT episodes is shown in Figure 56.

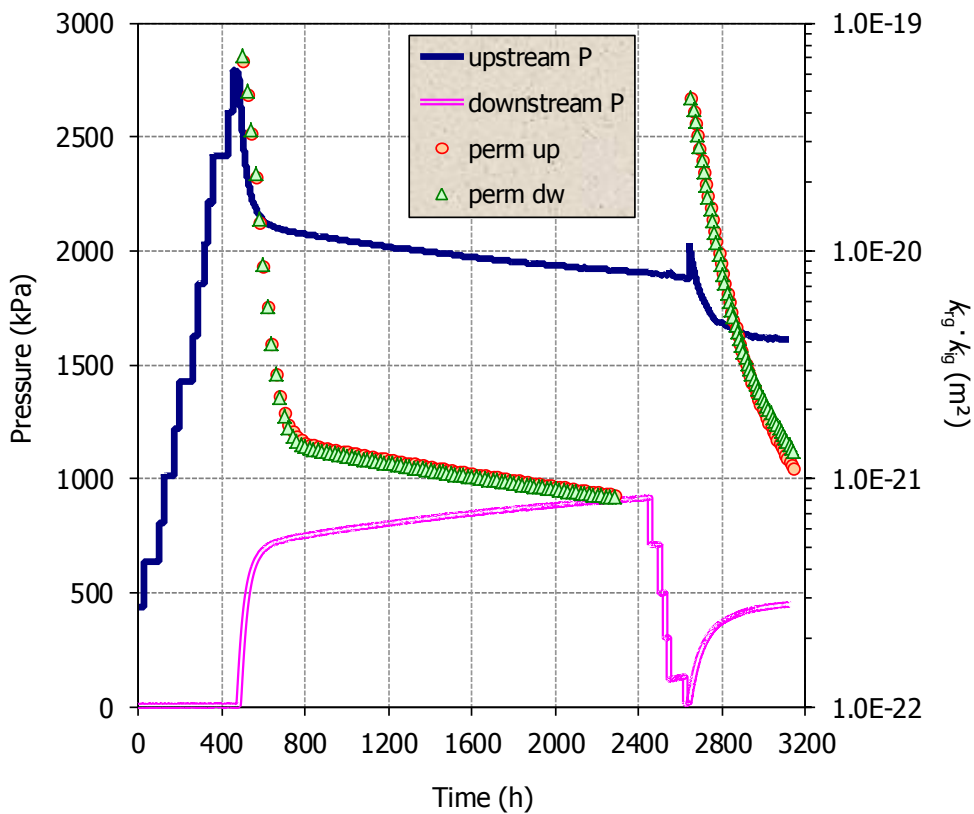


Figure 55: Evolution of pressure in the upstream and downstream deposits during Phase 4 of test JB1.7_38 and permeabilities computed from it.

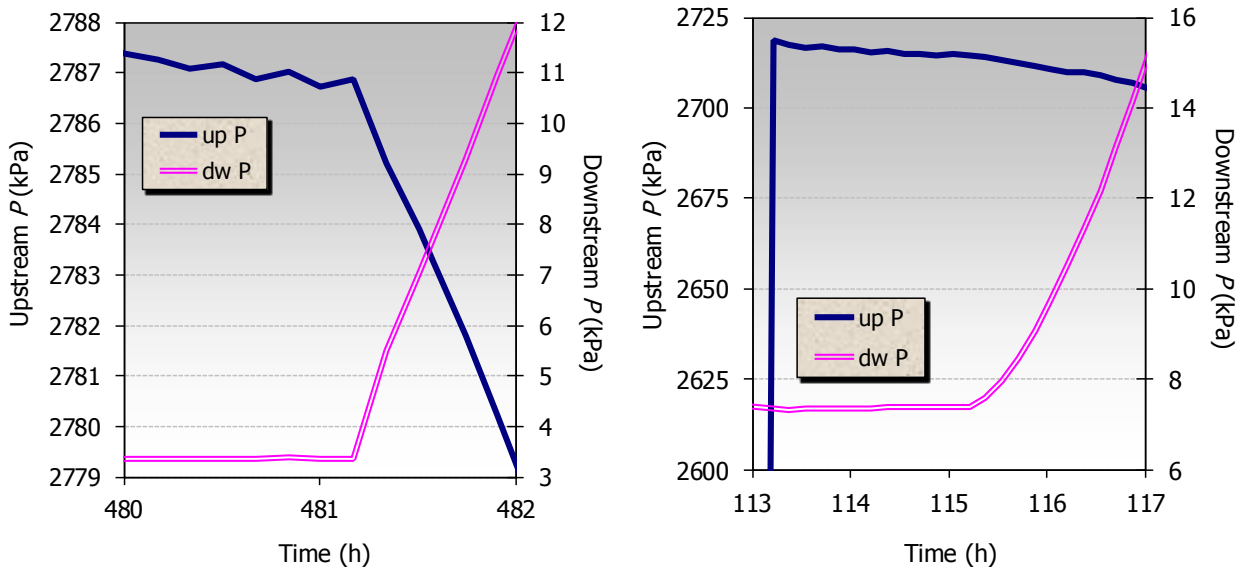


Figure 56: Evolution of pressure in the upstream and downstream deposits during the two breakthrough episodes of test JB1.7_38 during Phase 4

Figure 57 shows the appearance of the sample upon dismantling at the end of the test. The interface looked perfectly sealed, despite the fact that the initial opening was quite large (Figure 8). A lower density along the interface is to be expected, although this was not checked.



Figure 57: Appearance of sample JB1.7_38 at the end of the test

Test JB1.8_38

A bentonite sample was compacted at a nominal dry density of 1.8 g/cm³ (actual $\rho_d=1.77$ g/cm³) and cut longitudinally to create an interface. Upon cutting and placing in the stainless steel cell due to mass loss the dry density of the bentonite decreased considerably, to a value of 1.67 g/cm³. Saturation brought a new density reduction, due to the swelling of the bentonite and the slight deformation allowed by the cell and geotextile used as saturating interface. The characteristics and results of the different phases of the test are shown in Table XII. Figure 58 shows the evolution of pressure in the deposits during the test and the permeabilities computed from the fitted pressures. The two breakthroughs were very abrupt (Figure 59), the

second one occurring at a lower pressure, what could indicate that the interface remained a weakness zone even after gas flow almost stopped. It must be taken into account that the breakthrough tests were performed without water supply, for which reason the interface could not completely seal after the first breakthrough. The permeability decreased after the first breakthrough, although when calculated using the pressure in the downstream deposit it decreased by three orders of magnitude whereas when the pressure in the upstream deposit was used the decrease was smaller.

Table XII: Results of test JB1.8_38

Phase	Duration (days)	w (%)	ρ_d (g/cm ³)	S_r (%)	Saturation/BT P (MPa)	$k_{ig} \cdot k_{rg}$ (m ²)
1. Saturation	228	29.4	1.51	101	0.2-0.6-0.8-0.6	
2. Gas breakthrough	112	29.2	1.51	100	8.1	$5.4 \cdot 10^{-20}$ - $9.2 \cdot 10^{-23}$
					6.1	$1.6 \cdot 10^{-20}$ - $1.5 \cdot 10^{-22}$
3. Resaturation	203	29.5	1.53	104	0.4-0.6	
4. 2 nd gas breakthrough	95	29.2	1.53	103	7.8	$2.7 \cdot 10^{-18}$ - $2.8 \cdot 10^{-21}$
					7.4	$2.8 \cdot 10^{-18}$ - $2.7 \cdot 10^{-21}$

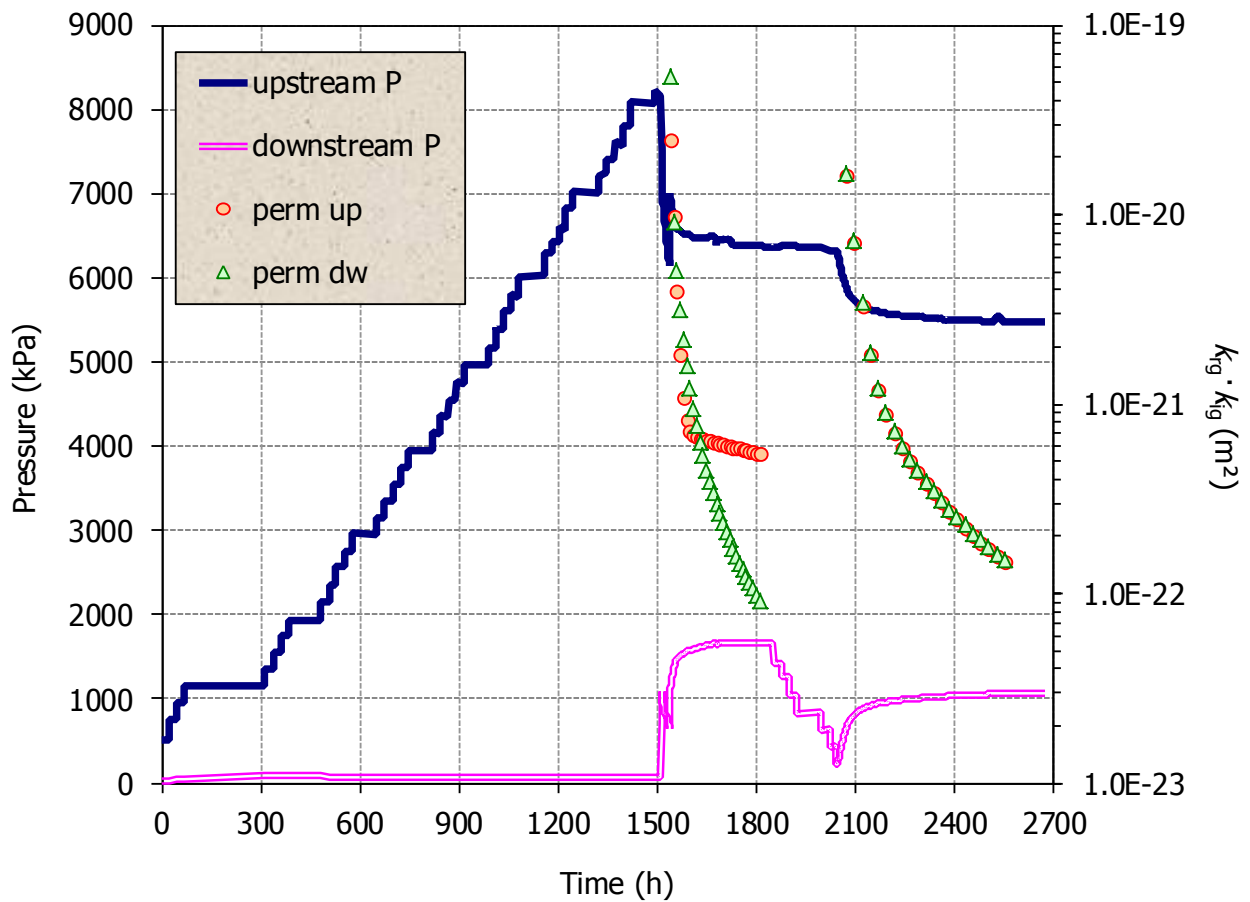


Figure 58: Evolution of pressure in the upstream and downstream deposits during Phase 2 of test JB1.8_38 and permeabilities computed from it

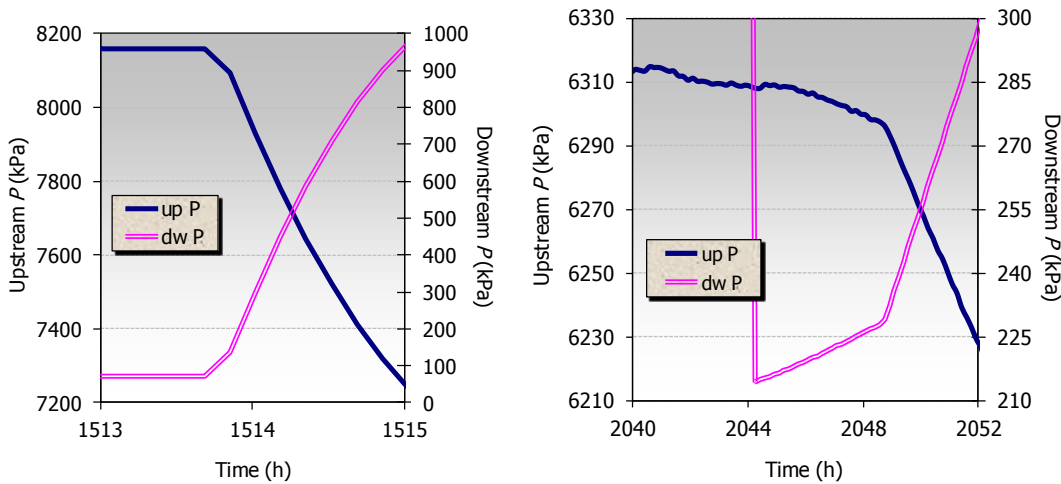


Figure 59: Evolution of pressure in the upstream and downstream deposits during the two breakthrough episodes of test JB1.8_38

Figure 60 represents the BT test results after resaturation. Both breakthroughs took place at a higher value than the last breakthrough in Phase 2. The flow decreased quickly afterwards in both cases and stopped in less than 1 h. After both breakthrough episodes the permeability decreased sharply. It has to be taken into account that these values were computed assuming two phase flow, whereas the mechanism of gas transport during breakthrough is probably different. Thus, they must be taken as indicative. Since flow stopped quickly, the sample did not dry between both episodes and the second breakthrough took place at a similar value than the first. The sealing after breakthrough was effective.

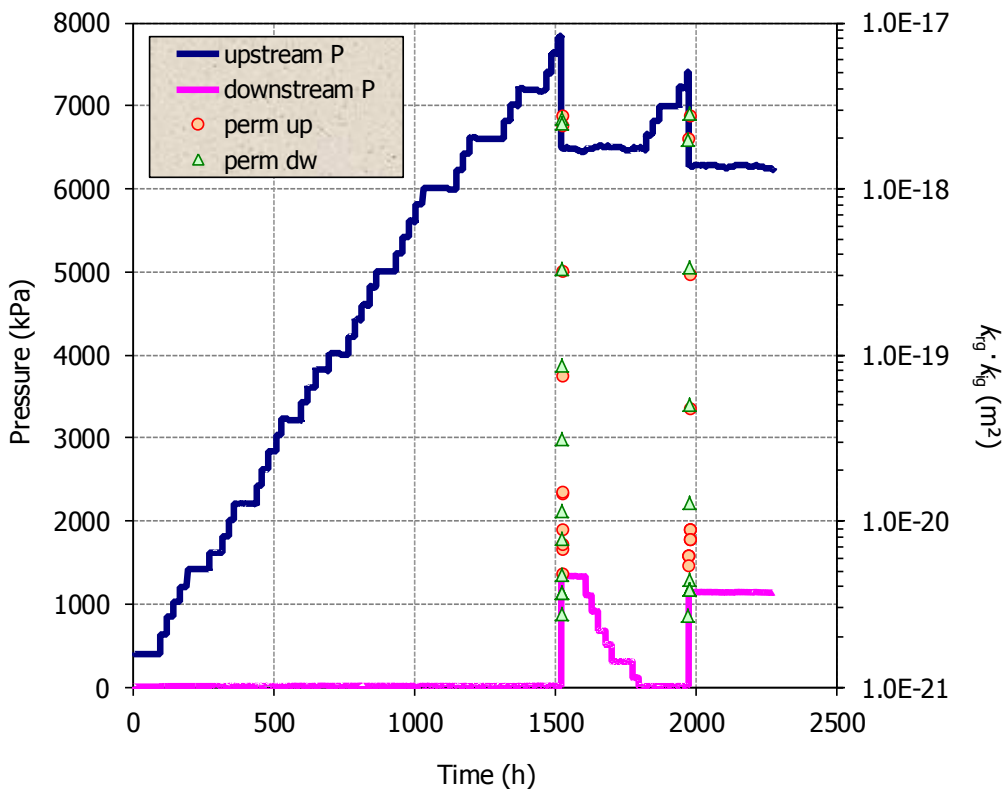


Figure 60: Evolution of pressure in the upstream and downstream deposits during Phase 4 of test JB1.8_38 and permeabilities computed from it

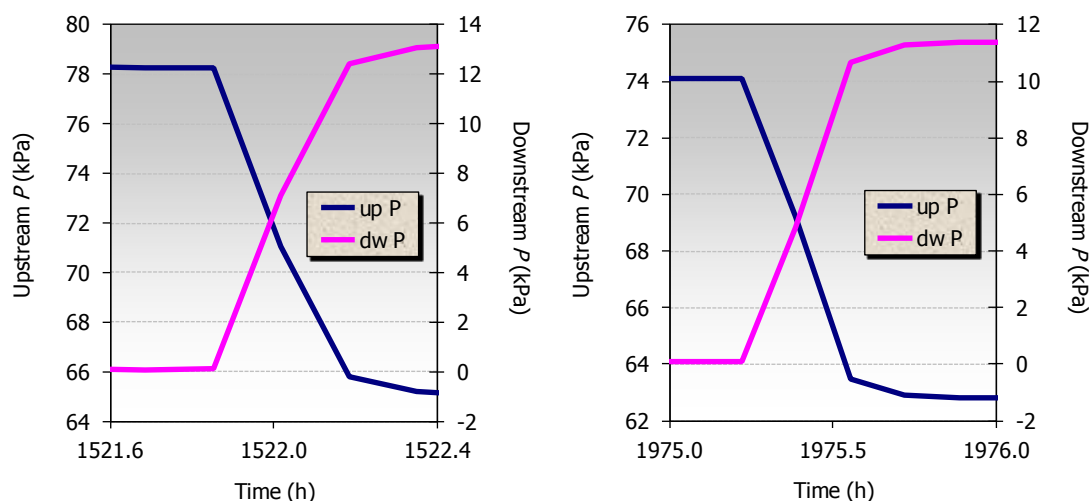


Figure 61: Evolution of pressure in the upstream and downstream deposits during the two breakthrough episodes of test JB1.8_38

4.3.2 Granite/bentonite interfaces

The preliminary test GB1 was carried out according to the procedure described in section 3.3.1. The dry density of the bentonite inside the cell was 1.56 g/cm^3 . The bentonite had initially water content of 17% and after saturation for 181 days, under a very low pressure (a 21-cm water column) for the first 69 days and under a pressure of 0.2 MPa afterwards, the water content was of 31.1%. The progress of saturation can be seen in Figure 62.

The cell was then dismantled to change the porous filters by dry ones and a gas breakthrough test started in the modified version of the setup described in section 3.1. A nitrogen gas pressure of 0.2 MPa was initially applied on the top surface, while the pressure at the bottom was atmospheric. The gas outflow was continuously monitored. Afterwards, the injection pressure was increased in 0.1-MPa steps according to the sequence shown in Figure 63. No gas outflow or pressure decrease were observed until the injection pressure reached 0.7 MPa. Then the gas outflow increased as the injection pressure decreased, indicating the breakthrough of the interface (Figure 64). The outflow stopped because the gas deposit was exhausted. After a few hours the test was restarted and breakthrough took place for an injection pressure of 0.3 MPa. The water content at the end of the test was 29.7%, and the drying along the interface was clearly visible.

After this gas breakthrough test the cell was resaturated through the bottom surface under a low water pressure (21-cm high column) for 50 days and tested again for gas breakthrough following a pressure path similar to that shown in Figure 63. For a second time breakthrough took place at an injection pressure of 0.7 MPa (Figure 65). After breakthrough the air flowed through the sample for 48 h, what caused drying of the sample to an average water content of 21.1%. This flow took place under an average hydraulic head of 10 kPa, and the permeability computed from it considering that flow took place through the bentonite surface was $1.2 \cdot 10^{-8} \text{ m/s}$. However, the flow probably occurred along the interface. In fact, upon dismantling it was observed that the interface between the bentonite and the granite was particularly dry and the bentonite had slightly retracted along it (Figure 66). The water content of the ends of the sample was considerably lower than in the central part, particularly in the end through which gas injection took place, which was also the part of the column farther from the hydration surface.

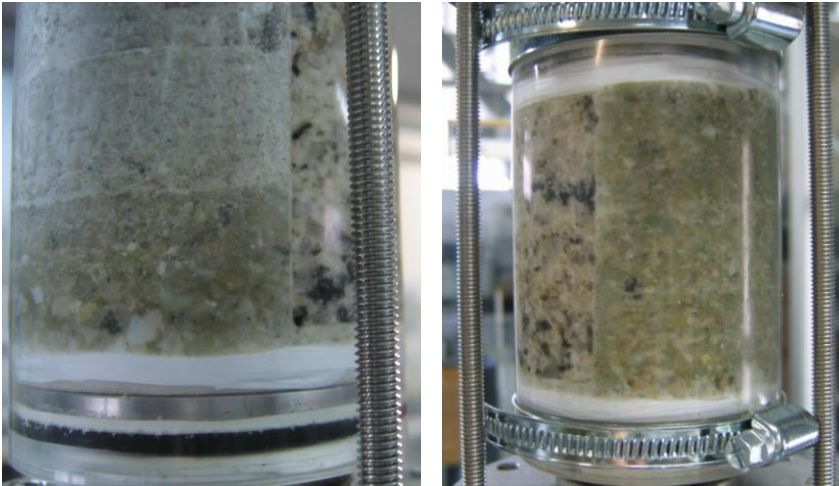


Figure 62: Evolution of saturation in the granite/bentonite interface test GB1 (12 days, left; 153 days, right)

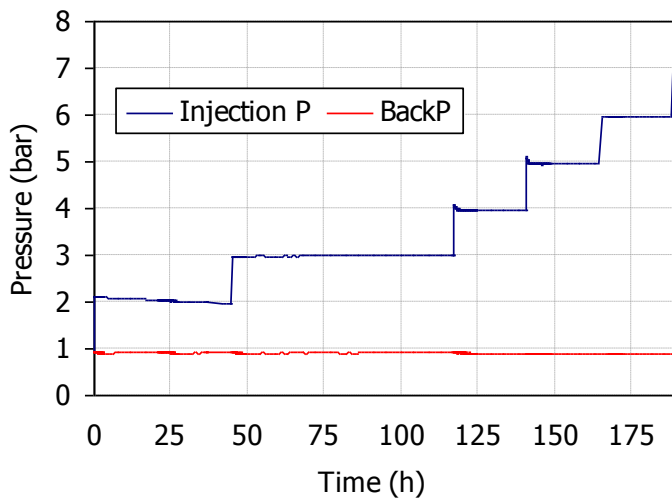


Figure 63: Pressure path followed in the granite/bentonite interface test GB1

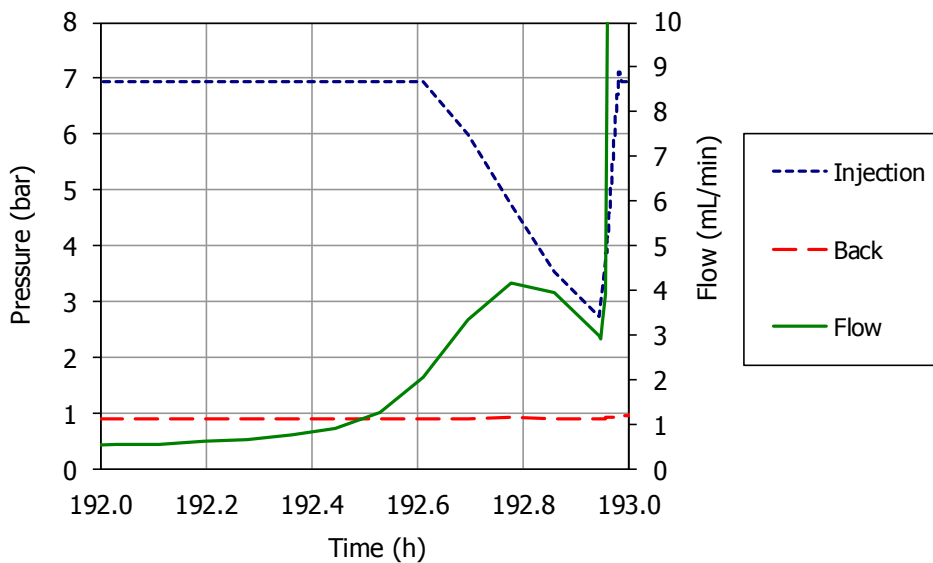


Figure 64: Breakthrough episode in the granite/bentonite interface test GB1

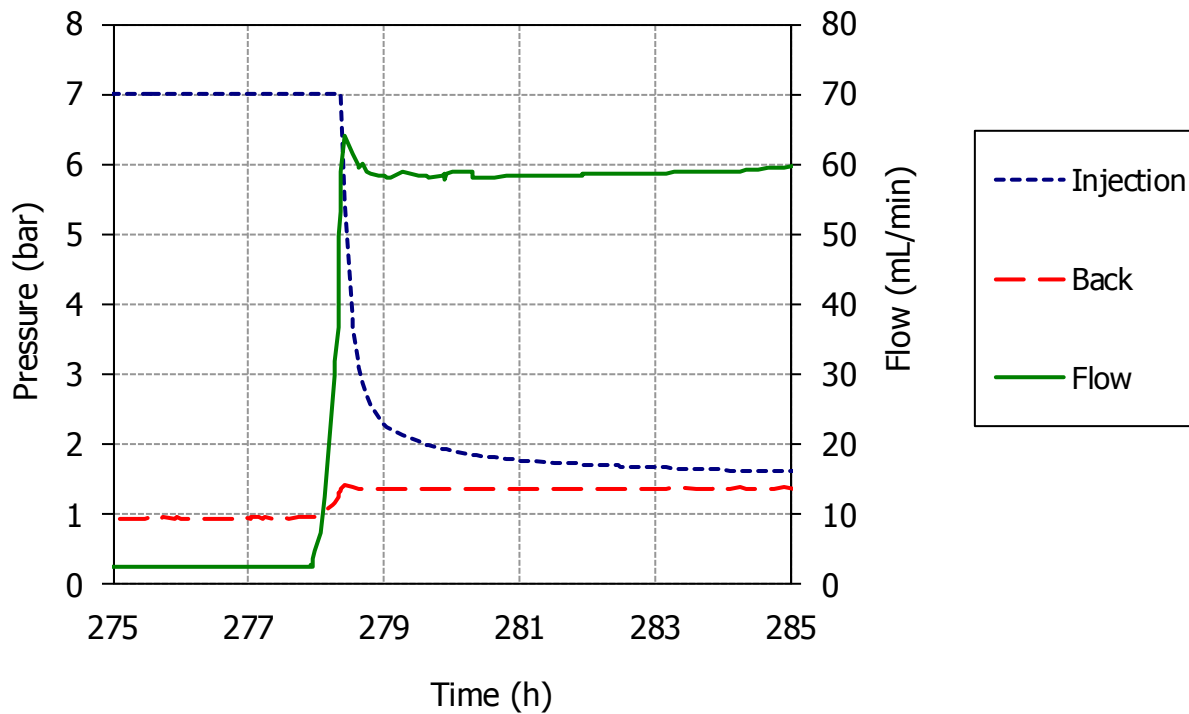


Figure 65: Second breakthrough measurement (after resaturation) in the granite/bentonite interface test GB1



Figure 66: Appearance of the granite/bentonite interface after the second gas breakthrough in test GB1

Another sample was prepared following the same procedure but with a higher bentonite density (test GB2). The bentonite blocks were initially compacted at a dry density of 1.90 g/cm^3 , although the density of the bentonite inside the cell, once all the voids filled, was 1.83 g/cm^3 . After 9 days of saturation under a very low pressure (a 21-cm water column), the methacrylate broke and the test had to be suspended.

5 Discussion

5.1 ANALYSIS OF THE KLINKENBERG EFFECT ON GAS PERMEABILITY

In gas flow through permeable materials with small pores, the mean free path of the molecules (that is, the mean distance between kinetic collisions) may become comparable to the pore size. The viscous drag is no longer transferred completely to the pore walls and the flow behaves as though there were slippage at the gas-solid interface. It is acknowledged that this would lead to the measured permeability becoming a function of pressure and to an overestimation in the permeability known as the gas slippage or the Klinkenberg effect. It is corrected for by making permeability measurements with gas at multiple pressure differences and constructing a graph of the measured apparent permeability ($k_{ig} \cdot k_{rg}$) against the reciprocal of the mean pressure in the samples. The mean pressure (P_{mn}) is the average of the upstream (P_{up}) and downstream (P_{dw}) pressures in Equation 4. The points should lie on a straight line which intersects the y -axis at $1/P_{mn} = 0$. This value effectively represents the permeability at which the gas is compressed by infinite pressure and becomes a near perfect liquid and is known as Klinkenberg apparent permeability.

This method was applied for the tests performed with the steady-state equipment, in which different upstream and downstream pressures were applied to measure gas permeability. The results were grouped according to the effective pressure applied and are shown in Figure 67 to Figure 74. The slopes of the fittings were in general very small, because the influence of the mean pressure on the permeability value was not significant. In some cases the slope was even negative, which invalidates the apparent permeability value obtained with this method, since it would be higher than the average of all the measurements obtained under different pressure conditions. Nevertheless, the apparent permeability values obtained applying the Klinkenberg method have been plotted in Figure 75, along with the average of all the permeability values measured in each sample for a given effective pressure. The Klinkenberg apparent permeability values obtained for a given effective pressure were on average the same as the average of all the values measured for the same effective pressure range. This would mean that the injection and backpressures applied did not have a large influence on permeability. For this reason it is considered that the Klinkenberg effect was not relevant in the range of pressures applied.

Figure 67 to Figure 74 show in addition that the effect of effective pressure on gas permeability was not always remarkable, and in many cases the same fitting was valid for the different effective pressures, probably due to the fact that they were well below the bentonite swelling pressure.

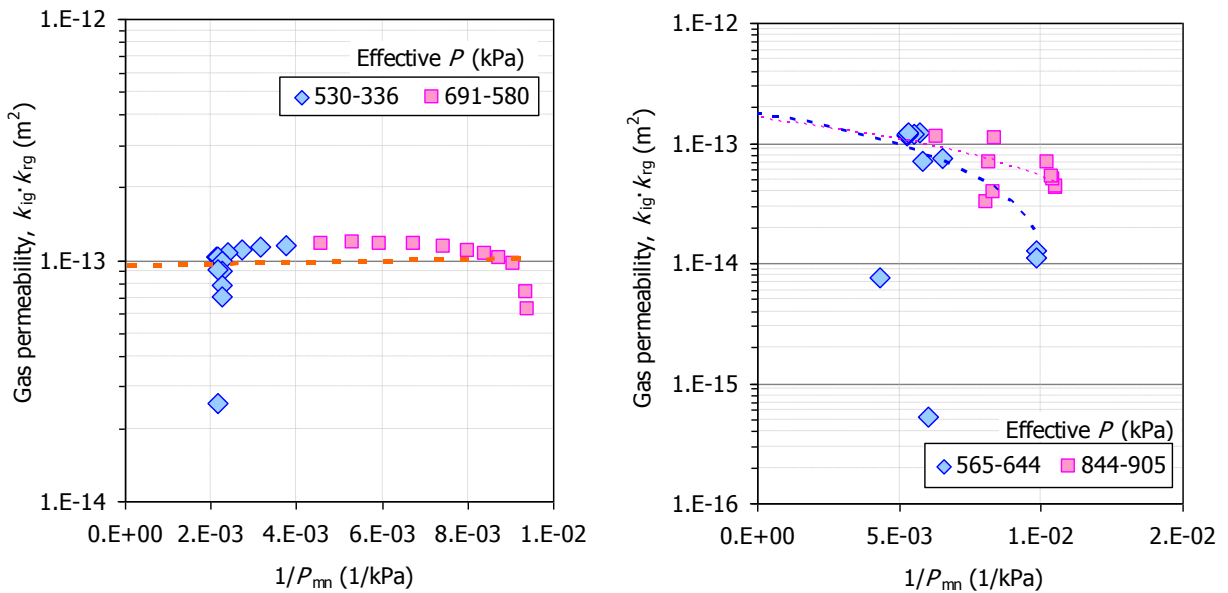


Figure 67: Measured permeability versus inverse of mean pressure (P_{mn}) for tests PGFBX1 (left) and PGFBX2 (right)

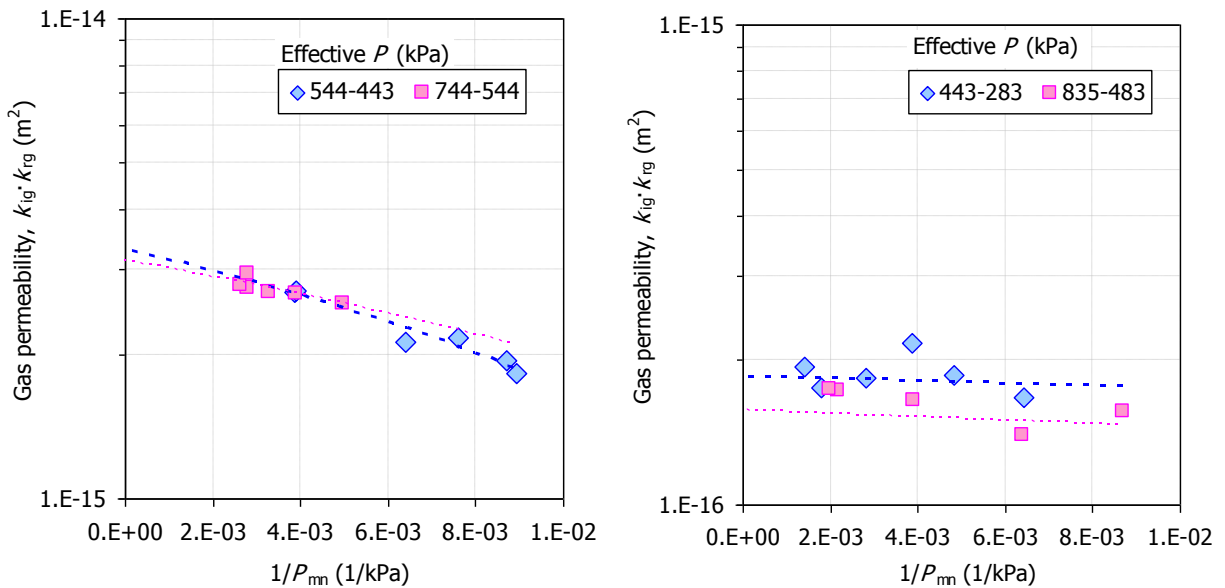


Figure 68: Measured permeability versus inverse of mean pressure (P_{mn}) for tests PGFBX3 (left) and PGFBX4 (right)

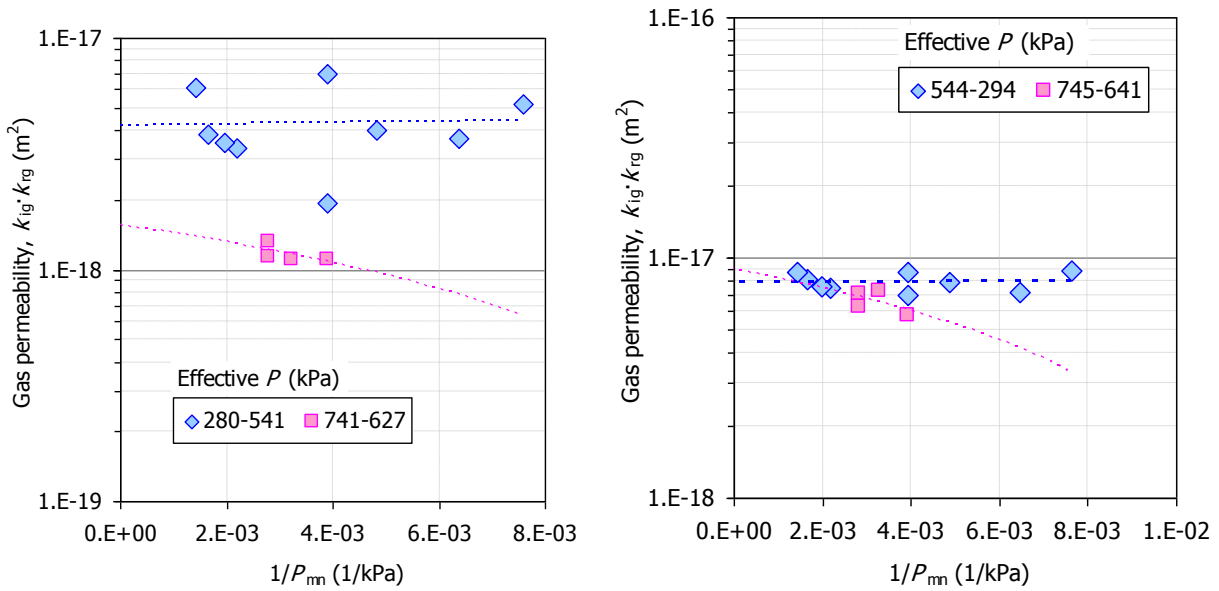


Figure 69: Measured permeability versus inverse of mean pressure (P_{mn}) for tests PGFBX5 (left) and PGFBX6 (right)

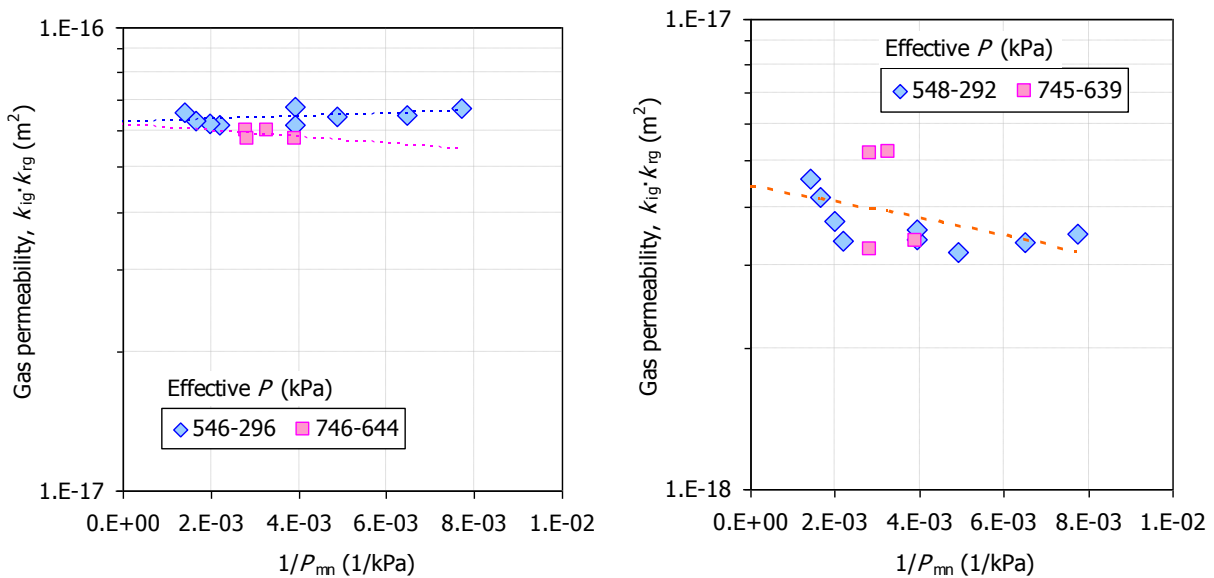


Figure 70: Measured permeability versus inverse of mean pressure (P_{mn}) for tests PGFBX7 (left) and PGFBX8 (right)

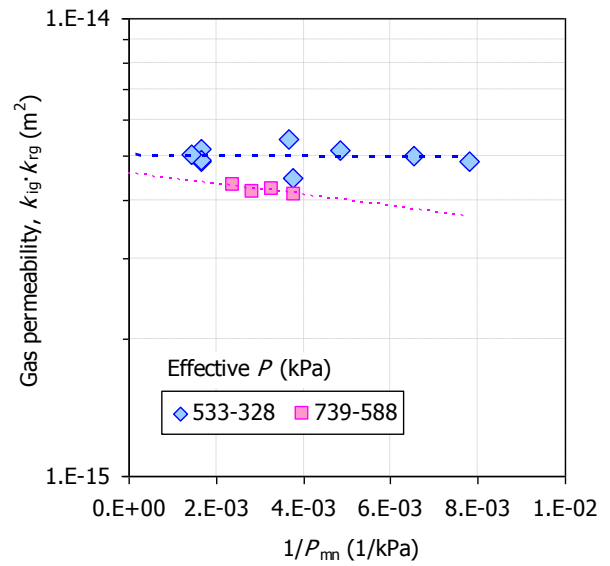
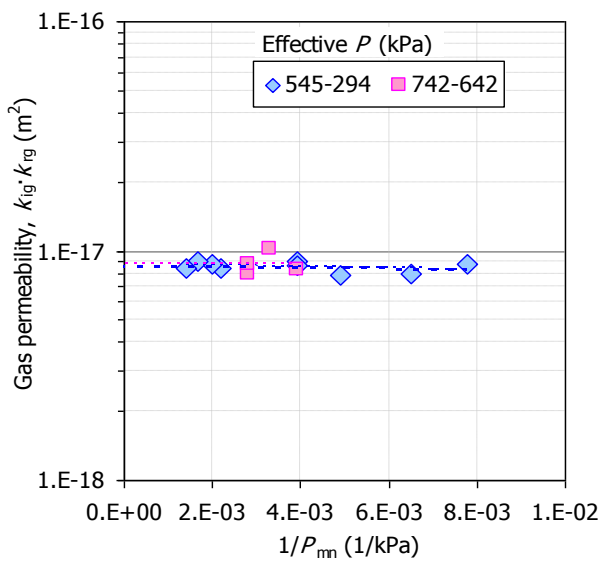


Figure 71: Measured permeability versus inverse of mean pressure (P_{mn}) for tests PGFBX9 (left) and PGFBX10 (right)

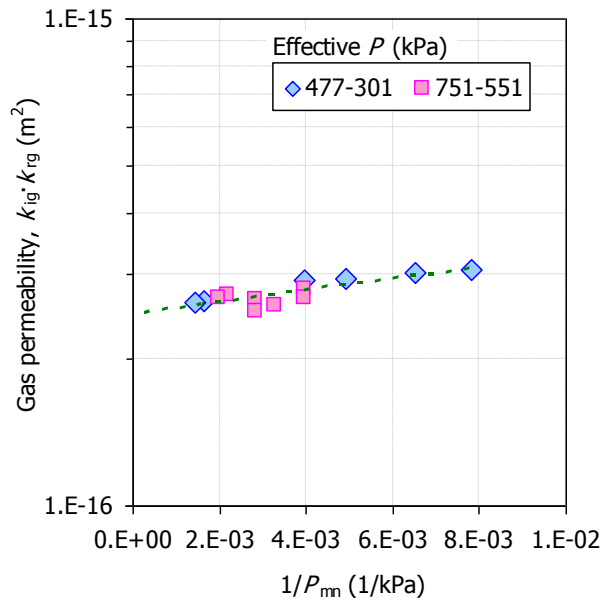
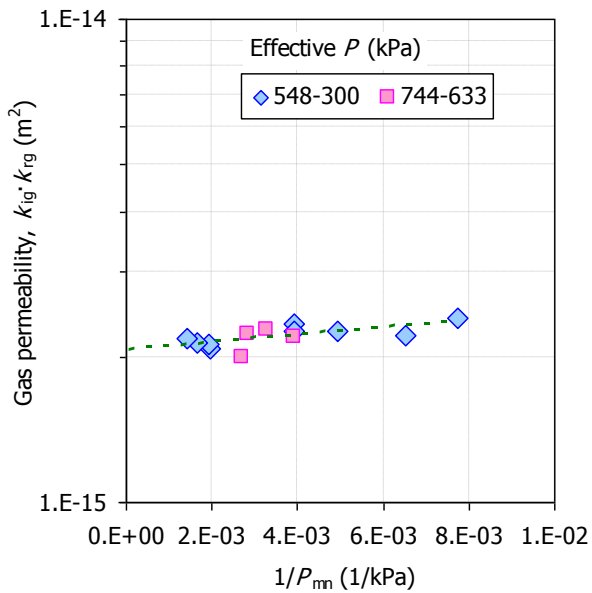


Figure 72: Measured permeability versus inverse of mean pressure (P_{mn}) for tests PGFBX11 (left) and PGFBX12 (right)

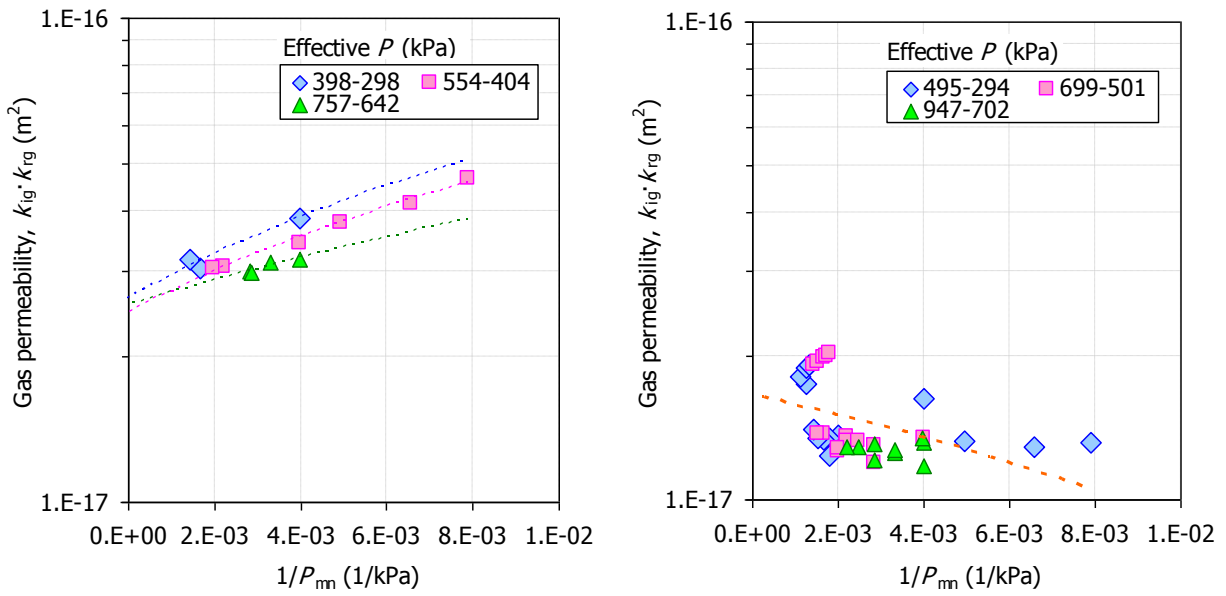


Figure 73: Measured permeability versus inverse of mean pressure (P_{mn}) for tests PGFBX13 (left) and PGFBX14 (right)

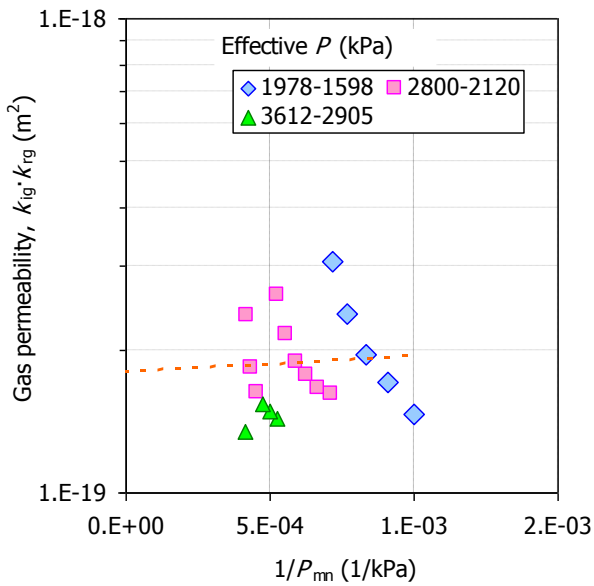


Figure 74: Measured permeability versus inverse of mean pressure (P_{mn}) for tests PGFBX16

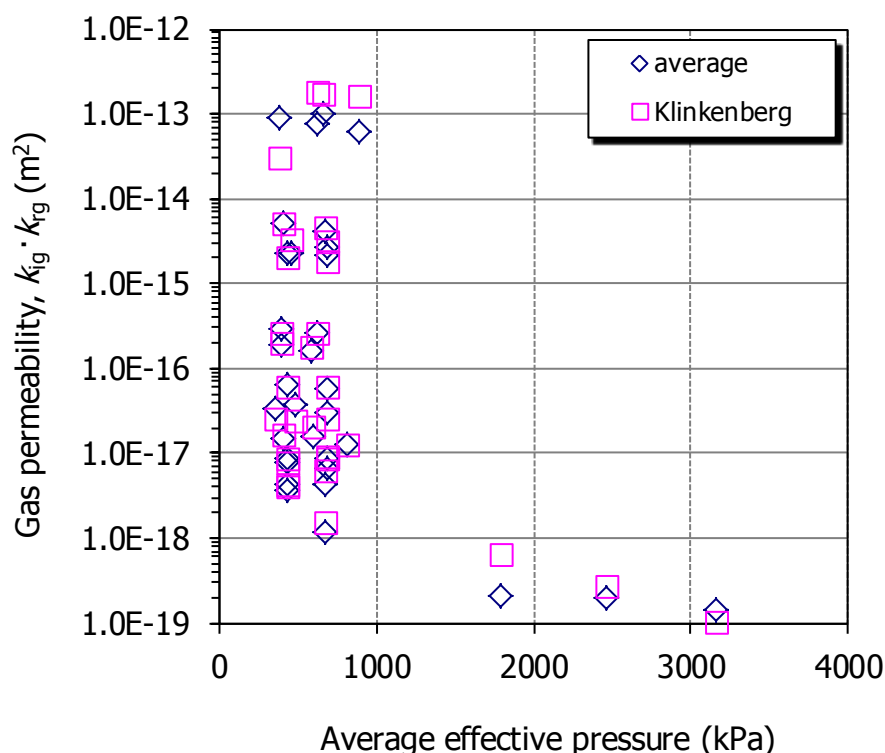


Figure 75: Gas permeability obtained applying different back and injection pressures for different ranges of effective pressure, calculated as an average of all the measurements or applying the Klinkenberg method. The measurements were performed in samples of different water contents and dry densities (Table I)

5.2 INTRINSIC AND RELATIVE GAS PERMEABILITY

During the FEBEX project, the gas permeability of samples of FEBEX bentonite compacted to different dry densities with different water contents was measured in a falling head permeameter under gas injection pressures just slightly above atmospheric, thus much lower than those used for the samples tested in FORGE (Villar & Lloret 2001, Villar 2002). It was found that the gas permeability was best correlated to the accessible porosity. Those results are plotted in Figure 76, in which the new results have also been plotted (Table I). The samples tested during FEBEX had lower degrees of saturation than those tested in FORGE, because the low injection pressures applied then did not allow for gas flow under high degrees of saturation. The new results obtained with highly saturated samples agree with those obtained in less saturated samples and with low injection pressure during FEBEX, and all of them fit in the new correlation shown in the Figure 76. A similar correlation can be found for the $k_{ig} \cdot k_{rg}$ value:

$$k_{ig} \cdot k_{rg} = 1.25 \cdot 10^{-12} (e(1-S_r))^{3.22} \quad [13]$$

If we made the degree of saturation 0 in Equation 13, we would obtain the intrinsic permeability value as a function of void ratio for the dry bentonite (k_{ig}), since the relative permeability to gas (k_{rg}) in a dry sample would be 1:

$$k_{ig} = 1.25 \cdot 10^{-12} e^{3.22} \quad [14]$$

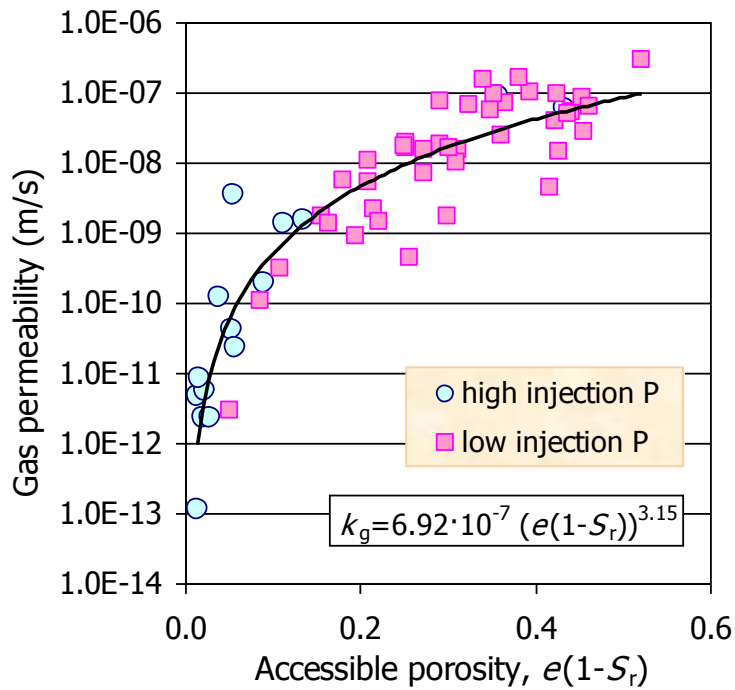


Figure 76: Gas permeability as a function of the accessible porosity for FEBEX samples tested during the FEBEX (low injection P) and the FORGE (high injection P) projects

These values cannot be actually measured, because the drying of the bentonite to such low degree of saturation would imply the modification of its microstructure by shrinkage. During FEBEX it was demonstrated that these intrinsic permeability values are much higher (up to 8 orders of magnitude) than those found for the saturated bentonite using water as permeating fluid, since the pore size distribution is greatly modified during hydration (Villar 2002, Villar & Lloret 2001).

The intrinsic permeability values thus obtained were introduced in Equation 4 for each test (last column in Table I) and then the relative permeability value for each sample tested, of a given e , was obtained. The values thus computed are plotted in Figure 77 as a function of the void ratio. They are very low because the degrees of saturation of the samples were very high, and it was found during FEBEX that the decrease of gas permeability for degrees of water saturation higher than a threshold value (between 65 and 80%, depending on the dry density) was very sharp, due to the discontinuity of the gas phase (Villar & Lloret 2001). Although there were not many results for each density, the relative gas permeability tended to be lower for higher dry densities. The values of relative gas permeability thus obtained during FEBEX have been plotted along with the new ones in Figure 78. Since the range of dry densities tested was between 1.5 and 1.9 g/cm³, there is a large dispersion of relative permeability values when they are plotted as a function of the degree of saturation. However, if they are plotted as a function of the accessible porosity, the following empirical correlation (with a $r^2=0.83$) has been found (Figure 78, right):

$$k_{rg} = 2.98 (e(1-S_r))^{2.94} \quad [15]$$

Finally, we could simply substitute Equation 14 in Equation 13 and obtain a general law relating relative gas permeability to degree of saturation that has been included in Figure 78 (left).

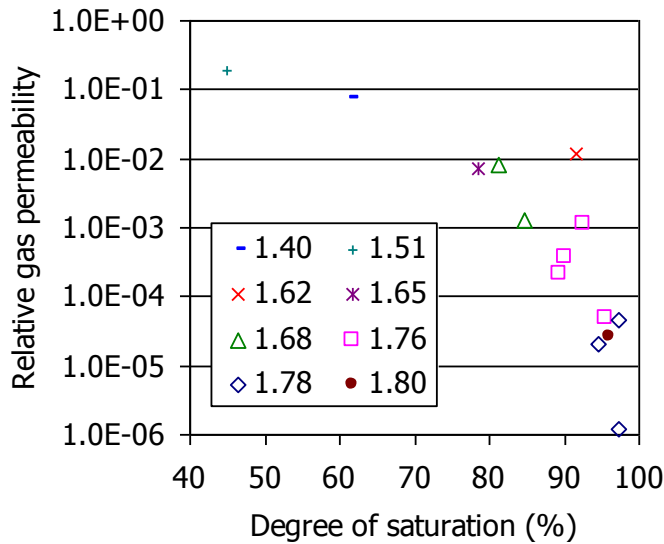


Figure 77: Relative gas permeability deduced from the new measurements as a function of degree of saturation for different dry densities (in g/cm^3)

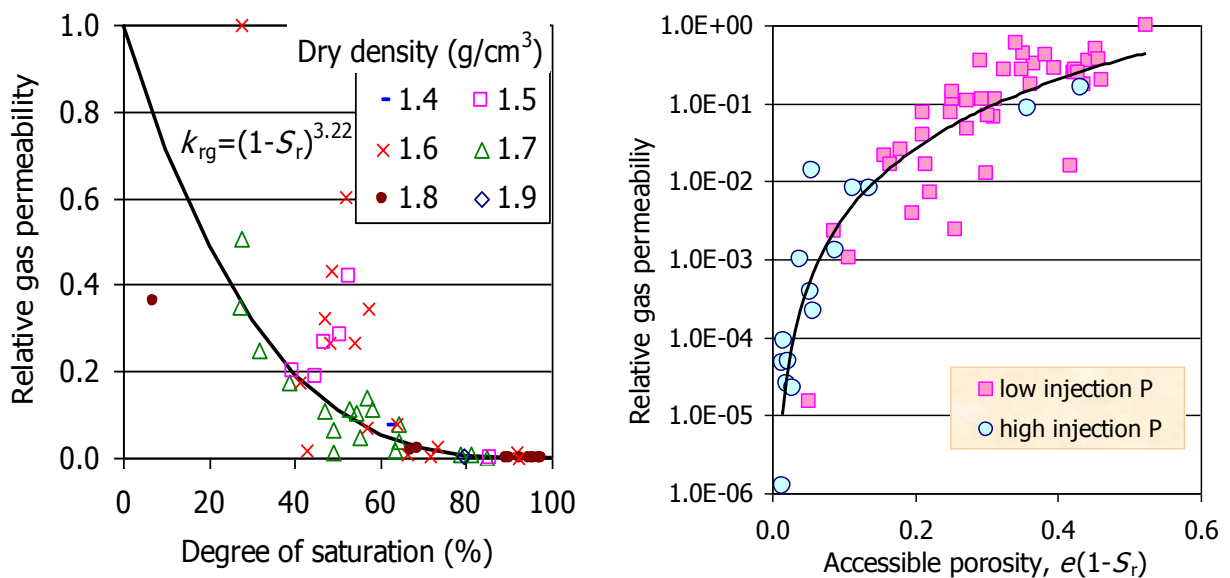


Figure 78: Relative gas permeability computed from the tests performed with compacted FEBEX bentonite during the FEBEX and FORGE projects

5.3 BREAKTHROUGH PRESSURE

The breakthrough pressure tests were performed in bentonite samples that had been completely saturated in stainless steel cylindrical cells. Through these samples a gas pressure gradient was applied, initially a low one, and then it progressively increased until flow through the sample took place, which was indicated by pressure decrease in the upstream deposit and simultaneous pressure increase in the downstream deposit. The hydraulic head at this moment was considered the breakthrough pressure. During the tests, the samples did not have any further water supply, and the swelling of the bentonite was considered enough to guarantee that gas did not flow between the bentonite and the cell walls.

The pressure changes were usually simultaneous in both deposits, although in some cases the pressure decrease in the upstream deposit occurred sometime before the beginning of the pressure increase in the downstream deposit (Figure 28, Figure 46, Figure 50). The first moment could be considered the air entry and the second one the actual breakthrough. The hydraulic head at both moments was very similar. In most cases, at the beginning of the test the pressure in the downstream deposit increased almost immediately a few kPa, what could be explained by the evaporation of water at the sample surface (the equilibrium water vapour pressure at 25°C is approximately 3 Pa). However, no water was generally observed in the downstream lines after dismounting of the tests.

In some cases, particularly when the sample had already experienced a breakthrough episode, the pressure changes were not so sharp (Figure 49). The hydraulic heads causing the subsequent breakthroughs in the samples analysed are shown in Figure 79. The second and third breakthroughs tended to take place at lower pressure gradients, what can be explained by the fact that the samples did not receive any water supply during the gas test, and they could slightly dry during it. In fact, the water content of the samples after the BT tests decreased systematically, although only an average of 0.8%. Horseman et al. (1999) considered that gas bubbles remaining in the pathways would help in their new opening. However, when the flow of gas stopped quickly after breakthrough, the following breakthrough would generally happen when a similar hydraulic head was reached again, what indicates that the gas passage sealed after the first breakthrough (Figure 37). After resaturation, the breakthrough pressures were similar to those obtained after the first saturation.

The breakthrough pressures obtained in the first breakthrough are shown in Figure 80 as a function of the dry density of the samples after saturation. The breakthrough pressure values increased clearly with dry density, and they were always higher than the swelling pressure of the bentonite. The results obtained in samples with a sealed joint have also been plotted in the Figure. The values are in the order of those obtained in samples of the same dry density without joint, what indicates that a sealed interface along the bentonite has no effect on the breakthrough pressure values. However, a granite/bentonite interface showed a much lower BT pressure of 0.7 MPa for a bentonite dry density of 1.56 g/cm³.

The effect of the size of the samples on the breakthrough pressures obtained was checked by using samples of two different heights (2 and 5 cm) and diameters (3.8 and 5.0 cm). Although there are not enough results to conclude, the shorter samples tended to show lower breakthrough pressures for similar dry densities.

The computation of gas permeability after breakthrough makes sense when the change in pressure in both deposits is gradual, because this means that two-phase flow along the sample has been established. So, in cases such as those shown in Figure 37 or Figure 51, the computation of permeability makes no sense, because the gas passage is “instantaneous” and takes place probably through processes other than two-phase flow. But usually flow decreased over time, as the pressure difference between both deposits decreased. Below a certain pressure difference no flow occurred and the pressures in both deposits remained unchanged – indicating the closing of pathways– until another pressure step was forced. In a few cases a stable permeability value was finally achieved (Figure 31, Figure 41).

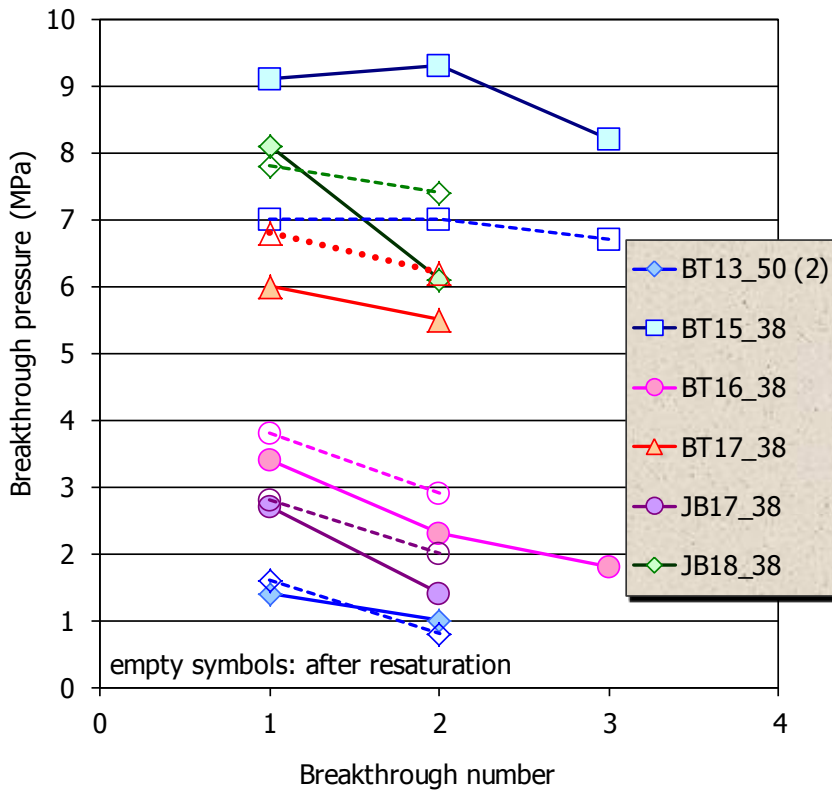


Figure 79: Subsequent gas breakthrough pressures measured after saturation (Phase 2 and 4) for samples of different dry density (indicated in Table III to Table XII)

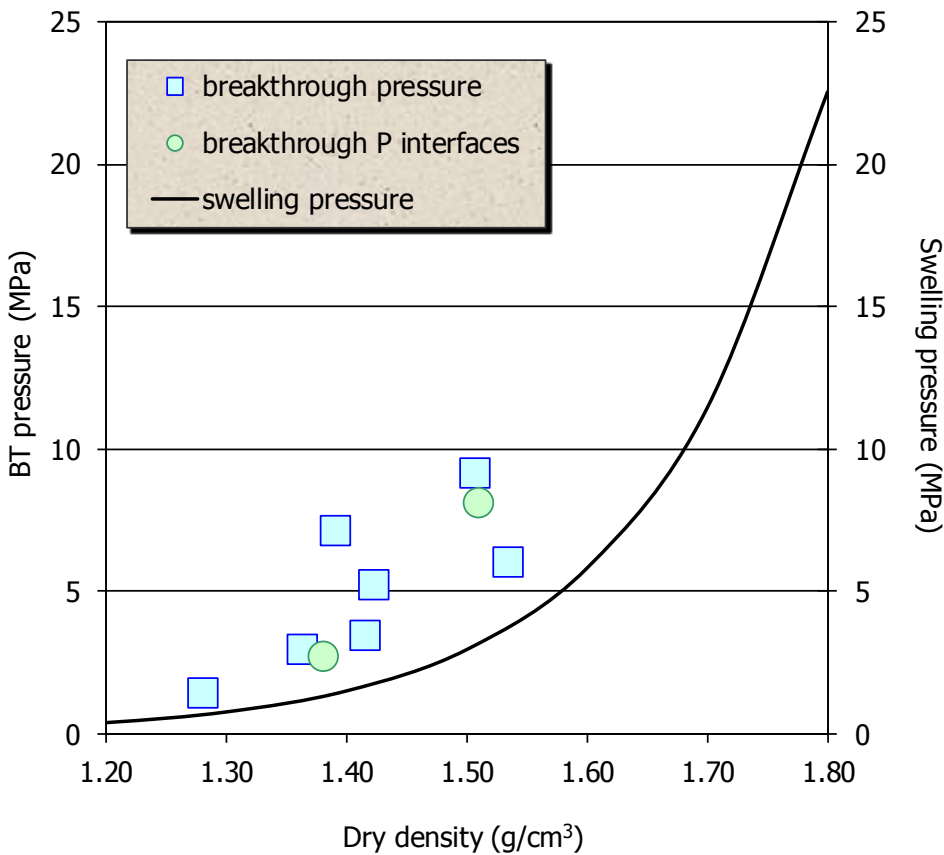


Figure 80: Gas breakthrough pressure values for saturated bentonite samples compacted at different dry density and theoretical swelling pressure

The gas permeability values computed after breakthrough are plotted in Figure 81 as a function of the dry density of the samples. Since the samples were saturated, lower dry densities overall indicate higher water contents. The permeability values correspond to the average of the values computed from the pressure increase and decrease once they were stable, which usually coincided. Nevertheless, in most cases permeability did not stabilise and just the lowest value obtained is plotted in the Figure. There is a trend for the permeability values to increase as the dry density decreases, i.e. as the water content increases. This could indicate that, although the flow took place specially through preferential pathways, the bentonite matrix had also an influence, maybe through the swelling pressure developed, which would condition the easiness of path's formation. Low density samples developing a lower swelling pressure would facilitate gas transport. Indeed the values given are only an estimation done considering that the flow is a two-phase flow. Surprisingly, the permeability after the subsequent breakthroughs tends to be similar, as if the microstructure was not modified after the first breakthrough, and this despite the fact that the samples were not resaturated between breakthrough episodes.

In any case, the permeability values are much lower than those measured for degrees of saturation below 97%. Figure 82 shows the values obtained in the breakthrough tests along with the values determined on compacted samples of FEBEX bentonite of degrees of saturation between 81 and 97% (Figure 12). Although in the latter case the dry density of the samples was higher, the gas permeability values were several orders of magnitude higher, which highlights the abrupt decrease of gas permeability as water saturation is approached.

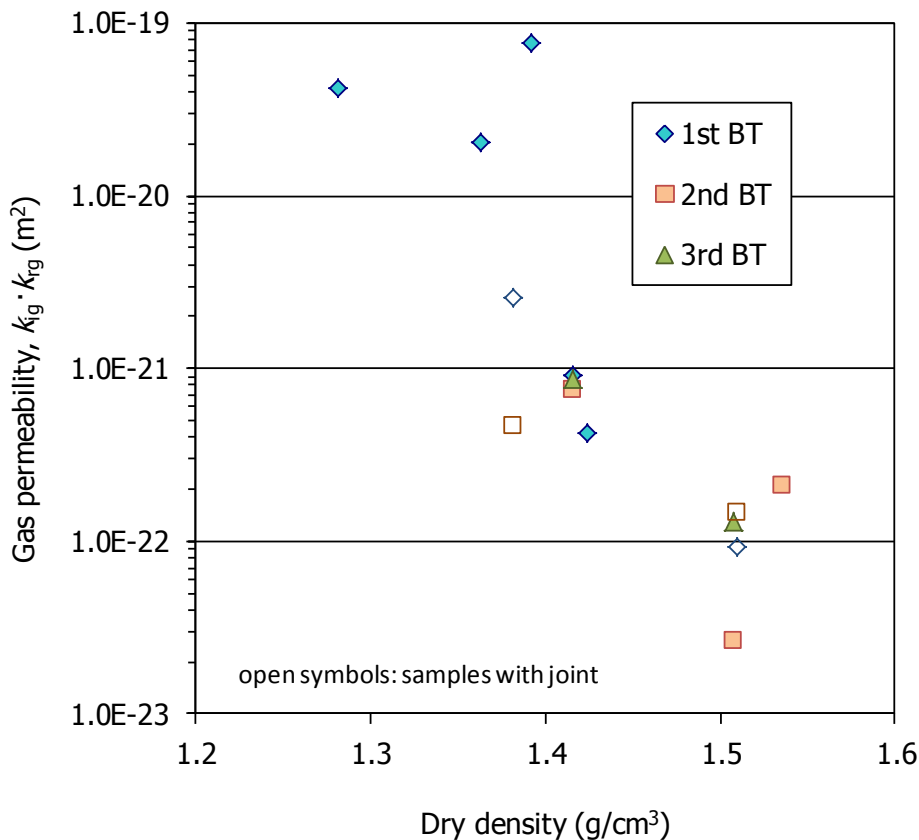


Figure 81: Gas permeability after breakthrough computed with Equation 10 in saturated bentonite samples of different dry density

deposits decreased below a certain value. This would indicate that the gas paths opened upon breakthrough were able to seal afterwards, despite the fact that no water supply was allowed during the gas tests. When the pressure gradient was increased again, breakthrough took place at values slightly lower than in the first case, particularly in the case of low density samples. However, after resaturation of the bentonite the same initial breakthrough pressures were usually found, pointing again to the perfect healing of the potential preferential pathways. The doubt remains if these breakthrough values would have been lower if the same pressure gradient steps had been kept for periods of time longer than 24 h.

The fact that the permeabilities computed after breakthrough were lower for lower dry density samples would indicate that despite the fact that flow took place through preferential pathways, that sometimes closed quickly after breakthrough and others remained open allowing a gradual decrease of gas flow, the bentonite matrix and its swelling conditioned the easiness of the path's formation. It has to be born in mind that the permeability values were computed assuming two-phase flow as gas transport mechanism for lack of a better approximation.

Consequently, gas migration would involve both two-phase flow (without significant deformation of the pore space) and microscopic pathway dilation. Two-phase flow seemed to take place for degrees of saturation lower than about 97% in compacted bentonite, whereas for higher degrees of saturation pathway dilation could be the predominant mechanism. The threshold pressure for gas entry into the bentonite was higher than the swelling pressure and seemed to be lower than the gas pressure required for fracturing (macroscopically) the material, since the samples were intact when the cells were dismantled. The stability of the pathways would depend on the degree of saturation and dry density of the samples. For not completely saturated bentonite, the gas pathways seemed to be stable, since for a given hydraulic gradient there was a stable flow. However, in almost completely saturated samples of bentonite, in which it was necessary to apply high pressure to induce flow (breakthrough pressure), when the pressure gradient dropped below a given value, flow stopped, what is interpreted as closing of the pathways. Upon increasing of the pressure gradient again, when the previous breakthrough pressure was reached once more, flow resumed. This can be interpreted as due to the reversibility of the closing-opening of paths previously opened. In any case, the drop in effective gas permeability when approaching full saturation is of several orders of magnitude.

Although there are not many results yet, it seems that a sealed interface along the bentonite has no effect on the breakthrough pressure values. On the contrary, a saturated granite/bentonite interface (bentonite dry density 1.56 g/cm^3) kept under constant volume allowed the passage of gas under a pressure of 0.7 MPa. After resaturation of this interface, the same breakthrough pressure was found. If the interface is allowed to dry, the pressure needed for gas passage decreases.

Acknowledgements

The laboratory work was performed by Ramón Campos and Juan Aroz, from CIEMAT. Vanesa Gutiérrez-Rodrigo had a grant for research personnel training from CIEMAT.

References

- ENRESA, 2000. FEBEX PROJECT. Full-scale engineered barriers experiment for a deep geological repository for high level radioactive waste in crystalline host rock. Final report. *Publicación Técnica ENRESA 1/2000*, Madrid, 354 pp.
- ENRESA, 2006. FEBEX Full-scale Engineered Barriers Experiment, Updated Final Report 1994-2004. *Publicación Técnica ENRESA 05-0/2006*, Madrid, 590 pp.
- HORSEMAN, S. T., HARRINGTON, J. F. & SELLIN, P. 1999. Gas migration in clay barriers: *Engineering Geology*, v. 54, p. 139-149.
- LLORET, A., ROMERO, E., VILLAR, M.V. 2004. FEBEX II Project Final report on thermo-hydro-mechanical laboratory tests. *Publicación Técnica ENRESA 10/04*, Madrid, 180 pp.
- L'AIR LIQUIDE, 1976. *Encyclopédie des Gaz*. Amsterdam: Elsevier. 1164 pp. ISBN-10: 0444414924
- LOOSVELDT, H., LAFHAJ, Z., SKOCZYLAS, F. 2002. Experimental study of gas and liquid permeability of a mortar. *Cement and Concrete Research* 32(9), 1357-1363.
- SCHIEDEGGER, A.E. 1974. *The physics of flow through porous media*. 3rd ed. Toronto: University of Toronto Press, 353 pp.
- SYSTAT SOFTWARE INC. 2002. Table Curve 2D. Automated Curve Fitting and Equation Discovery. Version 5.01.
- VILLAR, M.V., 2002. Thermo-hydro-mechanical characterisation of a bentonite from Cabo de Gata. A study applied to the use of bentonite as sealing material in high level radioactive waste repositories. *Publicación Técnica ENRESA 01/2002*, Madrid, 258 pp.
- VILLAR, M.V., LLORET, A., 2001. Variation of the intrinsic permeability of expansive clay upon saturation. 259-266 in *Clay Science for Engineering*. ADACHI, K. & FUKUE, M. (editors), Rotterdam: Balkema. ISBN 90 5809 175 9.
- VILLAR, M.V., GÓMEZ-ESPINA, R., 2009. Report on thermo-hydro-mechanical laboratory tests performed by CIEMAT on FEBEX bentonite 2004-2008. *Informes Técnicos CIEMAT 1178*, Madrid, 67 pp.
- VILLAR, M.V.; MARTÍN, P.L. & BARCALA, J.M. 2010. Description of experimental setups and procedures for CIEMAT gas transport tests of WP3. *Informe Técnico CIEMAT/DMA/2G207/01/10*, Madrid, 13 pp.
- Villar, M.V.; Martín, P.L.; Romero, F.J., Barcala, J.M. & Gutiérrez-Rodrigo, V. 2012a. Gas transport through bentonite: influence of dry density, water content and boundary conditions. In: Skoczylas, F.; Davy, C.A.; Agostini, F. & Burlion, N. (eds.): *Propriétés de Transfert des Géomatériaux*. Transfert 2012, Actes du Colloque: 379-389.
- Villar, M.V.; Gutiérrez-Rodrigo, V.; Martín, P.L.; Romero, F.J. & Barcala, J.M. 2012b. Results of the tests on bentonite (Part 2). FORGE Deliverable 3.27. Informe Técnico CIEMAT/DMA/2G207/07/12. December 2012. CIEMAT, Madrid, 52 pp.

